Development of extension over time during rifting of the Jeanne d'Arc Basin, offshore Newfoundland

by

©Caroline McIlroy

A Thesis submitted to the School of Graduate Studies in partial fulfillment of the requirements for the degree of

Master of Science

Department of Earth Sciences/Faculty of Science

Memorial University of Newfoundland

April 2014

St. John's Newfoundland

Abstract

The Jeanne d'Arc Basin formed during multiple rift events and passive subsidence associated with the opening of the North Atlantic Ocean through the Mesozoic and Cenozoic. It is typically reported that crustal thinning is greater than extension due to brittle faulting. Although there have been measurements of total extension from fault analysis along single transects across the basin or from change in crustal thickness, quantifying the extension using detailed fault analysis for the different rift phases and how it changes throughout the basin has not previously been attempted.

2D and 3D seismic data and well data were used to create time structure maps at the start of each rift phase. These maps were restored to their position before each rift phase using beta values derived from fault heave extension estimates. The restored maps were compared with restorations produced using change in crustal thinning to measure beta. It was established that fault heave measurements from the 2D data underestimate extension by approximately 50% when compared with measurements from the 3D data. This observation was incorporated into the extension estimates.

Extension was most significant during the Late Triassic to Early Jurassic rift phase in the Jeanne d'Arc Basin. The total amount of extension measured using fault heaves in this study corresponds closely with the total amount of extension measured using change in crustal thickness in the regional North Atlantic deformable plate model, for total extension with beta values generally around 2. This indicates that stretching is uniform with depth in this area. This detailed study can be used to refine the regional North Atlantic deformable plate model.

Time structure maps of the syn-rift and post-rift thickness were created for a larger area extending into the northern Jeanne d'Arc Basin and the southern Orphan Basin. The post-rift thickens dramatically northwards to overlie thin syn-rift in the north of the area. It is suggested that depth dependent extension caused by ductile flow of continental mantle lithosphere towards the rift axis led to large scale thermal subsidence in this area.

Acknowledgements

- I would like to say a special thank you to my supervisor Jeremy Hall for setting me up with the project and for his continued guidance and support.
- Thanks to the other members of my supervisory committee Sharon Deemer and Tom Calon.
- Many thanks to Peter Bruce for his constant help with the computers and software and for the many hours he spent converting my scans to SEGY and loading them into Seisworks.
- Thanks to Iain Sinclair for his insights into the Jeanne d'Arc Basin during my summer at Husky Energy.
- Software from Landmark and Petrosys.
- Funding from Husky, the Research and Development Corporation (RDC), Memorial University School of Graduate Studies (SGS), Jeremy Hall's Natural Sciences and Engineering Research Council (NSERC) Discovery Grant.
- Data from Canada-Newfoundland and Labrador Offshore Petroleum Board (CN-LOPB), Husky Energy, WesternGeco, Natural Resources Canada (NRC) Basin website.

- Data and models derived from a plate reconstruction study carried out by GeoArctic Ltd. and its subcontractors for the Petroleum Infrastructure Programme Rockall Studies Group (PIPCO RSG Ltd.). The project was jointly funded by the Irish Shelf Petroleum Studies Group (ISPSG) of PIP and Nalcor Energy (on behalf of the Offshore Geoscience Data Program with the Government of Newfoundland and Labrador).
- Thanks to Bridget Ady for producing the restored time structure maps using the GeoArctic Ltd. software. Underlying data for the GeoArctic plate model is derived from the work funded by ISPSG and Nalcor Energy.

Table of Contents

List of Tables

List of Figures

Chapter 1

Introduction

The Jeanne d'Arc Basin, on the Newfoundland continental shelf of the northwest Atlantic Ocean, formed during multiple rift events and passive subsidence associated with the opening of the North Atlantic Ocean through the Mesozoic and Cenozoic. This study aims to measure quantitatively the extension through time in the Jeanne d'Arc Basin.

The relationship between plate motion and continental deformation during crustal extension is complex. Plate tectonic models assume that the lithosphere is composed of rigid plates which move with respect to each other along discrete boundaries. This works well for oceanic lithosphere which is strong and dense, hence it can transmit stresses over great distances without significant deformation. Continental crust is comparatively weak because of its quartzo-feldspathic composition and greater radiogenic heat flow. This intrinsic weakness produces broad zones of distributed deformation during extension (e.g. the 70 km wide African rift). Previous rigid plate reconstruction models have moved plates around their pole of rotation leading to problems with overlap and under-fit of the restored plate margins (Srivastava et al.

1988, [46]). By allowing for multiple phases of extension which deform the plate edges prior to sea-floor spreading, these problems can be overcome.

1.0.1 Implications for petroleum geology

GeoArctic Ltd. and its subcontractors for the Petroleum Infrastructure Programme Rockall Studies Group (PIPCO RSG Ltd.) led a team of scientists, as part of the North Atlantic Petroleum Systems Assessment (NAPSA), to develop a new deformable/plate kinematic reconstruction of the North Atlantic between Ireland and Canada (GeoArctic Ltd. website, [13]). The GeoArctic Plate Model is derived from work funded jointly by the the Irish Shelf Petroleum Studies Group (ISPSG) of PIP and Nalcor Energy. The deformable plate model builds a detailed structural and paleogeographical history of the North Atlantic plate margins. This provides a new assessment of the depositional setting and provenance of reservoir rocks, source rock distribution, basin connectivity and can furthermore be used to inform discussion of palaeoclimate regimes and oceanographic currents. Therefore the new plate reconstruction can be used to make source and reservoir predictions pertinent to the petroleum geology of the Newfoundland and conjugate margins, which is an objective of NAPSA.

This study integrates GeoArctic's regional North Atlantic reconstructions with restorations of the Jeanne d'Arc Basin, which is the primary oil producing basin in the northwest Atlantic Ocean. The detailed mapping within the basin provides information on the orientation and timing of tectonic events that can be used to refine the regional North Atlantic deformable plate reconstruction.

The total amount of extension is measured using fault heaves in this study and compared with the total amount of extension measured using change in crustal thickness in the regional Noth Atlantic deformable plate model, to establish whether stetching is uniform with depth in this area.

1.1 Background Geology

1.1.1 Spreading of the North Atlantic

Sea-floor magnetic anomalies leave an account of the complex evolution of the North Atlantic which developed in stages from south to north (Fig. 1.1). Sea-floor spreading between Nova Scotia and Northwest Africa commenced in the Late Jurassic, around 150 Ma (Fig. 1.2; Srivastava et al., 1988 [48]). Immediately north of the Newfoundland-Azores Fracture Zone, the North Atlantic started spreading in the Early Cretaceous at around 115 Ma, separating Iberia from Newfoundland (Srivastava and Tapscott, 1986 [46]; Tucholke et al., 2007 [51]). Spreading propagated northward into the area between Galicia Bank and the Flemish Cap and into the Bay of Biscay in the mid-Cretaceous at around 100 Ma, and the Biscay Triple Junction formed at the intersection of the Mid-Atlantic Ridge and the Biscay spreading centre (Srivastava et al., 1988 [48]). Between 62-70 Ma seafloor spreading propagated into the Labrador Sea, separating Greenland and Labrador (Dickie et al., 2011 [8]). At the same time the Bay of Biscay spreading centre became inactive (Ziegler, 1989 [65]). In the early Eocene the Reykjanes Ridge started spreading, separating Greenland and the Rockall-Hatton Bank and creating a triple junction between the Mid-Atlantic Ridge, the Reykjanes Ridge and the Labrador Sea spreading centre. By the late Eocene sea-floor spreading in the Labrador Sea had ceased and the present-day configuration of the North Atlantic had been established (Fig. 1.1; Ziegler, 1989 [65]).

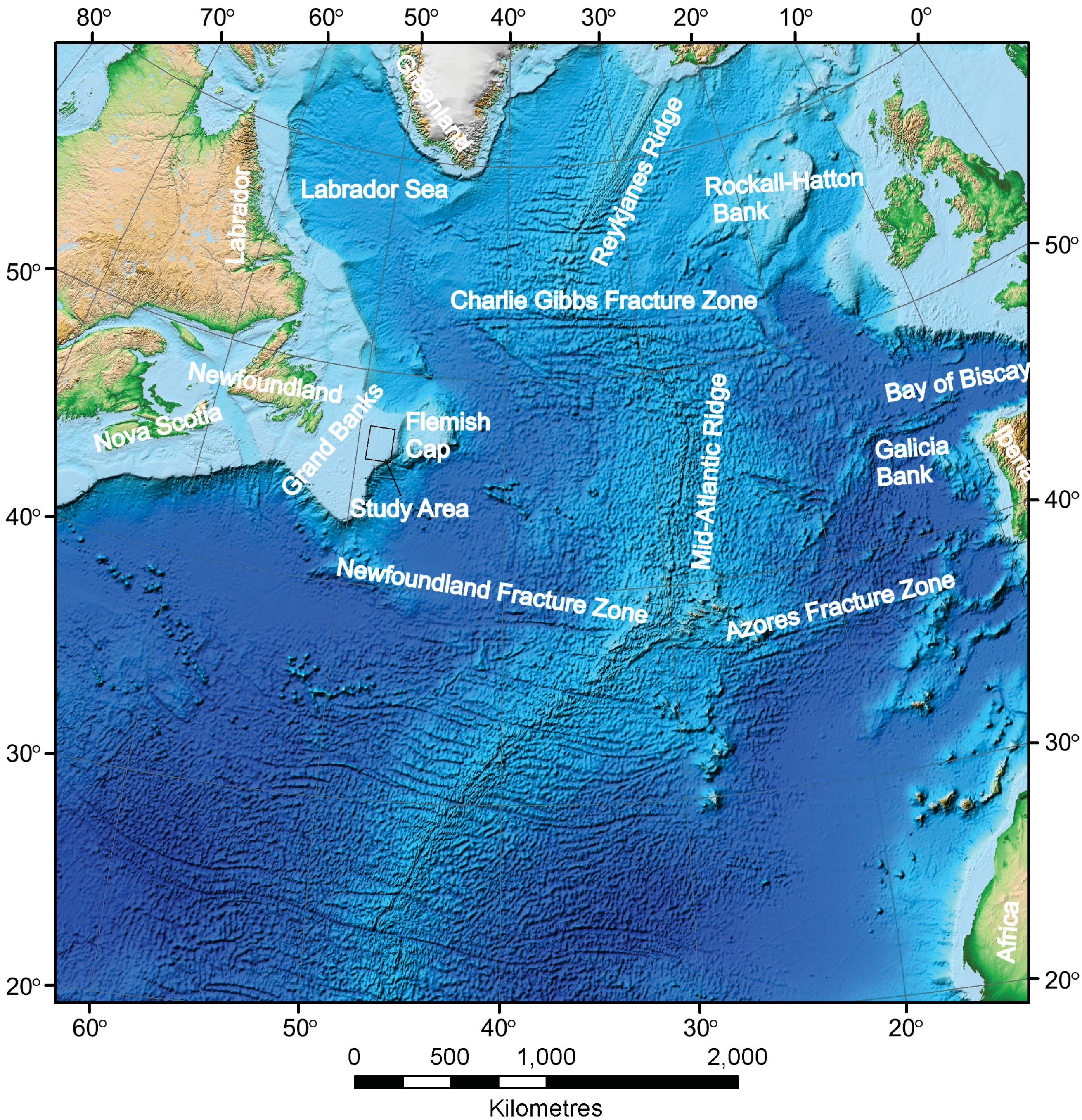

Figure 1.1: Bathymetric map showing the North Atlantic spreading centres.

1.1.2 The Southeast Newfoundland Margin

Rifting between Newfoundland and Iberia produced a magma-poor margin (Tucholke and Sibuet, 2007 [52]). It is bounded at the southern end by the Newfoundland-

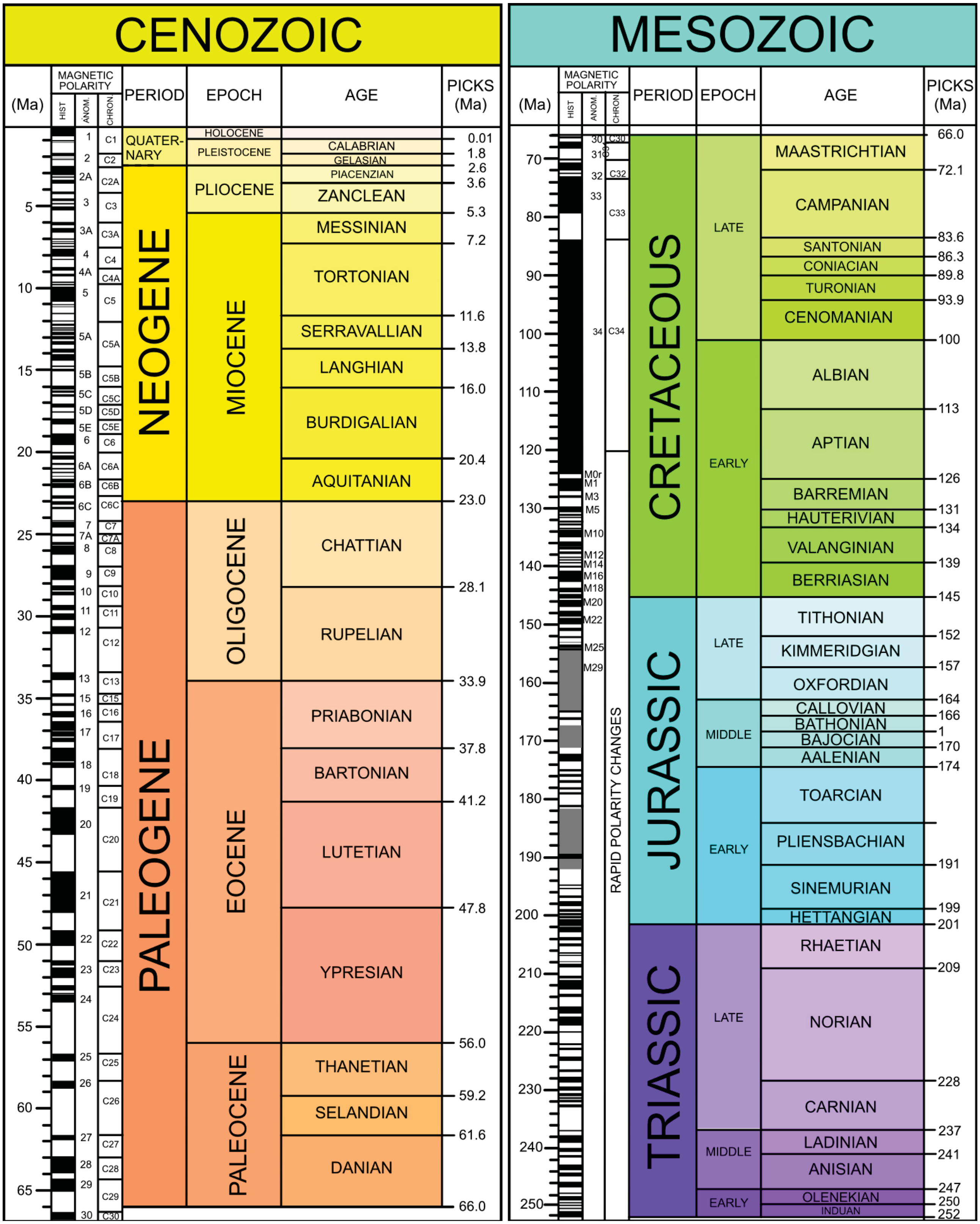

Figure 1.2: Geological timescale for the Cenozoic and Mesozoic, from the Geological Society of America, 2013 (Walker et al. 2013 [56]).

Gibraltar fracture zone, aligned with the southwestern edge of the Grand Banks (Fig. 1.3). The northern end of the rift is at the eastern tip of the Flemish Cap on the Newfoundland margin and the northwest edge of the Galicia Bank on the Iberian side.

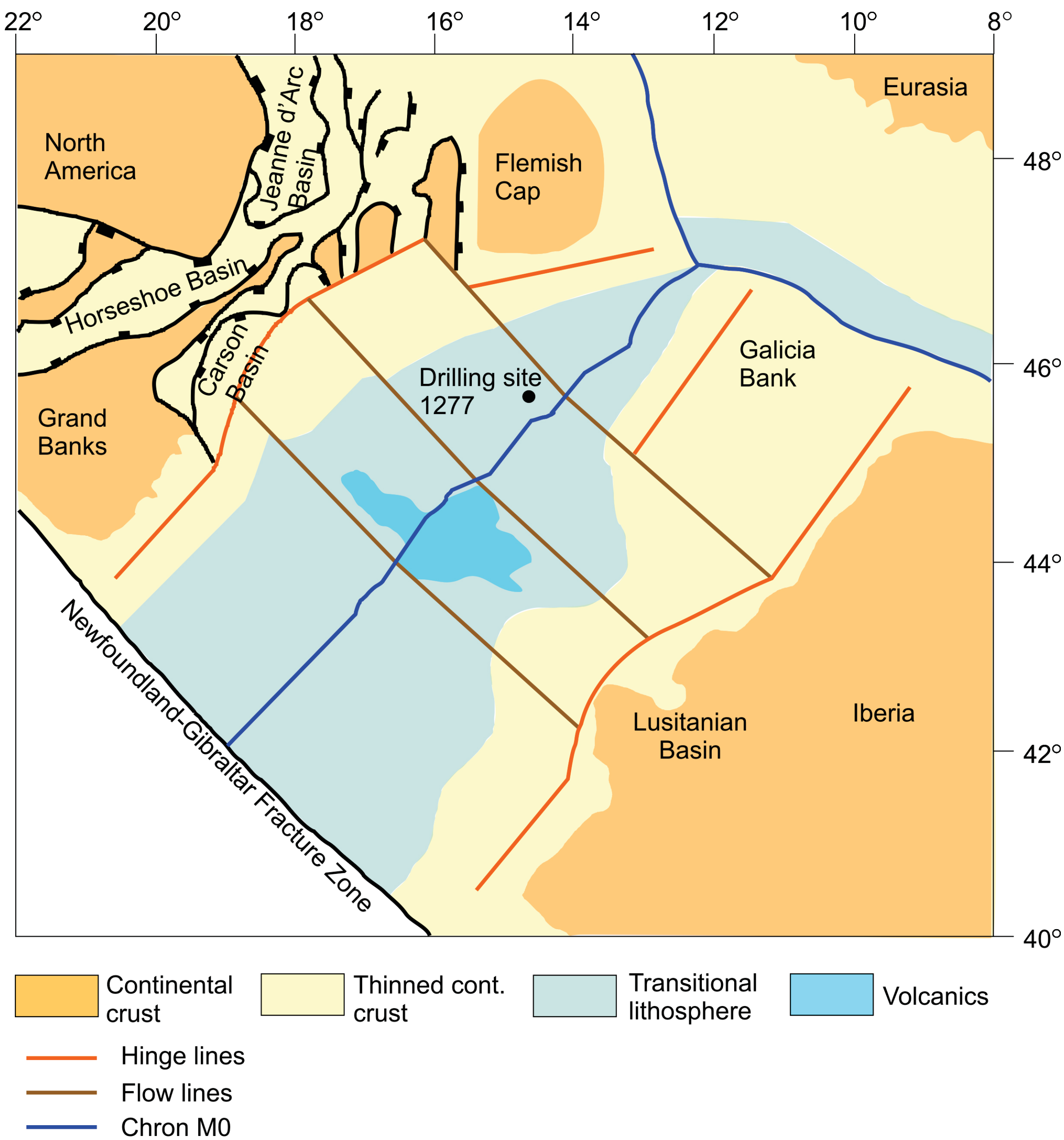

Figure 1.3: Plate reconstruction of the Newfoundland-Iberia rift at chron M0 (125 Ma), illustrating crustal and lithosphere domains (after Sibuet and Tucholke, 2012 [41]).

Rifting between Newfoundland and Iberia extended the approximately 30 km thick continental crust (Tucholke and Whitmarsh, 2012 [53]).

The pre-rift basement consists of Precambrian and Paleozoic rocks of the Avalon Zone which forms part of the Appalachian Orogen (Keen et al., 1987 [20]). Rifting in the Triassic to Early Jurassic created large deep rift basins on the Grand Banks, for example the Jeanne d'Arc, Horseshoe and Carson Basins and the Lusitanian Basin in Iberia, but it did not lead to continental breakup (Fig. 1.3; Tucholke and Whitmarsh, 2012 [53]). Following a period of widespread thermal subsidence, there was another phase of extension during the Late Jurassic and Early Cretaceous that culminated in seafloor spreading (Tucholke and Whitmarsh, 2012 [53]). The evolution from continental rifting and crustal thinning to seafloor spreading was complex.

Seaward of the zone of thinned continental crust, refraction studies across the rift infer a zone of transitional lithosphere (Lau et al., 2006 [23]). Magnetic anomalies over this zone are poorly developed, suggesting magnetization of serpentinites rather than igneous rocks (Tucholke and Sibuet, 2007 [52]). A strong component of magnetization can be produced by the serpentinization process, leading to magnetic anomalies correlatable to the magnetic timescale (Sibuet et al., 2007 [39]). Drilling at Site 1277 (Fig. 1.3) in the transitional lithosphere revealed that the basement is serpentinized mantle (Tucholke and Sibuet, 2007 [52]). There is debate as to the extent of transitional lithosphere, however it is proposed that it could be up to 200 km between Galicia Bank and Flemish Cap and greater than 400 km south of Galicia Bank (Sibuet and Tucholke, 2012 [41]).

The processes by which broad zones of mantle are exhumed with very little magma produced, followed by melt production and the formation of a new ridge is enigmatic. At a magma-poor rifted margin it is predicted that the potential temperature of the sublithospheric mantle beneath the continents is lower than beneath the oceans and may be as low as 1200°C (Reston and Morgan, 2004 [37]). As the temperature is too low for production of new oceanic crust, a broad zone of mantle is unroofed. It is suggested that initiation of true seafloor spreading at a magma poor margin requires a lateral influx of hotter suboceanic asthenosphere (Reston and Morgan 2004, [37]).

Sibuet and Tucholke, 2012 [41] propose that the upper mantle flowed ductilely from under the continent to be emplaced seaward of the brittlely thinned continental crust. Peron-Pinvidic and Manatschal, 2009 [33] infer exhumation of subcontinental mantle by detachment faults. This would produce a broader zone of transitional lithosphere on one side than the other, whereas there is evidence that the zone of transitional lithosphere is roughly equivalent on the Newfoundland and the Iberian side, thus Pérez-Gussinyé, 2013 [32] proposes that the mantle rose under its own bouyancy. A low initial temperature structure and very slow extension rates lead to the lower crust becoming brittle with progressive extension. Lower crustal embrittlement allowed seawater to penetrate to the mantle and caused serpentinization. Serpentinites are weak, hence crustal separation and mantle exhumation followed immediately after crustal embrittlement and the onset of serpentinization. This led to two breakup events: the rupture of the brittle continental crust and the rupture of the exhumed mantle at the start of oceanic crust emplacement (Tucholke and Sibuet, 2007 [52]). It is suggested that seafloor spreading started in the latest Aptian to earliest Albian leading to a break-up unconformity marking the final separation of sub-continental mantle lithosphere (Tucholke et al., 2007 [51]).

The Newfoundland Margin is further complicated by the motion of the Flemish Cap during rifting (Fig. 1.3). There is little evidence for significant extensional deformation of the Flemish Cap, and the continental crust thins rapidly on the eastern margin from 30 km to around 3 km over a distance of 80 km. This suggests that the Flemish Cap behaved as a microplate through the Mesozoic (Hopper et al., 2007 [16]; Welford et al., 2010 [58]). From chron M25 until chron M0 the Flemish Cap and Galicia Bank microplates remained attached to each other, producing extension in the Orphan Basin and Flemish Pass Basin landward of the Flemish Cap and in the Galicia Interior Basin landward of the Galicia Bank, as well as transtensional regimes northeast and southwest of Flemish Cap (Sibuet et al., 2007 [40]). Using Bouguer anomalies to compare the hinge zones, Sibuet et al., 2007 [40] argued that the Flemish Cap rotated 43° relative to Galicia Bank and Iberia and moved 200-300 km southeast with respect to North America.

1.1.3 The Jeanne d'Arc Basin

The study area is the Jeanne d'Arc Basin, located approximately 300 km east-southeast of St. John's, Newfoundland (Fig. 1.4). The oil-rich basin is economically important, containing the Hibernia, Terra Nova, White Rose and Hebron/Ben Nevis oil fields (Fig. 1.5). The Jeanne d'Arc Basin is an asymmetric half-graben trending north-northeast, containing in excess of 22 km of sedimentary fill. The basin extends almost 250 km in the north-south direction and about 80 km in the east-west direction. It is bounded to the west by pre-Mesozoic rocks of the Bonavista Platform and to the east by the Central Ridge (Fig. 1.5). The border fault to the west is the east-dipping, listric Murre fault (Fig. 1.5) which flattens in the mid-crust (Dentith and Hall, 1990 [6]). The gross morphology of the basin is attributed to the reactivation of planes of weakness in the Avalon basement, for example the listric border fault is localized on an older thrust-like dipping feature (Tankard et al., 1989 [50]).

The sedimentary evolution of the Jeanne d'Arc Basin reflects the regional tectonic

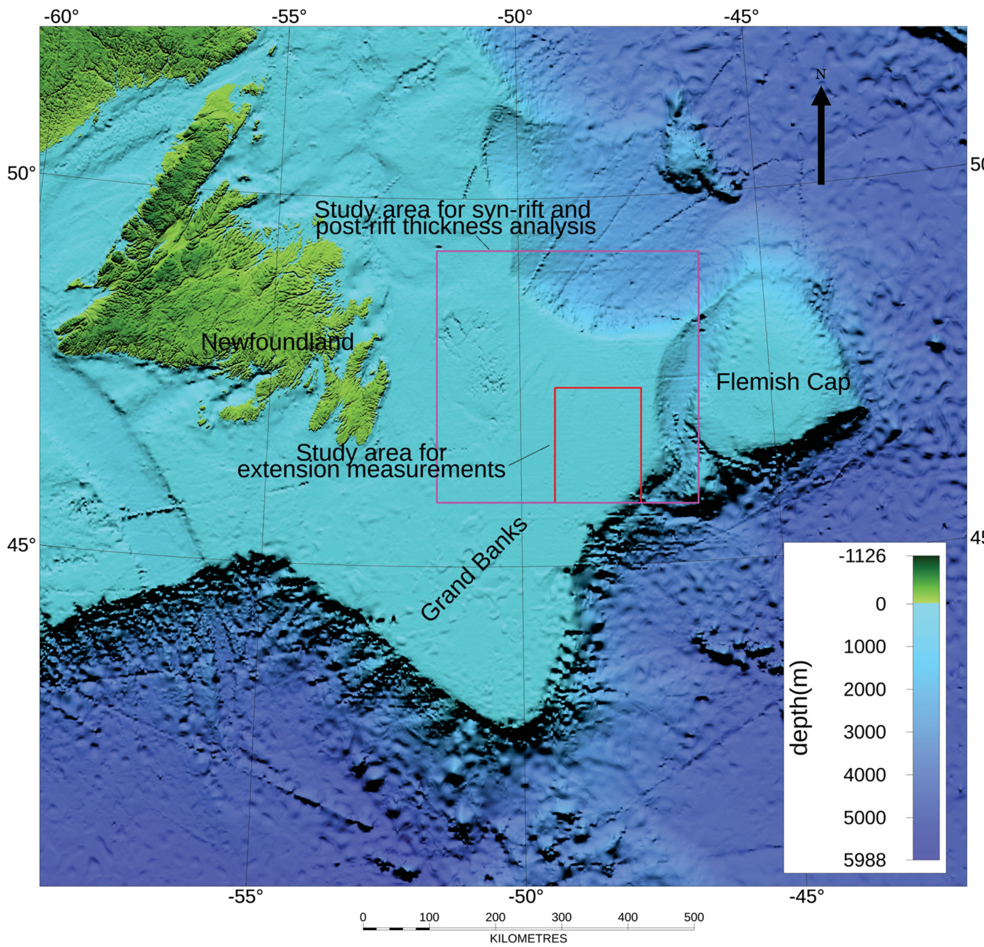

Figure 1.4: Bathymetric map showing the location of the study area on the Grand Banks, offshore Newfoundland.

episodes related to the opening of the Atlantic Ocean (Fig. 1.6). The Triassic to Early Jurassic rift phase (I) was dominated by evaporite deposition. The Late Jurassic to Early Cretaceous rift phase (II) was mainly characterized by coarse-grained siliciclastic sedimentation, thereby forming the hydrocarbon reservoirs of the Jeanne d'Arc Formation and the Hibernia Formation (McAlpine, 1990 [28]). The two rift phases were separated by a tectonically quiescent period during which limestones and fine-grained siliciclastic sediments were deposited. Hydrocarbons of the Jeanne d'Arc Basin are thought to have been generated from mudstones of the Egret Member of

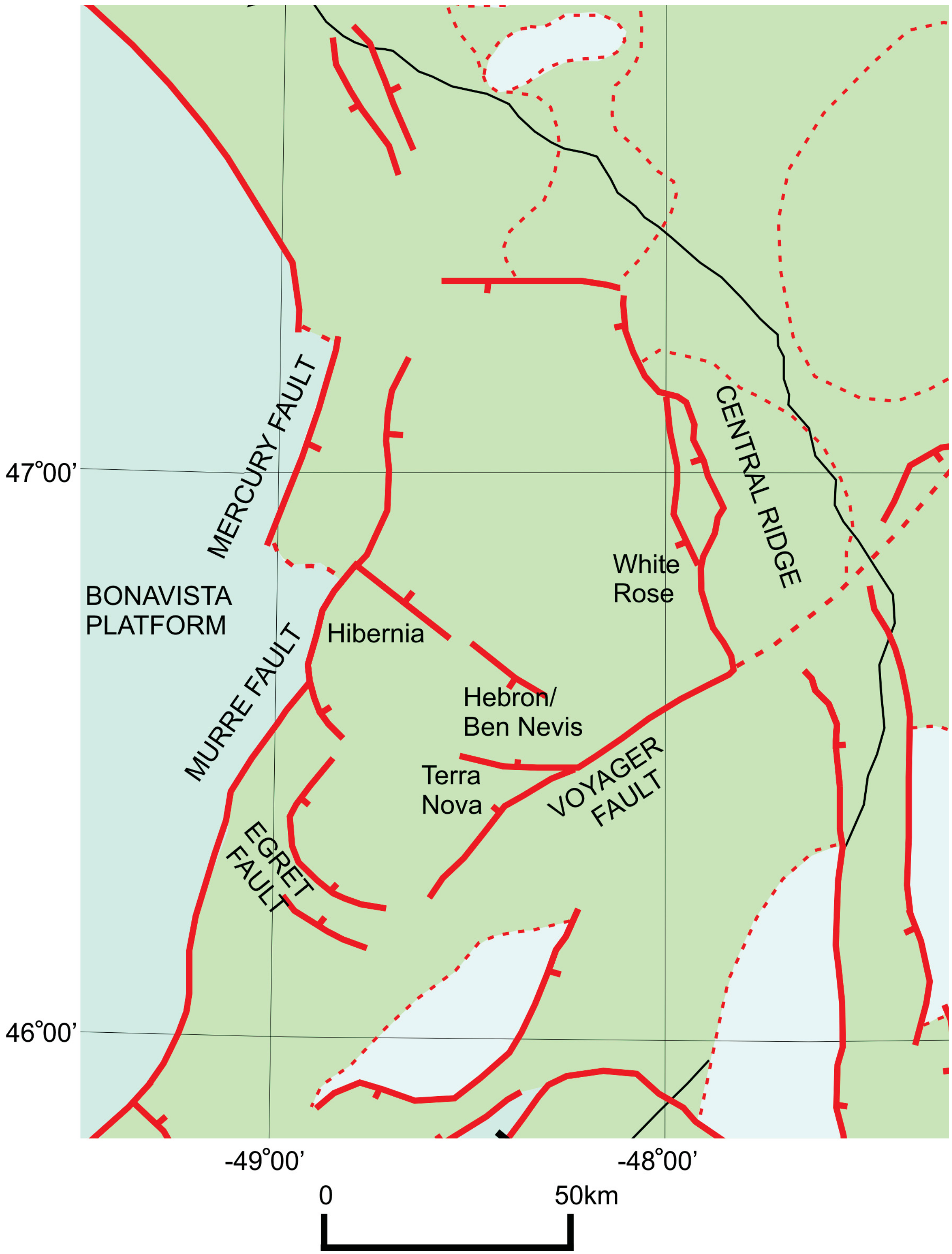

Figure 1.5: Map of the Jeanne d'Arc Basin showing the border faults and the oil fields (after CNLOPB, 2003 [4]).

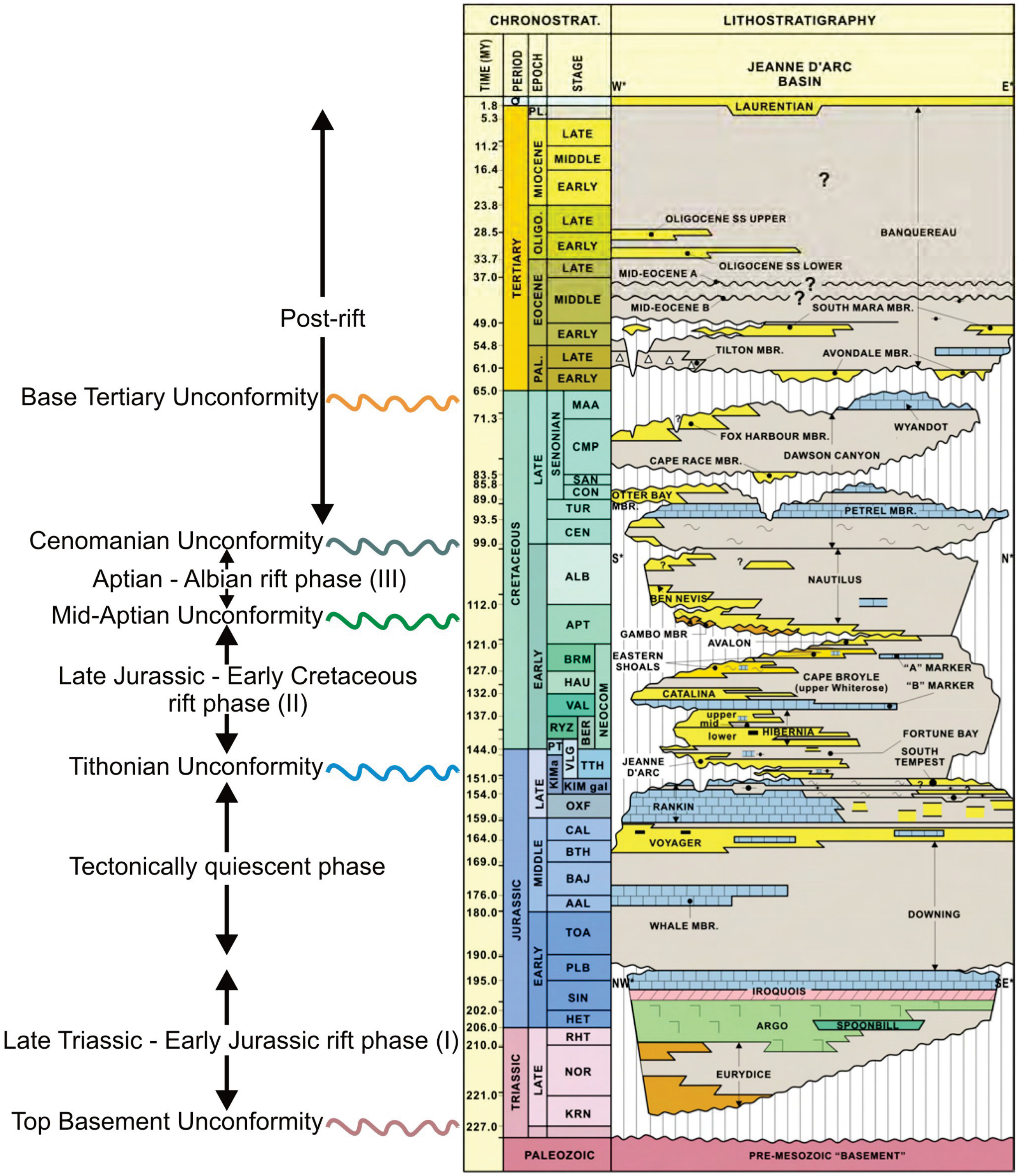

Figure 1.6: Stratigraphic column of the Jeanne d'Arc Basin, modified after Sinclair, 1993 [42] and incorporating McAlpine, 1990 [28] and Deptuck et al., 2003 [7].

the Rankin Formation deposited at the end of this period (McAlpine, 1990 [28]). The Aptian to Albian rift phase (III) was characterized by coarse-grained siliciclastic sediments of the Ben Nevis Formation which is the dominant hydrocarbon reservoir in the Hebron area. Regional subsidence in the Late Cretaceous and Cenozoic resulted in the deposition of fine-grained siliciclastic sediments and minor chalky limestones (McAlpine, 1990 [28]), which thicken dramatically northwards (Enachescu, 1987 [11]).

During rift phase I, extension was orientated northwest-southeast, resulting in northeast-southwest trending normal faults (Withjack and Schlische, 2005 [63]). Extension was accommodated along a system of listric faults synthetic to the Murre Fault, with rotation of the synrift succession into the fault plane and development of synthetic and antithetic planar faults (Tankard et al., 1989 [50]). The Murre fault formed as a series of en echelon faults separated by tilted relay ramps (Sinclair, 1995 [43]; Tankard et al., 1989 [50]). Relay ramps form between the tip lines of offset listric faults, which have the same sub-horizontal detachment at depth. The relay ramp deforms ductilely, keeping the hanging-wall block interconnected to the footwall block (Larsen, 1988 [22]). Tankard et al., 1989 [50] propose that increasing extensional strain led to the breakdown of the relay structures and the development of transfer faults offsetting the normal faults. The Early to Middle Jurassic was dominated by passive subsidence and halokinesis (Sinclair, 1995 [43]). The full range of salt structures have been imaged: steps, pillows, swells, ridges, walls and classic diapirs, which penetrate the Base Tertiary Unconformity and may even reach the seafloor as is the case with the Adolphus diapir in the north of the basin, indicating multistage salt growth (Enachescu, 1987 [11]).

Faults resulting from the Early Mesozoic extension were reactivated in an east-west direction during rift phase II associated with the North Atlantic rift and opening. There is a major basin-wide unconformity in the mid-Aptian (Sinclair and Withjack, 2008 [45]). This has been variously suggested as a “breakup” unconformity, marking the separation of the Grand Banks from Iberia (Tankard and Welsink, 1987 [49]; Tankard et al., 1989 [50]) and a rift onset unconformity, documenting the start of a late phase of extension (Driscoll et al., 1995 [9]). The Jeanne d’Arc Basin was affected by Aptian to Albian southwest-northeast extension in the Orphan Basin to the North, which preceded the opening of the Labrador Sea (Tankard et al., 1989 [50]). The extensional stress rotated to a northeast-southwest orientation during rift phase III. Aptian to Albian northwest-striking syn-depositional normal faults are common across the Jeanne d’Arc Basin, however there is debate as to the origin of these faults (Sinclair and Withjack, 2008 [45]). The geology of the basin at this time was strongly affected by northward downward tilting of the basin (Sinclair and Withjack, 2008 [45]). It has been suggested, based on seismic interpretation, that the Aptian to Albian faulting does not involve basement and can be accounted for by: 1) salt flow (McAlpine, 1990 [28]); or 2) gravity driven detachment within the Mesozoic succession initiated by the northward plunge of the basin coupled with southwest-northeast extension (Tankard and Welsink, 1987 [49]). However, although some of the northwest-southeast oriented faults detach in the Mid-Jurassic strata, a few continue into the basement (Sinclair, 1995 [43]). It has been proposed that deep seated northeast-southwest directed crustal extension during the Aptian to Albian produced widespread west- to northwest- striking basement involved and detached supra-salt normal faults (Sinclair and Withjack, 2008 [45]). The salt and mudstone units decouple the deep-seated faults from the coeval faults in the overlying Jurassic and Cretaceous strata (Sinclair and Withjack, 2008 [45]). The pattern of folding and faulting in the Jeanne d’Arc Basin resembles analog models of basement involved extension (Sinclair and Withjack, 2008 [45]; Withjack and Callaway, 2000 [61]). The 90° rotation of extensional stresses in rift phase III is inferred to have caused oblique-slip fault reactivation of basement blocks and local structural inversion (Sinclair, 1995 [43]). These structural responses include 'pop-up'-blocks, reverse faults and forced folds. Transpressional structures are recognized over a wide range of scales from relatively large scale reverse faults visible on seismic data to small-scale reverse faults seen in core (Sinclair, 1995 [43]).

1.2 Research Objectives

Although there is broad agreement about the rifting phases involved in the development of the Jeanne d'Arc Basin, there are no previously published attempts to measure the deformation through time in the basin and use it as a contribution to a regional deformable plate reconstruction. This thesis attempts to provide these new insights.

Research objectives were to:

- Compare the total amount of extension measured using fault heaves in this study with the total amount of extension measured using change in crustal thickness in the regional Noth Atlantic deformable plate model to establish whether stetching is uniform with depth in this area.
- Establish the timing and direction for the different rift phases within the Jeanne d'Arc Basin.
- Quantify the extension for each rift phase by measuring fault heaves.
- Analyse the complex interactions between the fault sets from the second and

third rift phases.

- Compare extension estimates using 2D seismic and 3D seismic.
- Produce time structure maps for the unconformities representing the start of each rift phase.
- Restore the time structure maps to their position before each rift phase using beta values derived from the fault heave extension estimates as input into GeoArctic's proprietary PlateDEF software and the deformable/plate kinematic model (GeoArctic Ltd. website, [13]).
- Compare the restored maps with GeoArctic's maps produced using crustal thinning to estimate extension.
- Produce time structure maps for the syn-rift and post-rift thickness across the Jeanne d'Arc Basin and into the southern Orphan Basin. Relate the northward thickening of the post-rift thickness to the syn-rift thickness.
- Establish a rifting history for the Jeanne d'Arc Basin and relate it to the evolution of the North Atlantic.

Chapter 2

Data and Methods

2.1 Data

2.1.1 Introduction

A combination of seismic and well data were used to create regional time structure maps and fault maps across the study area to analyze the rift phases within the Jeanne d'Arc Basin (Fig. 2.1). A larger area was used to explore the thickness variation and spatial distribution of the post-rift and syn-rift sequences across the Jeanne d'Arc Basin and into the southern Orphan Basin (Fig. 2.2). There is a huge quantity of publicly available seismic data, but few surveys with regional coverage and no publicly available recent regional surveys. Three regional 2D seismic surveys from the early 1980s were chosen to provide regional coverage. Scans of the seismic lines were converted to SEG-Y files using Tif2segy, a script that utilizes Seismic Unix and Netpbm image tools by Andrew MacRae (Tif2segy website [25]). The seismic lines were loaded into Landmark's Seisworks software using the navigation from the Natural

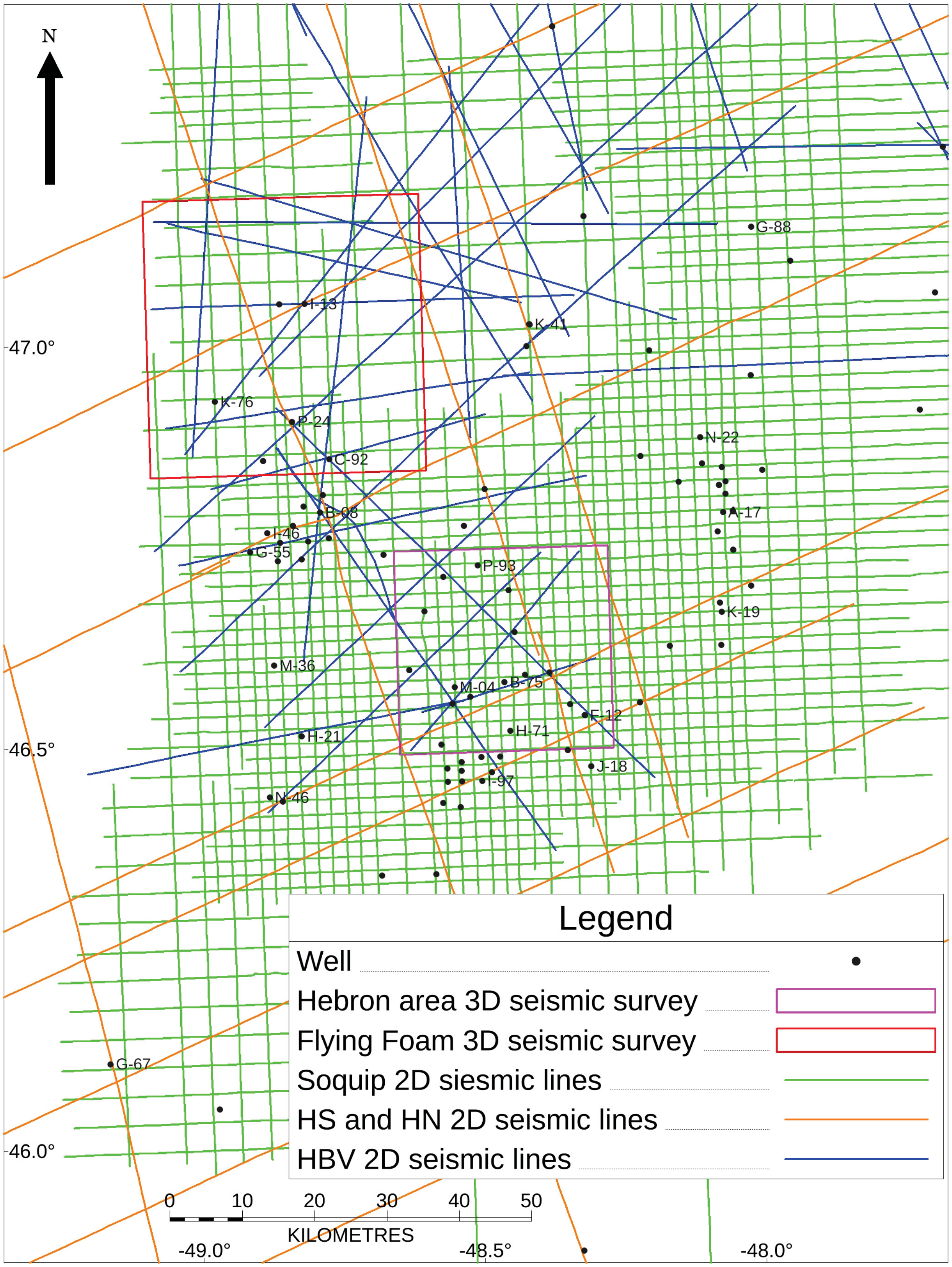

Figure 2.1: Map of the study area showing wells, 2D seismic and 3D seismic used.

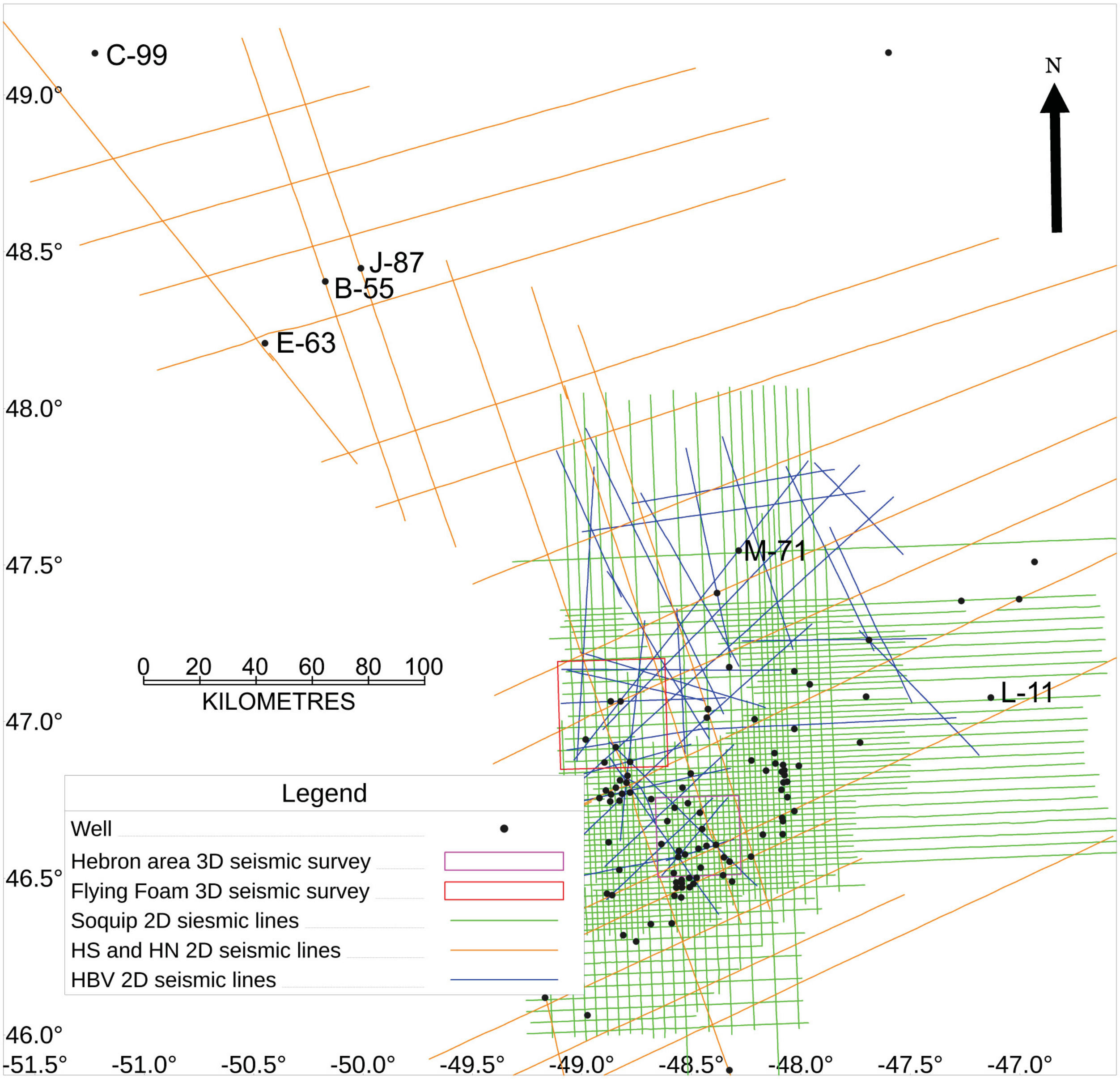

Figure 2.2: Map of the extended area used for studying syn-rift and post-rift thickness, showing wells, 2D seismic and 3D seismic.

Resources Canada (NRCAN) Basin website [2]. Two 3D seismic datasets were used to provide more local detail and to establish whether a wide-spaced grid of 2D seismic leads to an underestimation of extension. The quality (as well as the continuity) of the 3D data was superior to the 2D data (Figs. 2.3 - 2.7). Well data from 111 wells were used to tie in with the seismic.

2.1.2 SOQUIP 2D seismic data

Paper and microfiche copies of seismic lines from the 1983 SOQUIP survey, for example line 83-5084 (Fig. 2.3), were obtained from the Canada-Newfoundland and Labrador Offshore Petroleum Board (CNLOPB). The data were recorded on a 120-channel streamer with a shotpoint interval of 25 m and a group interval of 25 m, using a 3000 m cable. The source was a 66.777l / 13789.5 kPA airgun array offset 275 m from the nearest streamer group producing 60 fold multiplicity with a record length of 7 s or 8 s at a 2 ms sample rate. Data were processed using a velocity filter, designature, equalization, velocity analysis (every 3 km), normal moveout and stack, predictive shortgap deconvolution and Kirchhoff F-K domain wave equation migration.

2.1.3 HBV 2D seismic data

Paper copies of seismic lines from the 1983 HBV survey, for example line HBV83-225A (Fig. 2.4), were obtained from the CNLOPB. The data were recorded on a 120-channel streamer with a shotpoint interval of 26.667 m and a group interval of 26.667 m, using a 3173.33 m cable. The source was a 4500 P.S.I airgun array offset 221 m from the nearest streamer group producing 60 fold multiplicity with a record length of 7 s at a 2 ms sample rate. Data were processed using a velocity filter, designature, equalization, velocity analysis (3 km), normal moveout and stack, predictive shortgap deconvolution and Kichoff F-K domain wave equation migration.

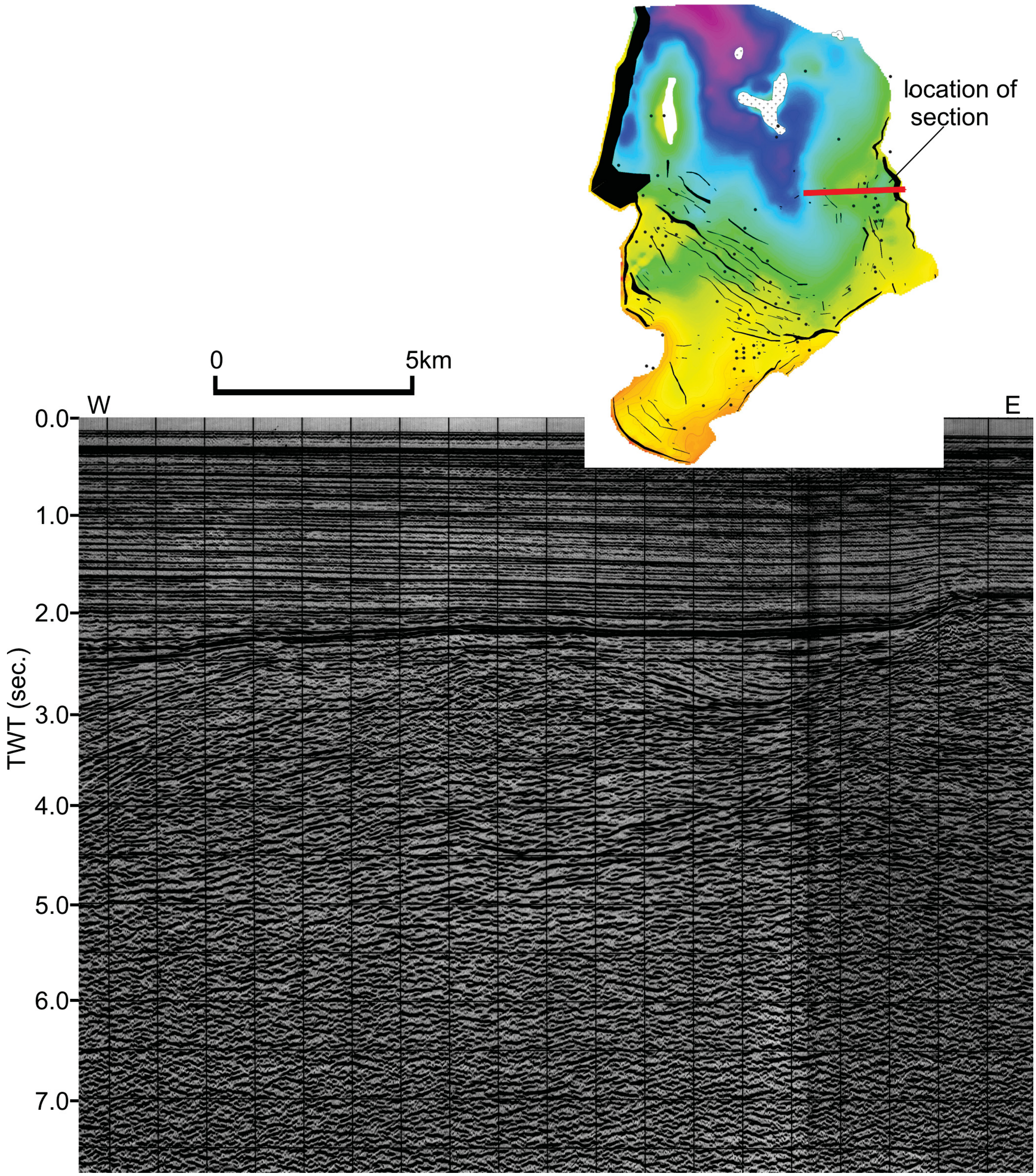

Figure 2.3: Seismic line 83-5084 across the Voyager fault zone and the White Rose area, from the 1983 SOQUIP 2D survey. Data courtesy of CNLOPB. The location of the section is illustrated on the time structure map at the Mid-Aptian Unconformity (Section 3.2.3).

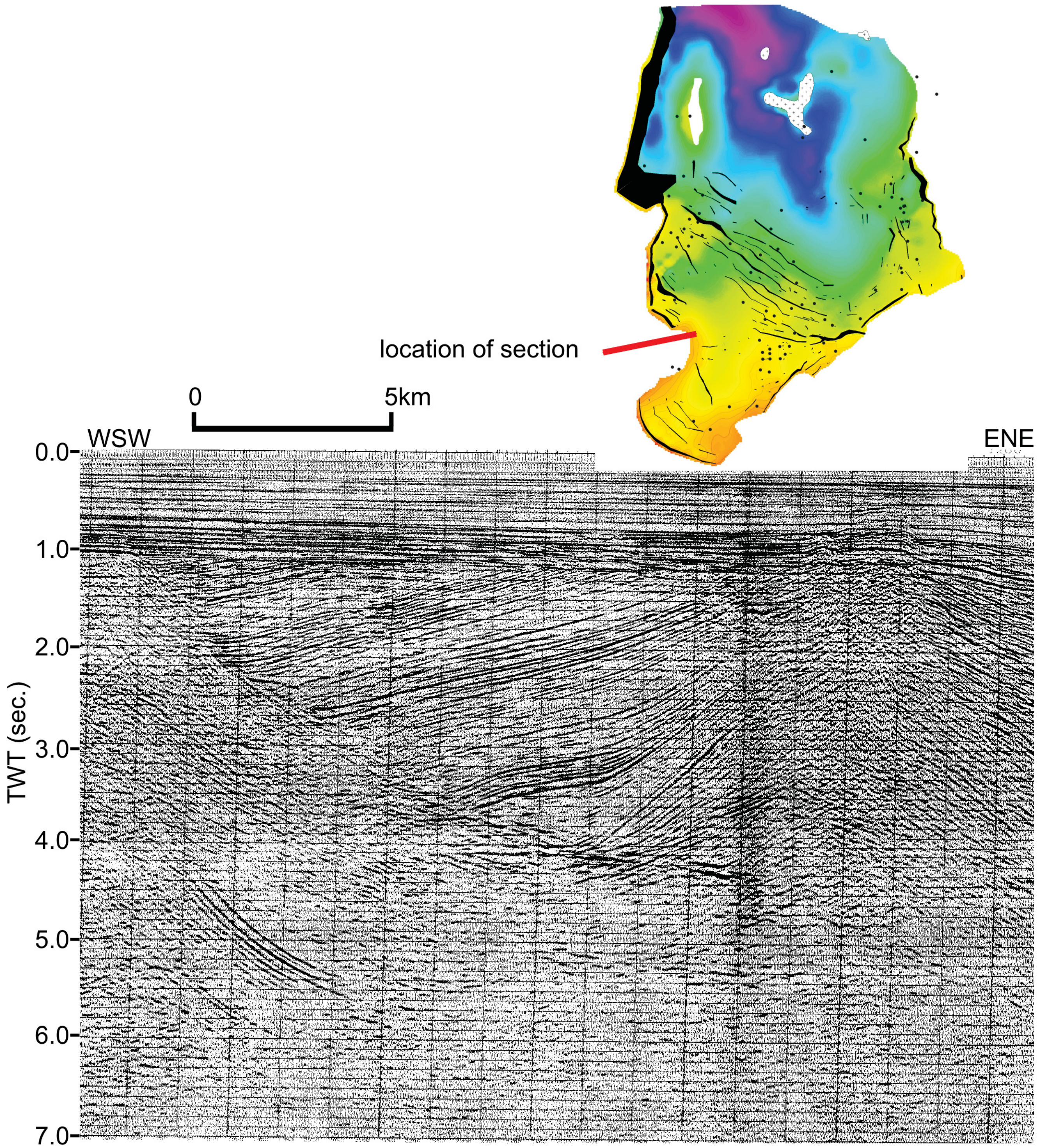

Figure 2.4: Seismic line HBV83-225A from the 1983 HBV 2D survey across the Murre fault and a salt ridge. Data courtesy of CNLOPB. The location of the section is illustrated on the time structure map at the Mid-Aptian Unconformity (Section 3.2.3).

2.1.4 SEFEL Geophysical Ltd. HS and HN 2D seismic data

Microfiche copies of seismic lines from the 1982 SEFEL Geophysical Ltd. HS and HN 2D surveys, for example line HS-12A (Fig. 2.5), were obtained from the CNLOPB.

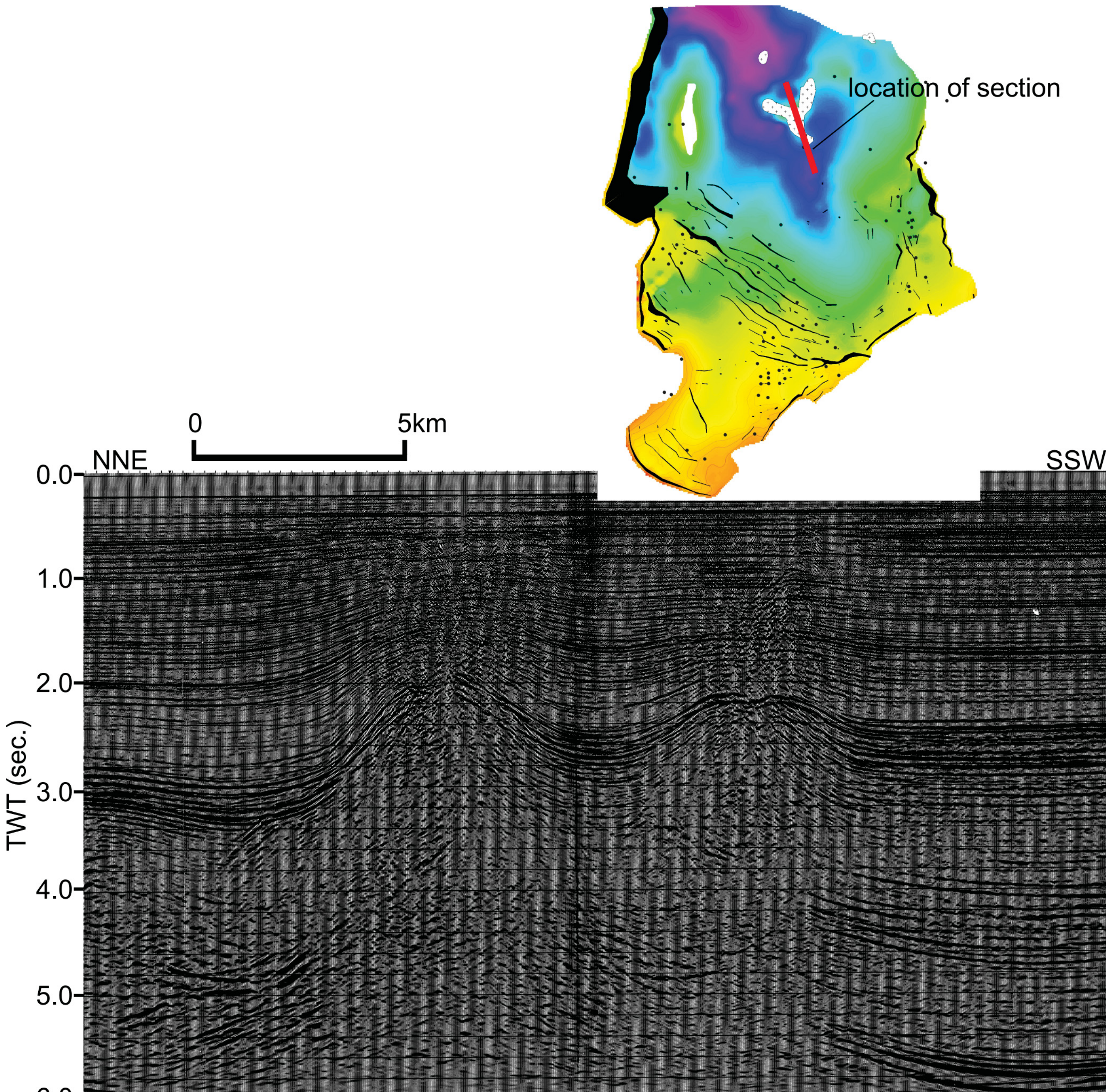

Figure 2.5: Seismic line HS-12A from the 1983 HS 2D survey showing the Adolphus salt diapir. Data courtesy of CNLOPB. The location of the section is illustrated on the time structure map at the Mid-Aptian Unconformity (Section 3.2.3).

The data were recorded on a 60-trace streamer with a shotpoint interval of 25 m and a group interval of 50 m, using a 3000 m cable. The source was a 2000 P.S.I airgun array offset 300 m from the nearest streamer group producing 60 fold multiplicity with a record length of 6 s and 7 s at a 2 ms sample rate. Data were processed using velocity analysis, normal moveout and stack, predictive shortgap deconvolution and wave equation migration.

2.1.5 Flying Foam 3D seismic data

The 1995 Flying Foam 3D seismic survey, courtesy of Western Geco, was incorporated into the Seisworks project. Figure 2.6 shows a northwest-southeast arbitrary line from the Flying Foam dataset. The data were recorded using 4 streamers, 192 channels per streamer and a nominal fold of 32. The source was a 2000 PSI triple airgun array with a shot point interval of 25 m, 40 hydrophones/group, 25 m group interval and 4800 m streamer length. The record length was 9.5 s at a 2 ms sample rate. The data were processed using SEG-D conversion, spherical divergence correction, exponential gain, inverse filter, deconvolution, 3D binning, normal moveout and stack and one pass phase shift migration.

2.1.6 Hebron area 3D seismic data

3D seismic data and well data from the Hebron area were available in the office at Husky Energy during the summer of 2012. Figure 2.7 shows a north-northeast-south-southwest arbitrary line from the Hebron dataset. These data were able to better inform the 2D mapping in the Hebron area, better constrain the extension directions across the basin, provide a view of fault interactions and allow a comparison between

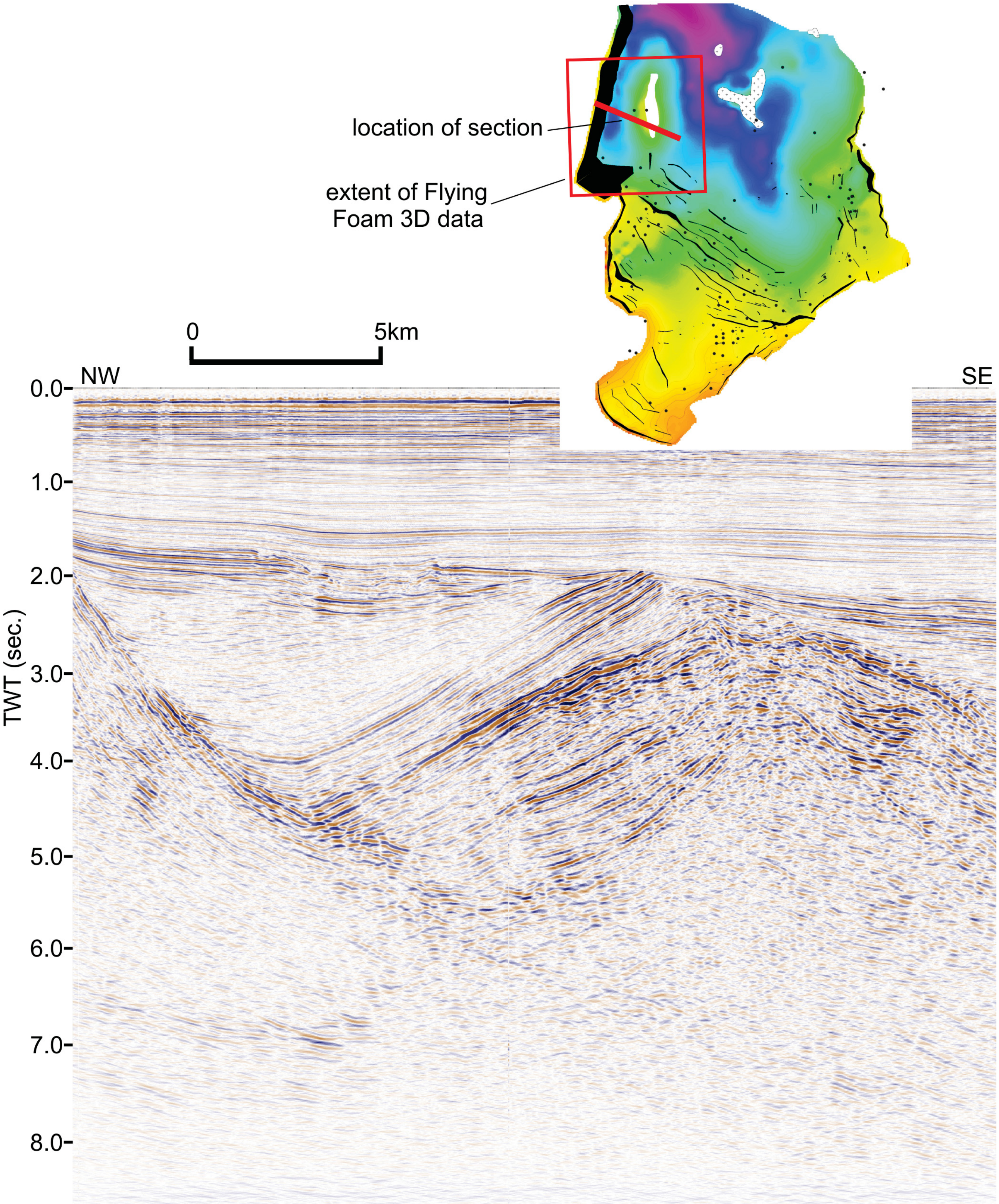

Figure 2.6: Seismic section from the Flying Foam 3D survey across the Mercury fault and the Flying Foam fold. Data courtesy of WesternGeco. The location of the section is illustrated on the time structure map at the Mid-Aptian Unconformity (Section 3.2.3).

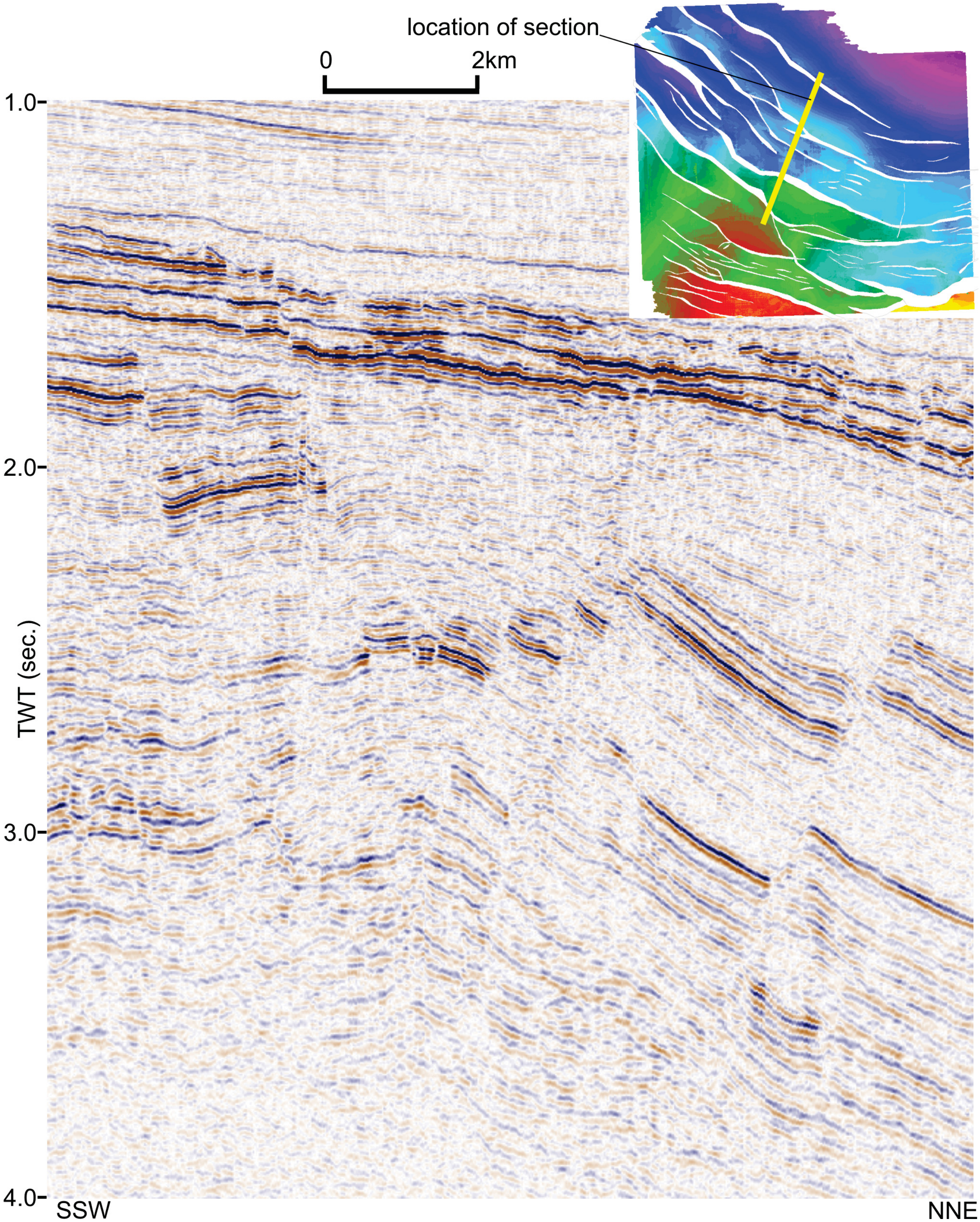

Figure 2.7: Seismic section from the Hebron area 3D survey across predominantly northwest-southeast striking faults. Data courtesy of Husky Energy. The location of the section is shown on a time structure map at the Mid-Aptian Unconformity from the Hebron area (Section 3.2.3).

the 2D and the 3D mapping. The data extends to 7 s two way time, however the resolution becomes poor below 4 - 4.5 s two way time.

2.1.7 Well data

Well data from 111 wells were taken from the Natural Resources Canada (NRCAN) Basin website [2], for example for the Archer K-19 well (Table 2.1). Time depth tables created by the CNLOPB, for example for the Archer K-19 well (Table 2.2), were used to convert the data to the time domain for correlation with the seismic data.

Year	Author	Depth	Top	Bottom	Formation
2007	CNLOPB	MD		1929	BANQUEREAU FM
2007	CNLOPB	MD	1908 m	1929 m	SOUTH MARA MB
2007	CNLOPB	MD	1929 m	1929 m	(BASE TERTIARY UNCONFORMITY)
2007	CNLOPB	MD	1929 m	2016 m	DAWSON CANYON FM
2007	CNLOPB	MD	1929 m	1960 m	PETREL MB
2007	CNLOPB	MD	2016 m	2016 m	(CENOMANIAN UNCONFORMITY)
2007	CNLOPB	MD	2016 m	2091 m	NAUTILUS FM
2007	CNLOPB	MD	2091 m	2218 m	BEN NEVIS FM
2007	CNLOPB	MD	2218 m	2218 m	(APTIAN UNCONFORMITY)
2007	CNLOPB	MD	2218 m	2609 m	HIBERNIA FM
2007	CNLOPB	MD	2218 m	2403 m	HIBERNIA UPPER ZONE
2007	CNLOPB	MD	2403 m	2609 m	HIBERNIA LOWER ZONE
2007	CNLOPB	MD	2609 m	2892 m	FORTUNE BAY FM
2007	CNLOPB	MD	2892 m	2892 m	(TITHONIAN UNCONFORMITY)
2007	CNLOPB	MD	2892 m	4299.3 m	RANKIN FM
2007	CNLOPB	MD	3278 m	3602 m	(UPPER KIMMERIDGIAN SOURCE ROCK)
2007	CNLOPB	MD	3640 m	3825 m	("LOWER TEMPEST" SANDSTONES)
2007	CNLOPB	MD	3942 m	4287 m	(LOWER KIMMERIDGIAN SOURCE ROCK)
2007	CNLOPB	MD	4287 m	4299.3 m	PORT AU PORT MB

Table 2.1: Natural Resources Canada, Geological Survey of Canada, Geoscience Data Repository, BASIN website [2]: lithostratigraphic picks for the Archer K-19 well.

time	depth mss	depth MD	2 way time
490.00	897.95	919.65	980
500.00	916.53	938.23	1000
510.00	937.92	959.62	1020
:	:	:	:
:	:	:	:
:	:	:	:
:	:	:	:
1540.00	4202.83	4224.53	3080
1550.00	4243.57	4265.27	3100

Table 2.2: An extract from the CNLOPB time depth data for the Archer K-19 well. Logging company: Schlumberger, 7th November 1984.

2.2 Methods

2.2.1 Approach to interpretation

Thermal thinning of the mantle lithosphere by a mantle plume or upwelling of the asthenosphere caused by stress induced extension produces upward displacement of the asthenosphere-lithosphere boundary at the onset of rifting (Ziegler and Cloetingh, 2004 [66]). This produces doming of the rift zone and an unconformity forms. The unconformity at the start of each rift phase was mapped, along with the faults at the level of each unconformity. The Top Basement Unconformity (Fig. 1.6) was chosen to represent the base of the syn-rift for rift phase I, which preceded the separation of Nova Scotia and Africa (Fig. 1.1; Tankard et al., 1989 [50]). Uplift at the start of rift phase II caused erosion and incision into the underlying strata, especially in the south of the basin, producing the Tithonian Unconformity (Fig. 1.6; Sinclair et al., 1999 [44]). Rift phase II preceded seafloor spreading between Iberia and Newfoundland (Fig. 1.1). The Mid-Aptian Unconformity (Fig. 1.6) was chosen to represent the base of the syn-rift for rift phase III (Driscoll et al., 1995 [9]). The Cenomanian Unconformity and the Base Tertiary Unconformity (Fig. 1.6) were mapped to analyze whether there was significant extension during the Late Cretaceous and Cenozoic.

Seismic and well data were used to identify and interpret the unconformities, which were loop correlated across the study area (Fig. 2.8). The Top Basement Unconformity was only present in the Hibernia I-46 and Murre G-67 wells from the extension study area (Fig. 2.1) and in the Bonanza M-71, Bonavista C-99, Sheridan J-87, Cumberland B-55, Linnet E-63 and Kyle L-11 from the larger study area (Fig. 2.2). Top Basement is hard to interpret on the seismic data and becomes deeper than the depth extent of the seismic data in the northeast of the basin. It was interpreted subjectively as the base of reflective layering (avoiding multiples) and tied to wells where possible. The interpreted unconformities were gridded and mapped using Petrosys software to produce time structure maps. Faults were interpreted on each seismic line, loop correlated and mapped across the basin at the level of each unconformity. The faults were colour coded according to strike and dip, such that the predominantly north-south striking faults were purple for east dipping and blue for west dipping, and the predominantly northwest-southeast striking faults were red for northeast dipping and green for southwest dipping (see 2.2.2 for further explanation of fault groups). The faults became hard to interpret at depth in the seismic sections. A comparison between the 2D data (Fig. 2.8) and the Hebron 3D data (Fig. 2.9) illustrates the superior quality of the more recent 3D data.

The Base Tertiary Unconformity, the Mid-Aptian Unconformity and the Tithonian Unconformity were interpreted across the Hebron area using 3D seismic and well data in the office of Husky Energy (Fig. 2.9). In addition, the Early Cretaceous "B" Marker Limestone and the Late Cretaceous Petrel Limestone were mapped. The Hebron 3D seismic data did not extend deep enough to image the Top Basement Unconformity. Faults were interpreted and mapped across the Hebron area at the

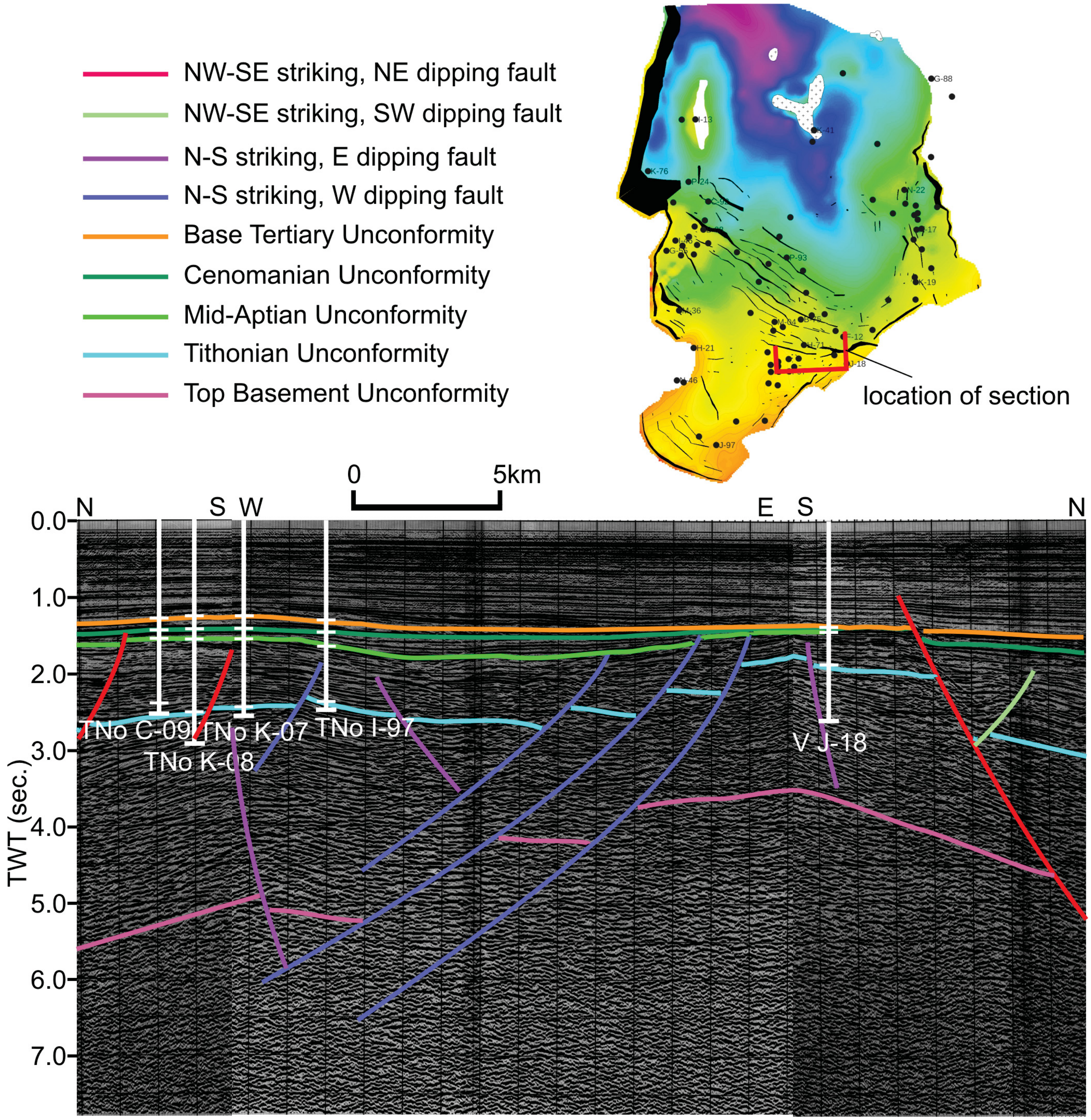

Figure 2.8: Seismic section from the SOQUIP 2D survey, illustrating well ties. Data courtesy of CNLOPB. The location of the section is illustrated on the time structure map at the Mid-Aptian Unconformity (Section 3.2.3).

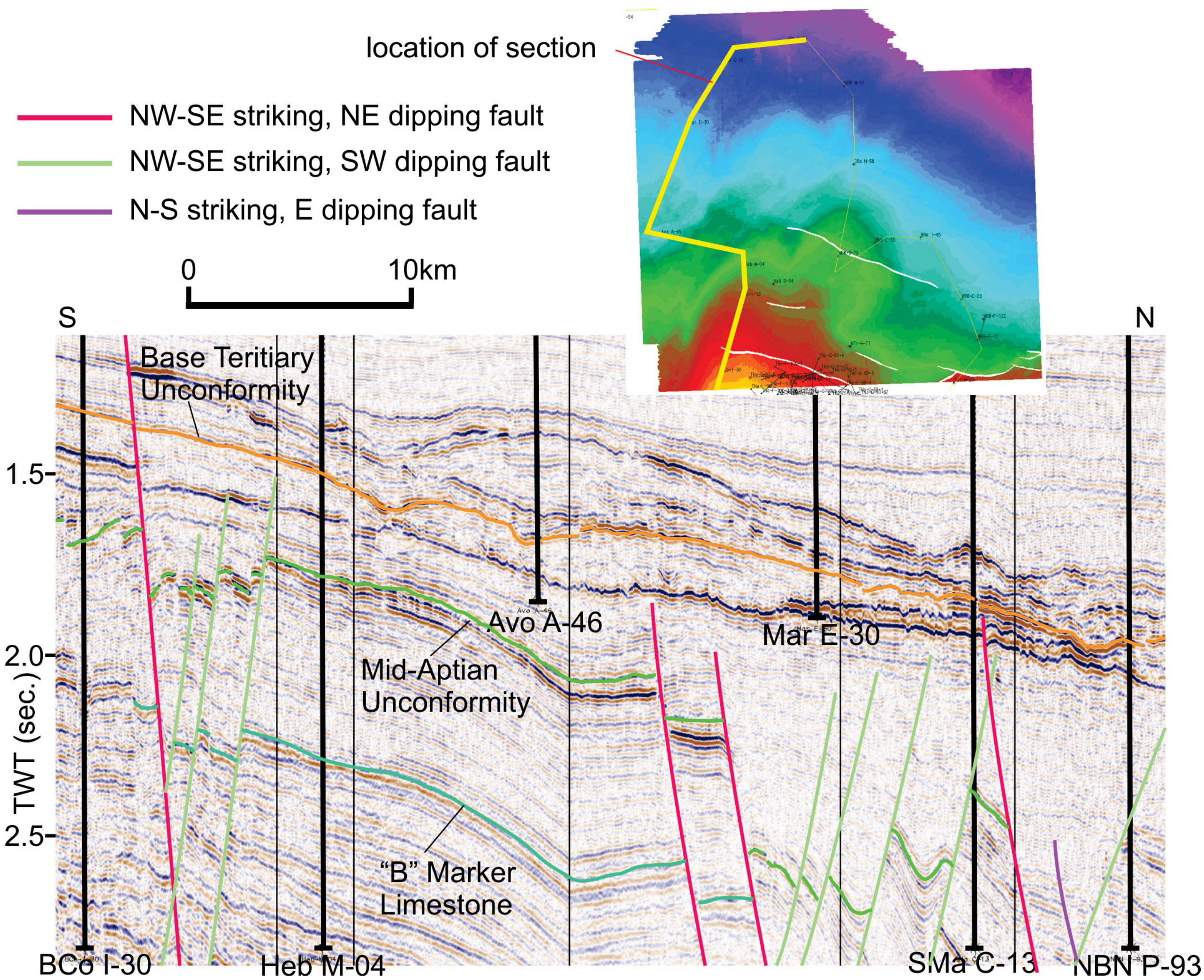

Figure 2.9: Seismic line from the Hebron 3D area showing well ties. Data courtesy of Husky Energy. The location of the section is shown on a time structure map at the Base Tertiary Unconformity from the Hebron area (Section 3.2.5).

level of each unconformity and horizon, with emphasis on the earlier faults and on the interaction between faults.

2.2.2 Extension directions

Extension was measured in three directions corresponding to the interpreted directions for each of the three proposed rift phases. The basins on the Grand Banks initially formed during rift phase I (Withjack and Schlische, 2005 [63]). The border fault zones in these basins, including the Murre, Mercury and Voyager faults in the Jeanne d'Arc Basin, strike predominantly northeast-southwest (Fig. 2.10). The extension direction is assumed to be northwest-southeast, perpendicular to this regional strike direction. The early extension phase was active during the Late Triassic to Early Jurassic (228 Ma - 186 Ma), followed by a period of thermal subsidence in the Early to Late Jurassic (186 Ma - 150 Ma) (Sinclair, 1995 [43]; McAlpine, 1990 [28]).

Subsequent faulting along and close to the border faults is strongly influenced by the orientation of the border faults. The extension direction for the later two rift phases was estimated by looking at the new faults formed towards the centre of the basin, using the Hebron area 3D seismic data. Fault mapping at the Tithonian Unconformity level shows that faults most active during rift phase II are predominantly north-south striking (Section 3.2.2), suggesting that the extension direction is east-west, perpendicular to this fault trend. This north-south striking fault trend continues to the south across the Terra Nova area (Lethbridge, 2012 [24]; Fig. 1.5). Fault mapping at the Mid-Aptian Unconformity using the 3D Hebron area data shows that faults active during rift phase III are predominantly northwest-southeast striking (Section 3.2.3). The extension direction during rift phase III is assumed to be northeast-southwest, perpendicular to the fault trend. A series of lines was chosen across the basin in the three assumed extension directions (Fig. 2.11). The exact location of the lines was carefully chosen to allow analysis of major changes in faulting, and to cross the basin in areas where the faulting is better imaged.

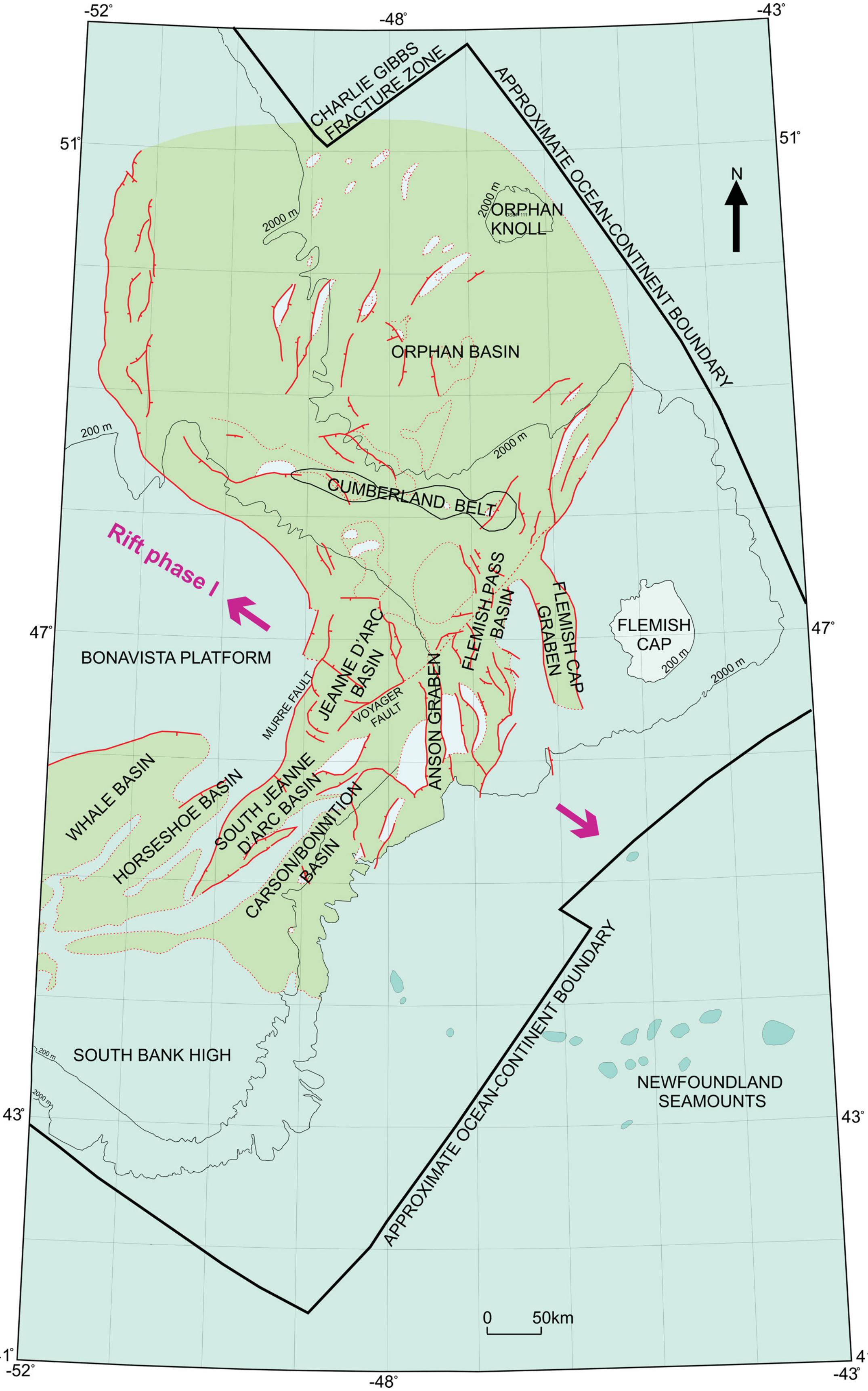

Figure 2.10: Basins on the Grand Banks of Newfoundland, illustrating the predominant northeast-southwest strike of the border faults (after CNLOPB, 2003 [4]).

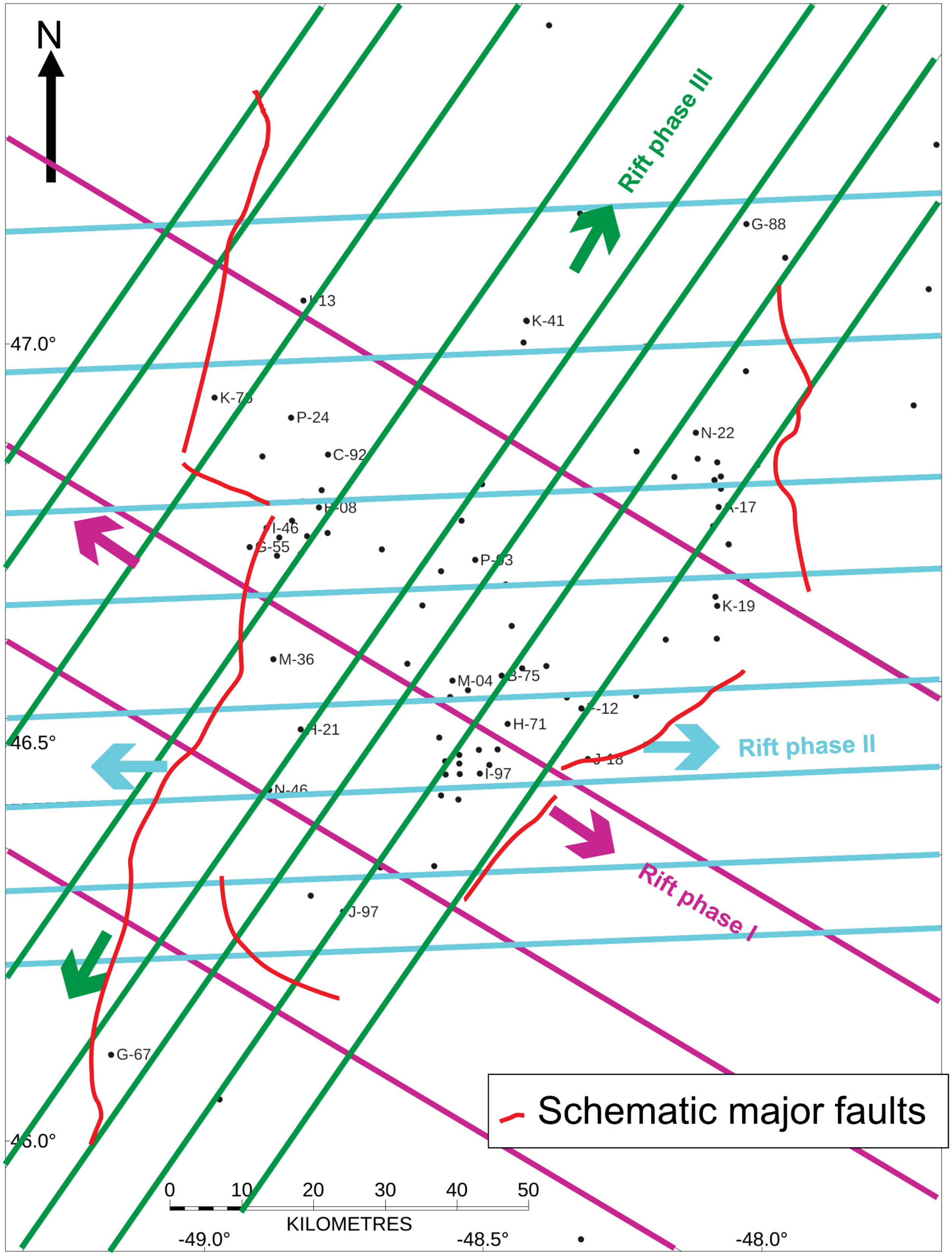

Figure 2.11: Analysis lines across the study area parallel to the extension directions. Fault heaves were summed along each of these lines.

2.2.3 Measuring extension

Extensional movement on a listric fault produces a rollover anticline. If simple shear in a vertical plane is assumed (Fig. 2.12), thinning and stretching of the beds is necessary to conserve area (Gibbs, 1983 [14]). Bed thinning can be achieved by numerous antithetic and synthetic faults in the roll-over.

Vertical simple shear may be mechanically unrealistic and antithetic and synthetic faults in the hanging wall are commonly not vertical (White et al., 1986 [60]). Inclined simple shear is potentially a better approximation with angular shear accommodated along slip planes at an angle to the vertical (Fig. 2.13). Deformation of the hanging wall by homogeneous inclined simple shear may be a simplification of a complex deformation in the hanging wall with the angle of shear varying with depth (Withjack et al., 1995 [62]) and possibly temporally and spatially (Dula, 1991 [10]).

It has been suggested that antithetic faults accommodate shear above a concave fault bend and synthetic faults above a convex fault bend. The heave is equal to the hori-

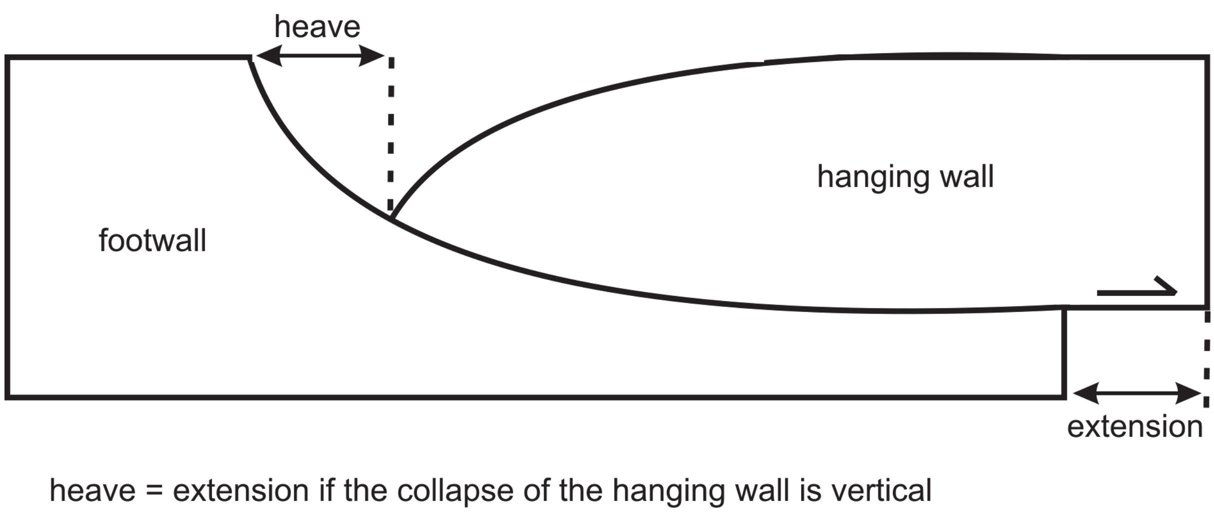

Figure 2.12: Measuring extension assuming vertical simple shear (after Gibbs, 1983 [14]).

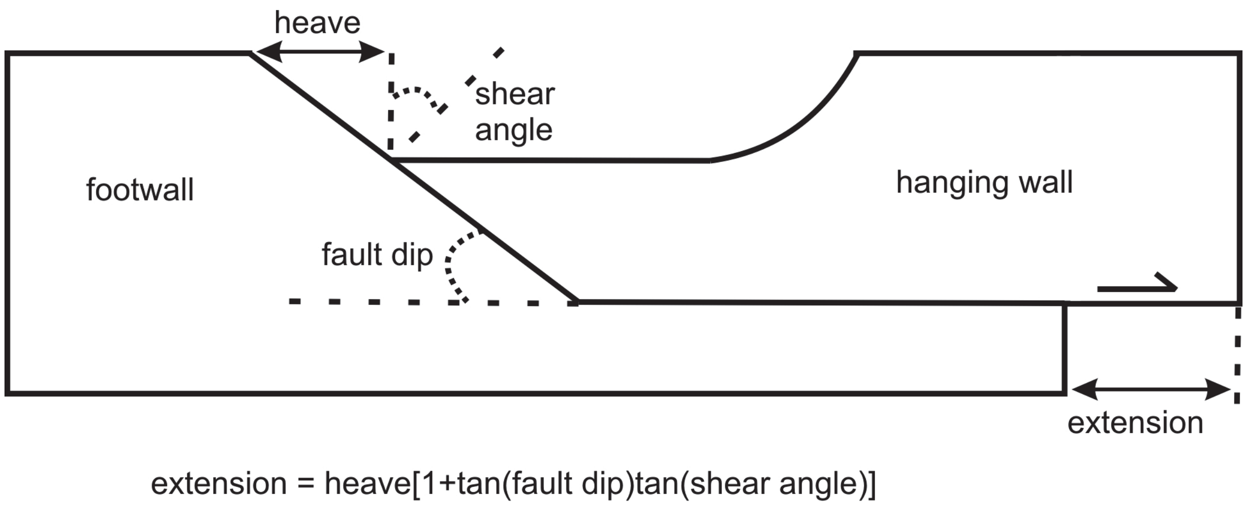

Figure 2.13: Measuring extension assuming inclined simple shear (after White et al., 1986 [60]).

zontal extension assuming vertical shear, less than the horizontal extension assuming antithetic shear and more than the extension assuming synthetic shear (Xiao and Suppe, 1992 [64]). An obvious drawback to measuring extension as inclined simple shear is that it is necessary to know the angle of shear. On a migrated time section horizontal distance is conserved making heave easy to measure, whereas to measure angles it is necessary to depth convert, leading to inaccuracies if the velocities are not well constrained (Sclater and Celerier, 1989 [38]). Marrett and Allmendinger, 1992 [27] and Walsh et al., 1991 [57]) suggest that heave provides a reasonable approximation of extension where the dip of the strata is low (<10°).

The quality of the available seismic and velocity data for this study does not allow an accurate measure of the angle of shear to be made. Hence vertical simple shear was assumed and heave was measured to give an approximation of the extension. For faults of limited strike length motion must be predominantly dip slip. Assuming dip slip motion on most of the faults, the heave was measured perpendicular to the strike of the fault (Fig. 2.14). To obtain the component of heave in the analysis direction a

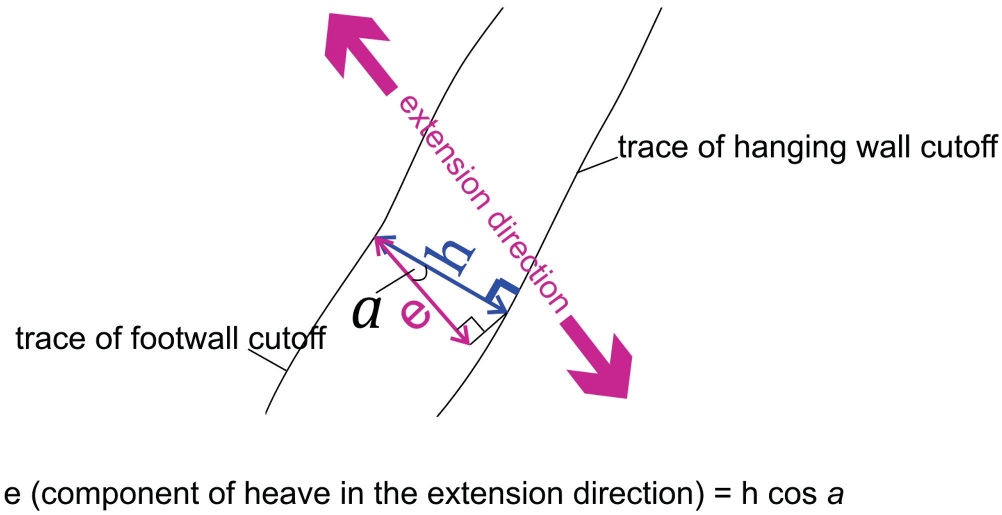

Figure 2.14: Calculating the component of heave in the extension direction.

correction was applied to faults that are not perpendicular to the extension direction (Fig. 2.14). The extension across each fault for a given rift phase was calculated by subtracting the heave associated with the subsequent rift phase from the heave associated with that rift phase (Fig. 2.15). An estimation of the extension along each line was made for each time interval by summing the extension across each fault for that rift phase.

There are obvious limitations with assuming dip slip motion, particularly concerning fault motion associated with rift phase III. The 90° rotation of extensional stresses in the Aptian to Albian is inferred to have caused oblique-slip fault reactivation of earlier northeast-southwest and north-south striking faults (Sinclair, 1995 [43]). Without being able to identify piercing points it is impossible to establish the true motion on the faults, however there is compelling evidence for oblique slip. There is in excess of 7.75 km of heave across the east-west striking Murre-Mercury connector (Fig. 2.16). To avoid a space issue at the intersection between the Murre-Mercury connector and the Mercury fault it is necessary for there to be left-lateral oblique slip along the Mercury fault. If motion is assumed to be in a northeast-southwest

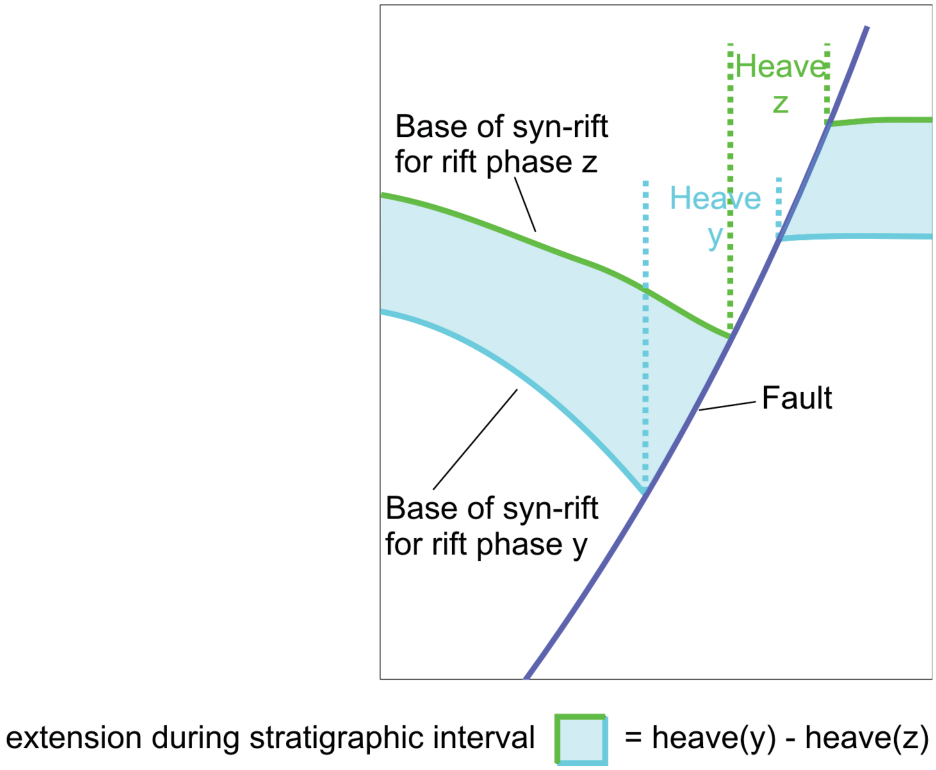

Figure 2.15: Schematic cross-section perpendicular to the strike of a pure dip slip normal fault, assuming vertical simple shear, illustrating the extension during a specific stratigraphic interval.

direction, a comparison of the heave across the Murre-Mercury connector with the extension measured in an oblique direction across the Mercury fault gives a similar extension value (Fig. 2.17). Oblique slip is discussed further in Section 3.4. Along the border faults at the Mid-Aptian level, extension was measured as oblique slip in a northeast-southwest direction.

An estimation of extension was made by summing fault heaves along the measurement lines at the Tithonian Unconformity level and the Mid-Aptian Unconformity level using the Hebron 3D seismic data. This provided a comparison between the measurements made using the 2D data and the 3D data.

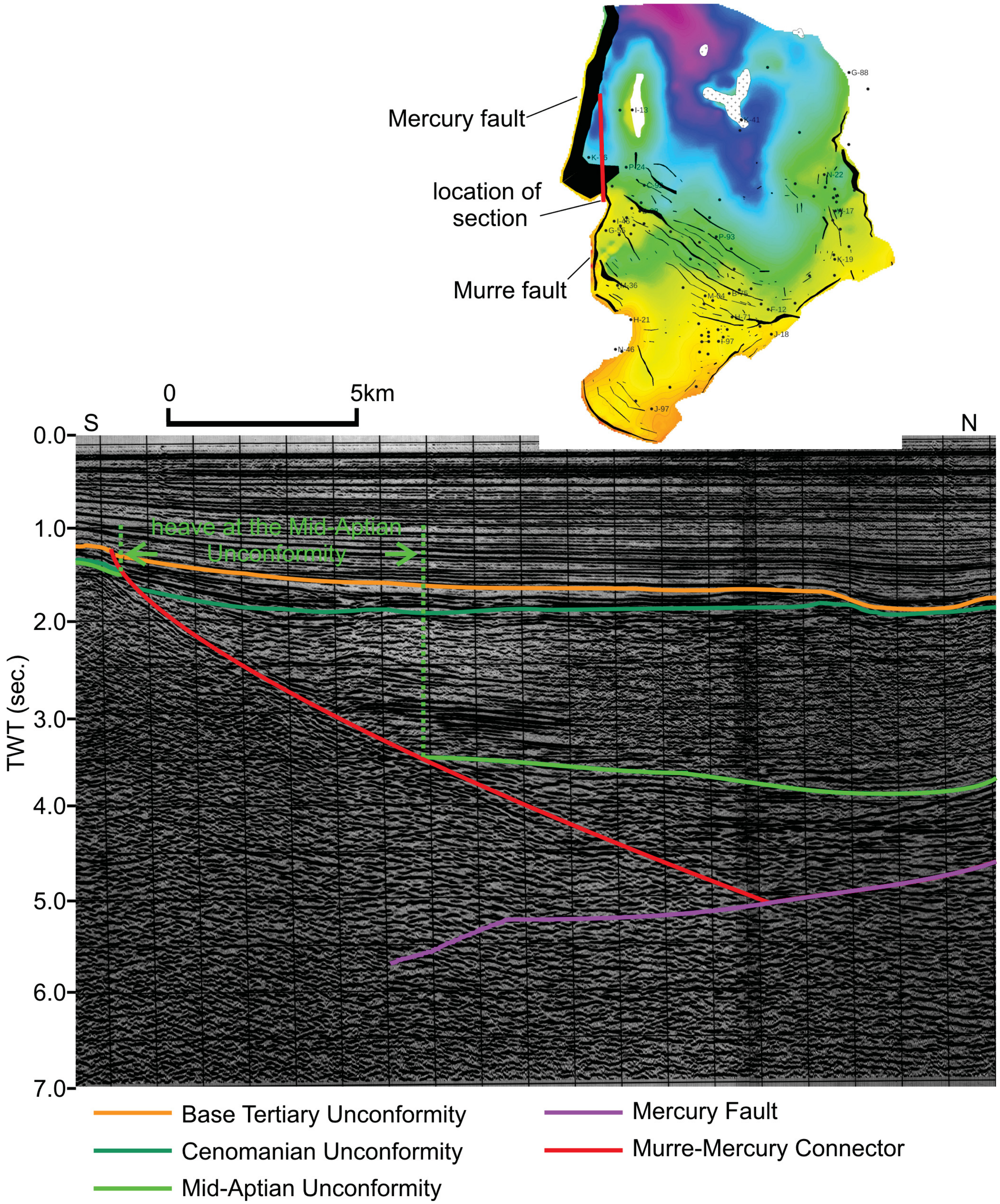

Figure 2.16: Interpreted north-south seismic profile from the SOQUIP survey across the Murre-Mercury connection, illustrating the substantial heave at the Mid-Aptian Unconformity level. Data courtesy of CNLOPB. The location of the section is illustrated on the time structure map at the Mid-Aptian Unconformity (Section 3.2.3).

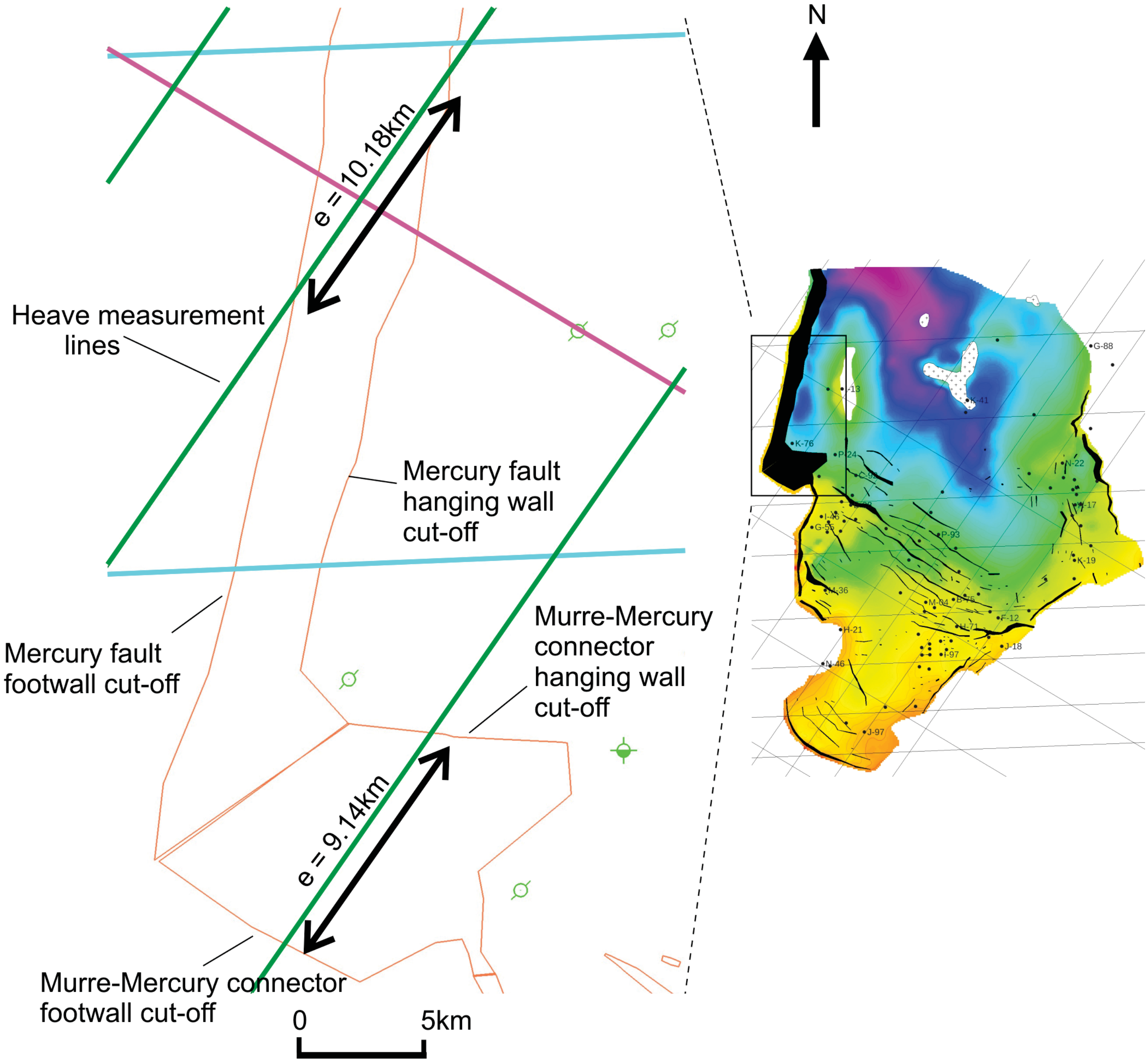

Figure 2.17: Measuring extension during rift phase III assuming slip is in the northeast-southwest direction. The location of the faults is illustrated on the time structure map at the Mid-Aptian Unconformity (Section 3.2.3).

2.2.4 Restoring the time structure maps to before each rift phase

The extension estimates were used to restore the time structure maps of the unconformities to their position before each rift phase using GeoArctic's proprietary

PlateDEF software, which models deformable plate margins (GeoArctic Ltd. website [13]). The GeoArctic plate model is derived from work funded jointly by the Irish Shelf Petroleum Studies Group (ISPSG) of the Petroleum Infrastructure Programme (PIP) and Nalcor Energy. A grid of stretching factors, beta, is required as input into the PlateDEF software. Equation 2.1 illustrates that beta(β) is a measure of the ratio of extended length(l) to unextended length(l-e).

$$\beta = \frac{l}{l - e} \tag{2.1}$$

Beta was calculated along the northeast-southwest analysis lines at the Aptian Unconformity level, along the east-west analysis lines at the Tithonian Unconformity level and along the northwest-southeast analysis lines at the Top Basement Unconformity level. Beta was not calculated at the Cenomanian Unconformity nor the Base Tertiary Unconformity because the amount of extension measured produces beta factors not significantly different from 1.0.

Beta values have local meaning when the extension, or complementary thinning, is continuously variable, which is valid for crustal thinning estimates used by GeoArctic. When extension occurs across discrete faults as in the basin fill studies here, beta values are best estimated across windows including several faults, to produce values that can be used in the GeoArctic software. Beta factors along each line were calculated every 5 km using a 20 km window (Fig. 2.18; eqn. 2.2), and a moving average was calculated in order to create a smoother beta. A 20 km window was chosen because the distance across the faulted centre of the basin is approximately 20 km. The calculated beta factors were gridded for each unconformity using a 5 k grid.

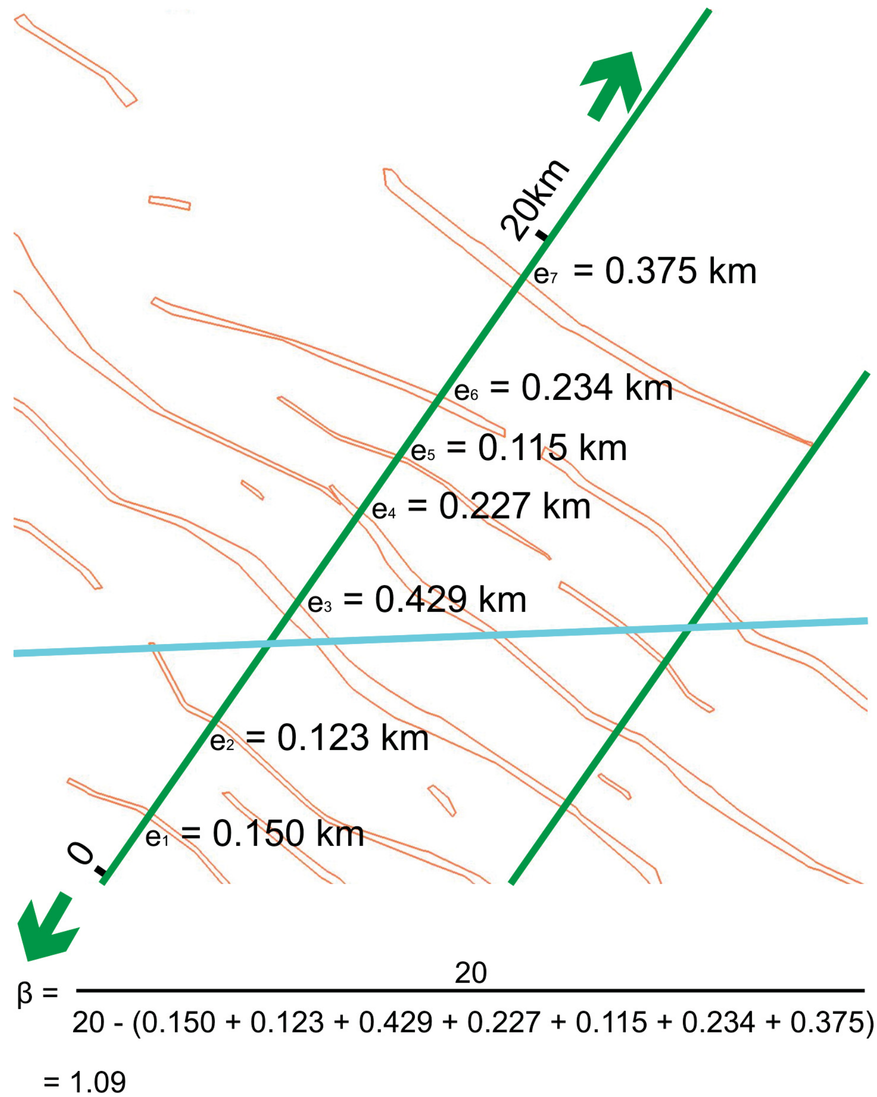

Figure 2.18: Measuring the stretching factor, beta using a 20 km window. Illustrated using faults at the Mid-Aptian Unconformity across the centre of the basin.

$$\beta = \frac{20}{20 - (\sum_{i=1}^{n} e_i)} \tag{2.2}$$

2.2.5 Underestimation of extension

It is often reported that crustal thinning is greater than extension due to faulting (Deemer et al., 2009 [5]; Reston, 2009 [36]). Possible reasons include differential stretching of brittle and ductile layers (Kusznir and Karner, 2007 [21]), sub-seismic faulting (Walsh, 1991 [57]), imaging and interpretation of cross cutting polyphase faults (Reston, 2009 [36]), plastic deformation in the rock body, underestimation of small faults (Marrett and Allmendinger, 1991 [26]) and sequential faulting (Ranero and Gussinyé, 2010 [34]).

There may be minor underestimation of extension due to plastic deformation in the rock body, for example some northwest-southeast faults, imaged in the Hebron 3D area do not penetrate the Mid-Aptian Unconformity, although the growth associated with the fault is above this level (Fig. 2.19). The fault must have nucleated below

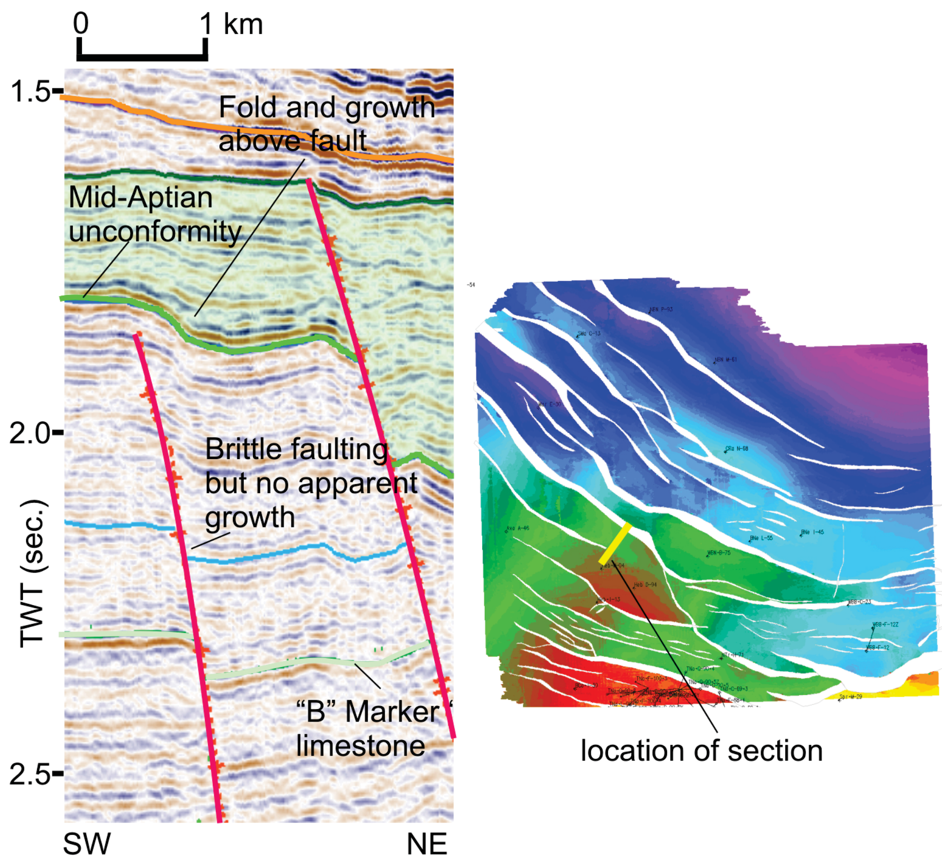

Figure 2.19: Short interpreted seismic profile from the Hebron area 3D data showing forced folding above a northwest-southeast trending fault. Data courtesy of Husky Energy. The location of the section is shown on a time structure map at the Mid-Aptian Unconformity from the Hebron area (Section 3.2.3).

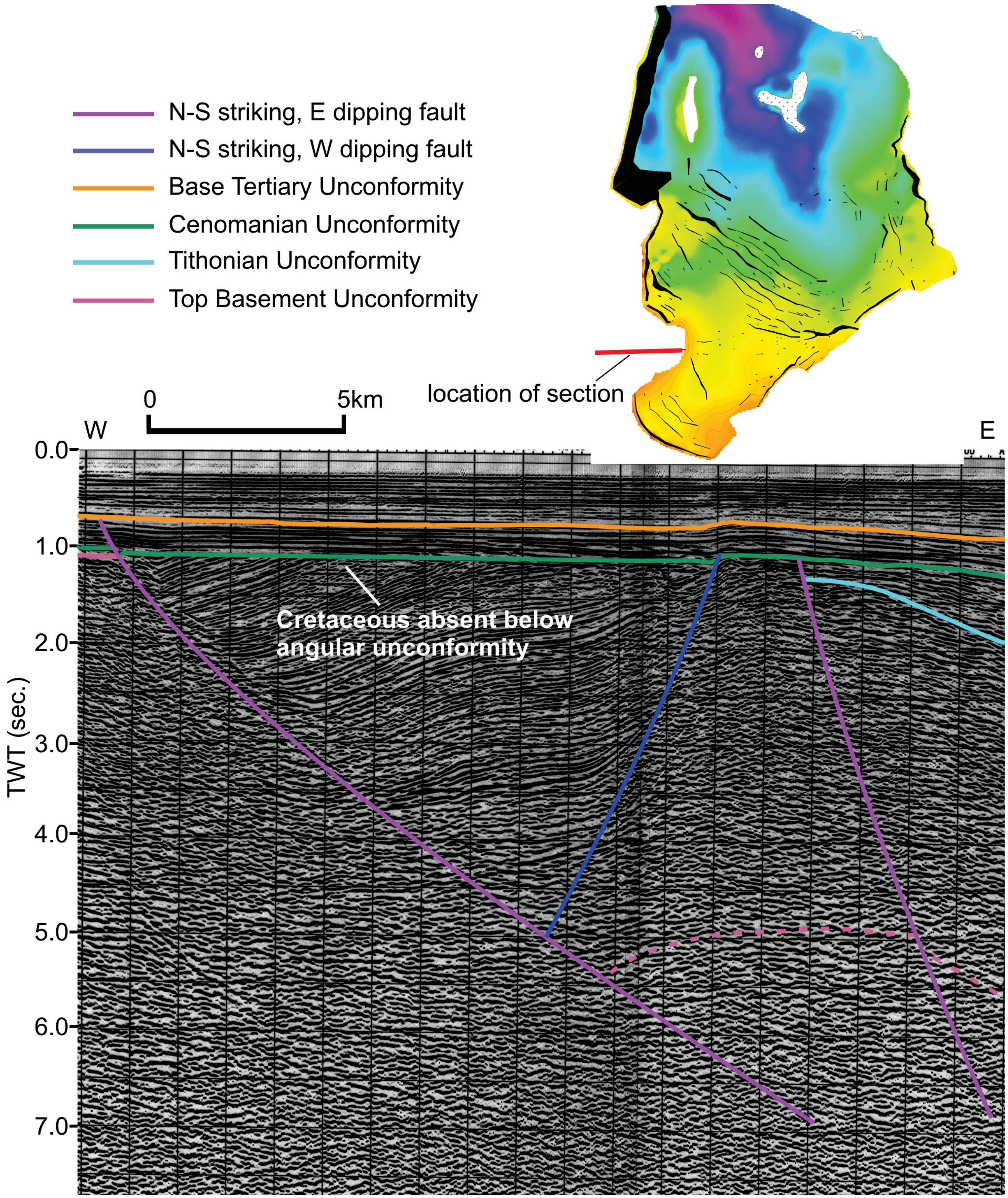

Figure 2.20: Interpreted east-west seismic profile from the SOQUIP survey illustrating the strong angular unconformity at the Cenomanian level. Data courtesy of CNLOPB. The location of the section is illustrated on the time structure map at the Mid-Aptian Unconformity (Section 3.2.3).

the surface and failed to propagate above the Mid-Aptian, hence the extension is expressed as ductile folding not brittle faulting above the Mid-Aptian. By measuring fault heaves this extension will be included in rift phase II not in rift phase III as predicted by the growth above the fault.

A source of potential error in estimating extension is erosion, particularly towards the edges of the southern part of the basin, where the Cenomanian Unconformity is a strong angular unconformity (Fig. 2.20). It is unclear whether there was no Early Cretaceous sedimentation or if it has been removed by erosion. The absence of Early Cretaceous sediments leaves no record of fault movement along the Murre fault during rift phase II or III in this area of the basin.

It is difficult to image completely the geometry of polyphase faulting with seismic sections (Reston, 2005 [35]; Reston, 2010 [36]). Detailed fault mapping of the Hebron area using the 3D data revealed complex fault interactions (Section 3.3). Fault mapping was difficult in areas of cross-cutting faults, even with the continuity of the 3D data. Comparing the extension measurements across the Hebron area using the 3D-data with the measurements across the same area using the 2D data, it is observed that the extension using the 3D data is approximately twice that using 2D data (Fig. 2.21 and Fig. 2.22).

2.2.6 Accounting for "missing" extension

In order to attempt to account for the extension discrepancy between the 2D and the 3D data, a second set of beta grids was created based on several assumptions:

- Measurement of heave across basin boundary faults provides a reasonable estimate of extension for those faults.

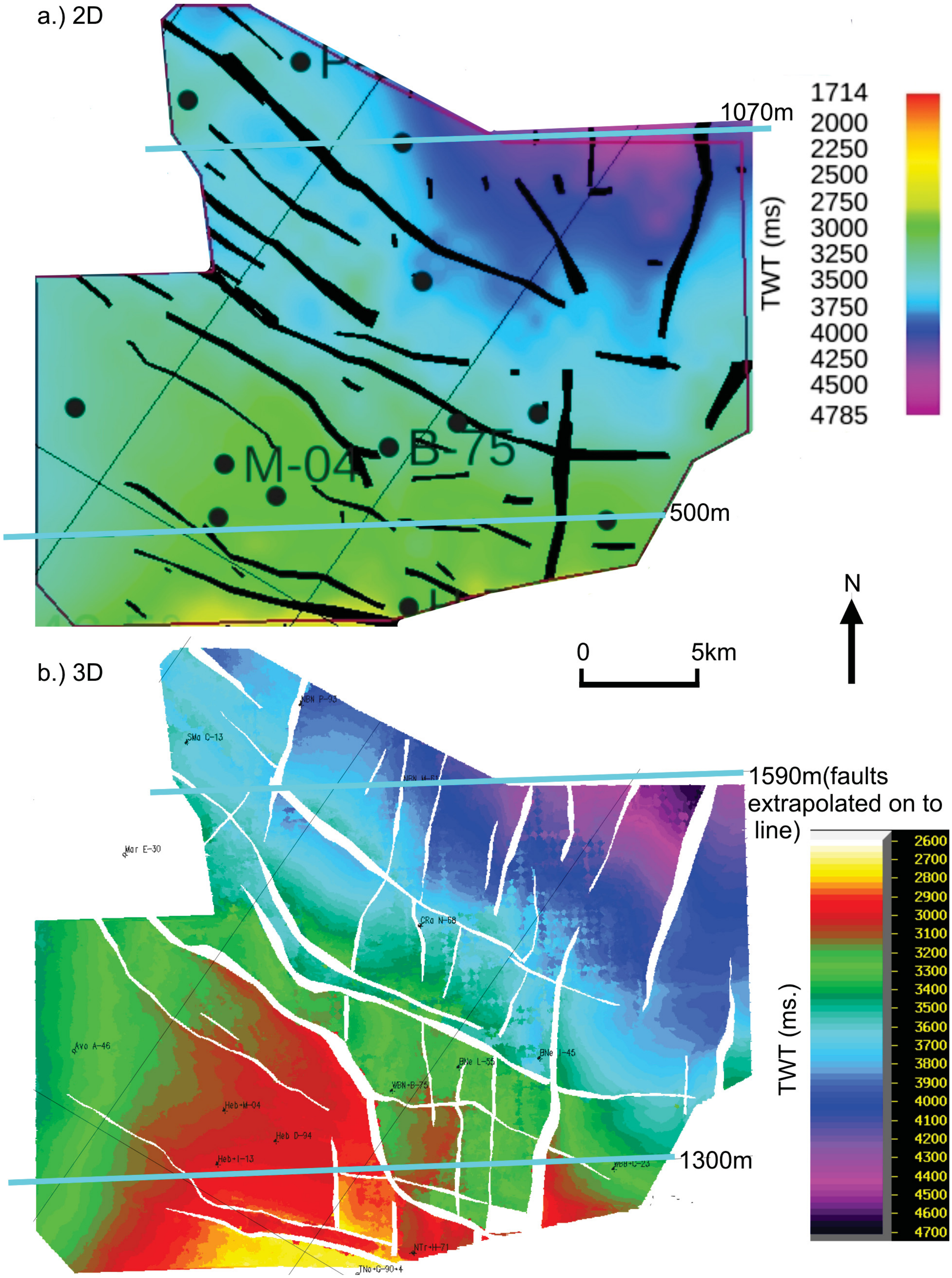

Figure 2.21: Timestructure at the Tithonian Unconformity across the Hebron area using a.) 2D data and b.) 3D data. Extension measurements along the east-west measurement lines are shown. Data courtesy of Husky Energy.

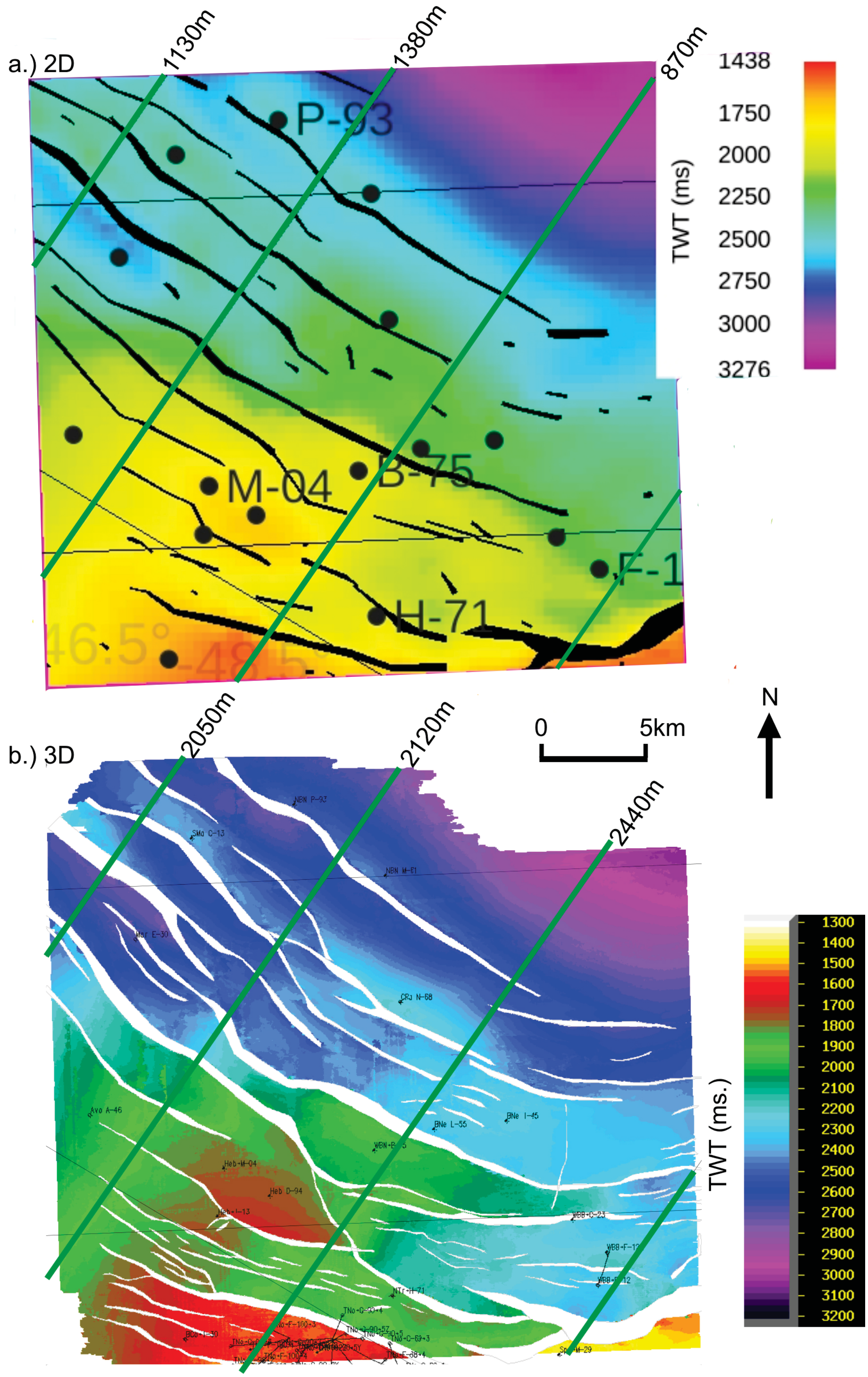

Figure 2.22: Timestructure at the mid-Aptian Unconformity across the Hebron area using a.) 2D data and b.) 3D data. Extension measurements along the northeast-southwest measurement lines are shown. Data courtesy of Husky Energy.

- Measurement of heave across internal basin faults from the 2D data underestimates extension by approximately 50%.
- Assuming double extension on the internal faults, approximately 45% of extension is on the boundary faults at the Tithonian Unconformity level. Although it was not possible to map the internal faults at the Top Basement level, it is assumed that 55% of the extension during the early rift phase was also accommodated by internal faults.

The new beta grids were created with the following parameters:

- The extension across the basin boundary faults remained as measured.
- At the Aptian Unconformity level and the Tithonian Unconformity level extension across the faulted areas of the basin interior was doubled.
- At the Top Basement level 55% of the extension was accommodated by interior faults. This "extra" extension was distributed evenly in the area between the basin boundary faults.

The new beta grids were used to restore the time structure maps to their position before each rift phase and compared with the first set of restorations.

2.2.7 Mapping the syn-rift and post-rift

The Late Cretaceous and Cenozoic post-rift stratigraphy thickens dramatically northwards in the Jeanne d'Arc Basin (Enachescu, 1987 [11]). To assess this thickening and relate it to thickness of the syn-rift stratigraphy, isochron maps of the post-rift and the syn-rift were produced. The Top Basement was interpreted as the base of the syn-rift and the Base Tertiary Unconformity as the top of the syn-rift. Both horizons were interpreted across the extended study area (Fig. 1.4) in the time domain using Landmark's Seisworks, and gridded and mapped using Petrosys. The Base Tertiary Unconformity map was subtracted from the Top Basement map to produce an isochron map of the syn-rift. The waterbottom was interpreted in Seisworks as the top of the post-rift, gridded and mapped in petrosys and subtracted from the Base Tertiary Unconformity map to produce an isochron map of the post-rift.

Chapter 3

Structure

3.1 Introduction

This chapter illustrates the timing and orientation of faulting in the Jeanne d'Arc Basin through a series of time structure maps, seismic profiles and isochron maps. Complexities arising from crossing conjugate faults, transpression during rift phase III and salt tectonics are discussed.

3.2 Changing fault patterns through time

The following time structure maps show a pronounced deepening of the basin northwards. Fault cut-offs are displayed on each map, revealing the changing fault pattern through time. Time structure maps combined with seismic profiles and isochron maps from the Hebron 3D data allow a more detailed view of the Hebron area, illustrating the timing and direction of fault growth during rift phases II and III.

3.2.1 Faults at the Top Basement Unconformity

The Top Basement Unconformity deepens northwards from around 1000 ms two way time in the southeast of the study area to 7500 ms two way time in the northwest of the mappable area (Fig. 3.1). This represents a depth range of approximately 0.95 km to 15 km depth. The northern extent of the Top Basement map is limited by the 7500 ms two way time extent of the seismic data. The Top Basement Unconformity represents the start of rift phase I in the Jeanne d'Arc Basin, during which time the border faults formed. The basin is bounded to the west by the northeast-southwest striking, east dipping listric Murre and Mercury faults (Fig. 3.2) and to the east by the predominantly northeast-southwest trending Voyager fault zone (Fig. 3.3). Extension during rift phase I is assumed to be in a northwest-southeast direction, perpendicular to the border fault trend. Figure 3.4 is an east-west seismic profile across the basin illustrating the Murre and Voyager faults and the internal basin faulting. It is not possible to image the Top Basement Unconformity across the smaller faults in the basin. Figure 3.5 is a north-south seismic profile illustrating the Voyager fault zone and the Adolphus salt diapir. The northwards deepening of the basin is evident on the section, such that the Top Basement Unconformity becomes deeper than the depth extent of the seismic.

The Egret fault forms the southerly limit of Cretaceous sediments in the basin (Fig. 3.6). In plan view the Egret fault appears to be a curved fault varying from north-south striking in the west to northwest-southeast further east. With only 2D data in this area it is not possible to say whether this is actually a curved fault or a north-south fault and a northwest-southeast fault that have grown towards each other.

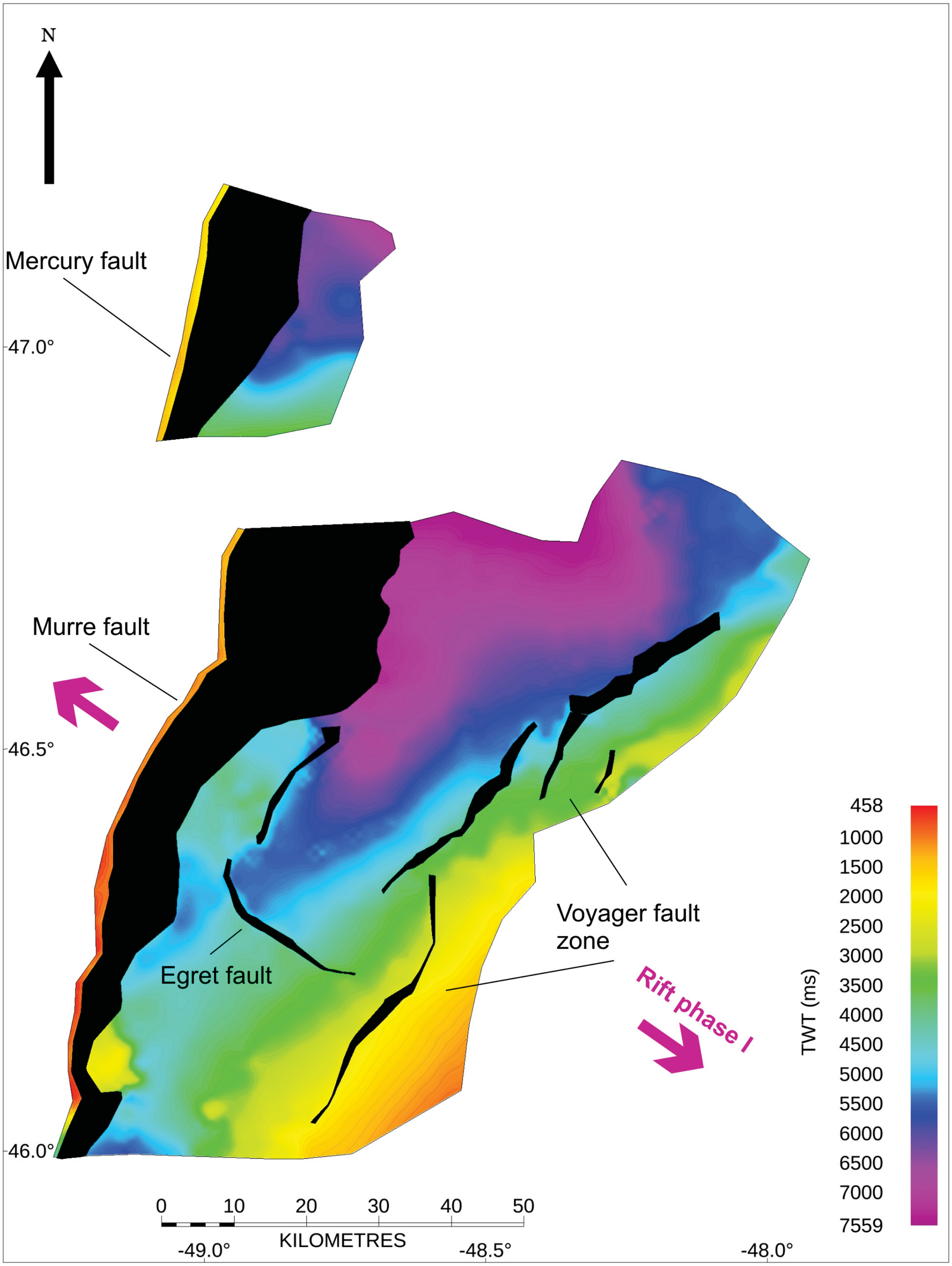

Figure 3.1: Time structure map of the Top Basement Unconformity. The fault gaps are shown in black.

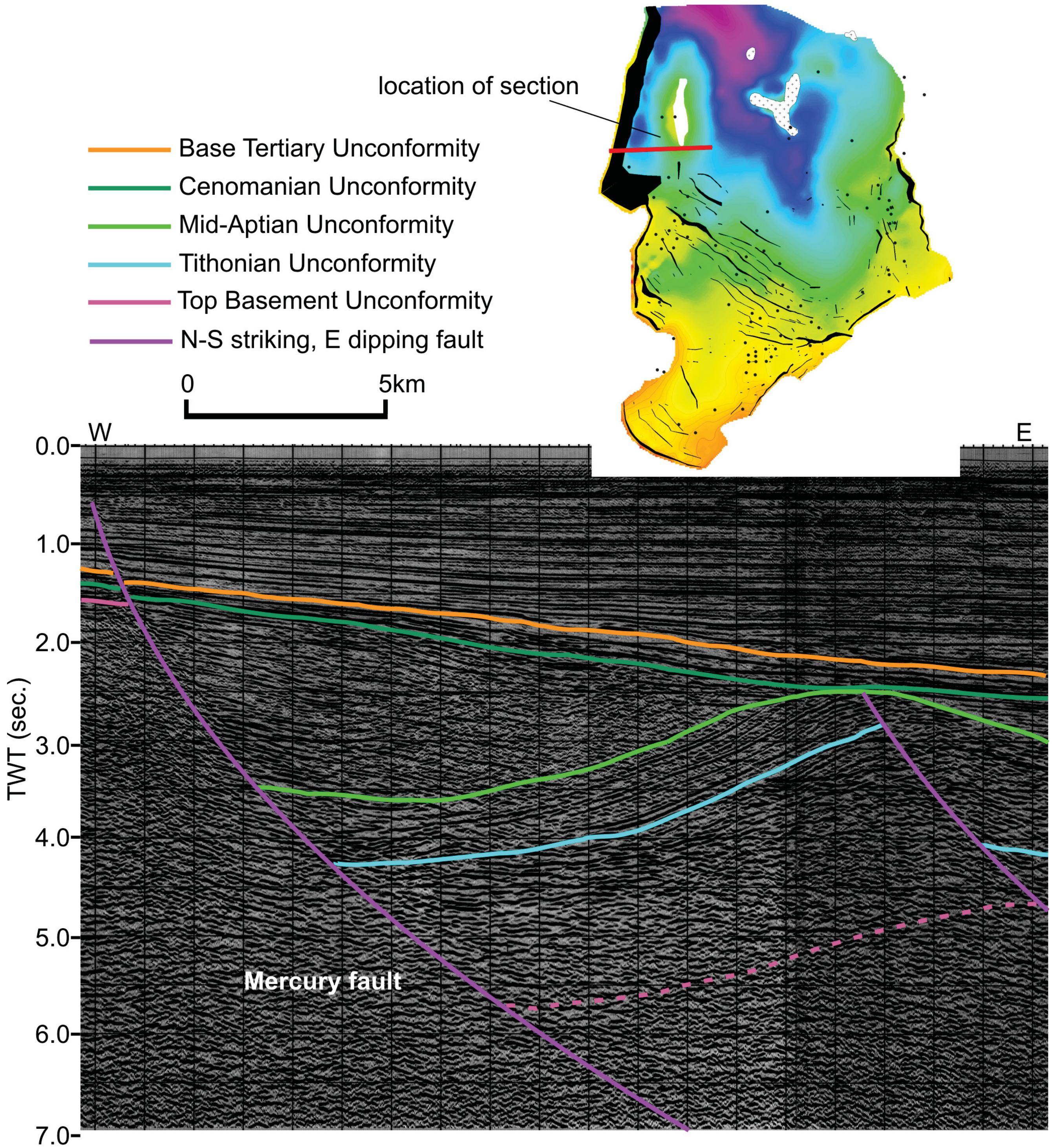

Figure 3.2: Interpreted east-west profile from the SOQUIP survey across the Mercury fault. Data courtesy of CNLOPB. The location of the section is illustrated on the time structure map at the Mid-Aptian Unconformity (Section 3.2.3).

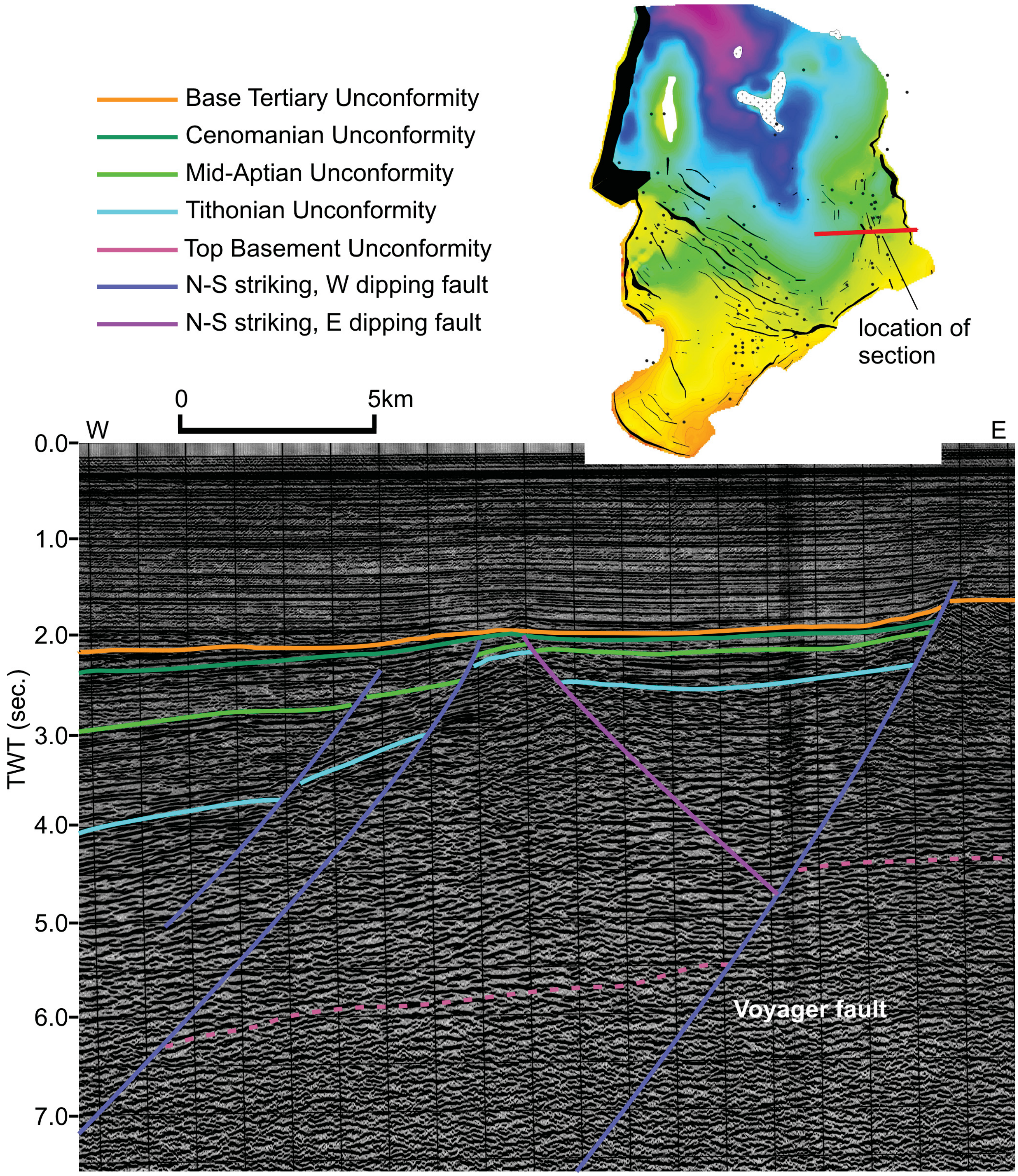

Figure 3.3: Interpreted east-west profile from the SOQUIP survey across the Voyager fault. Data courtesy of CNLOPB. The location of the section is illustrated on the time structure map at the Mid-Aptian Unconformity (Section 3.2.3).

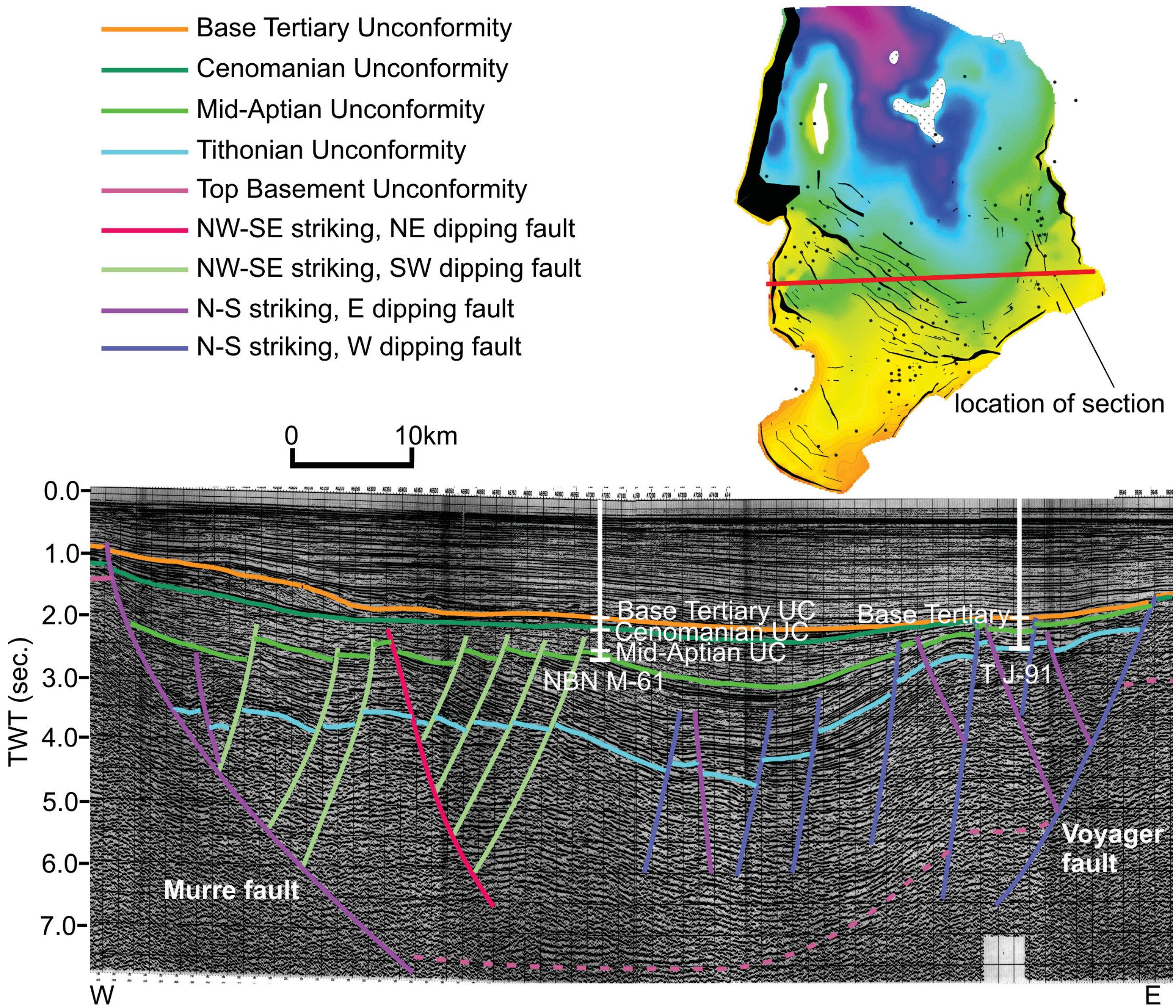

Figure 3.4: Interpreted east-west profile from the SOQUIP survey across the Jeanne d'Arc Basin. Note that the section is vertically exaggerated by approximately x3. Data courtesy of CNLOPB. The location of the section is illustrated on the time structure map at the Mid-Aptian Unconformity (Section 3.2.3).

3.2.2 Faults at the Tithonian Unconformity

The Tithonian Unconformity is mapped over a range from around 900 ms two way time in the south of the basin to 7000 ms two way time at the northern end of the basin (Fig. 3.7). This represents a depth range of approximately 0.86 km to 14 km.

The Tithonian Unconformity is cut by the huge Adolphus salt diapir and a smaller salt diapir in the north of the basin and there is deepening around the diapirs caused by salt withdrawal (Section 3.5). The border faults were reactivated during rift phase

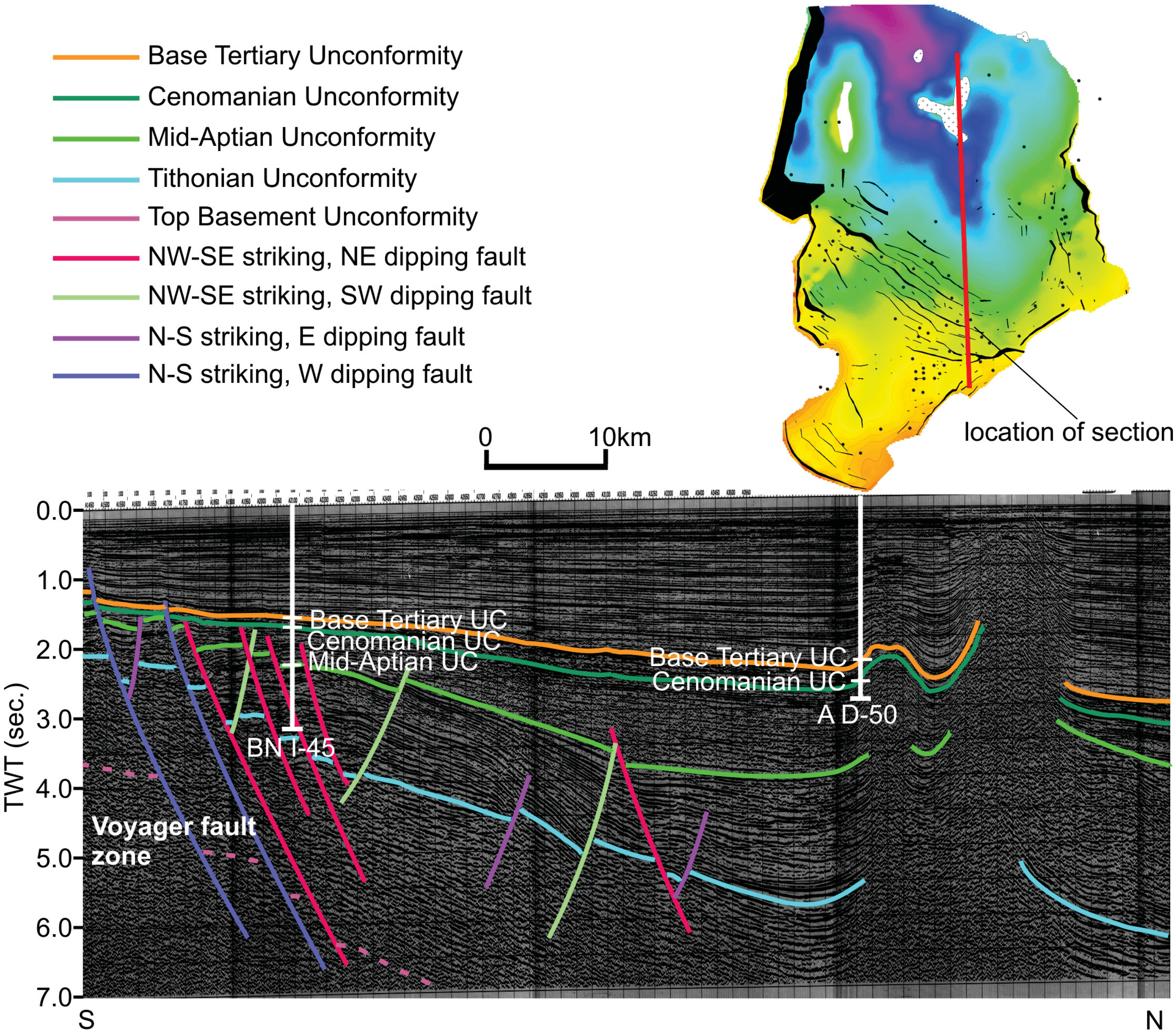

Figure 3.5: Interpreted north-south profile from the SOQUIP survey illustrating the Voyager fault zone, the Adolphus salt diapir and the northwards deepening of the basin. Note that the section is vertically exaggerated by approximately x3. Data courtesy of CNLOPB. The location of the section is illustrated on the time structure map at the Mid-Aptian Unconformity (Section 3.2.3).

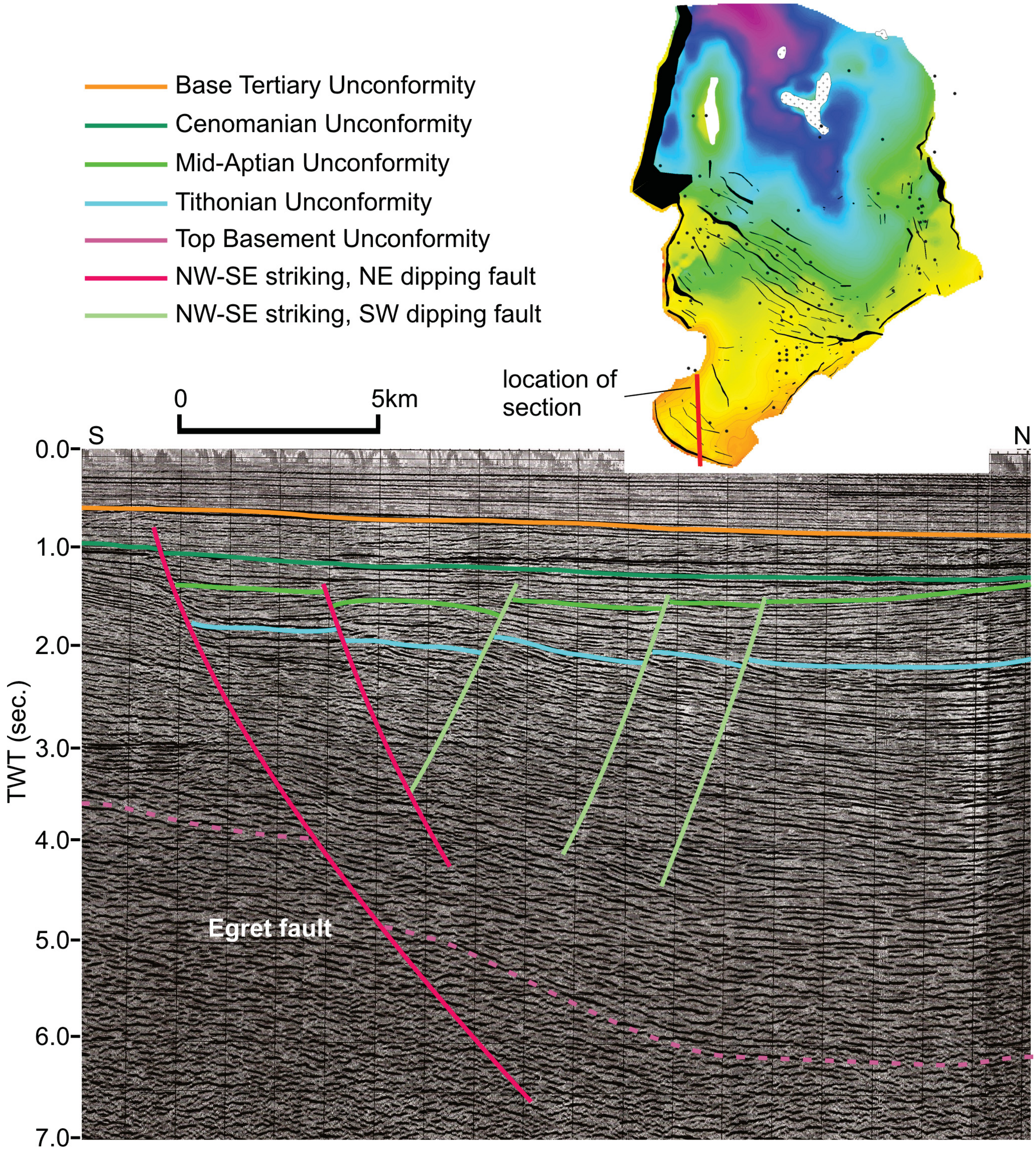

Figure 3.6: Interpreted north-south seismic profile from the SOQUIP survey across the Egret fault. Data courtesy of CNLOPB. The location of the section is illustrated on the time structure map at the Mid-Aptian Unconformity (Section 3.2.3).

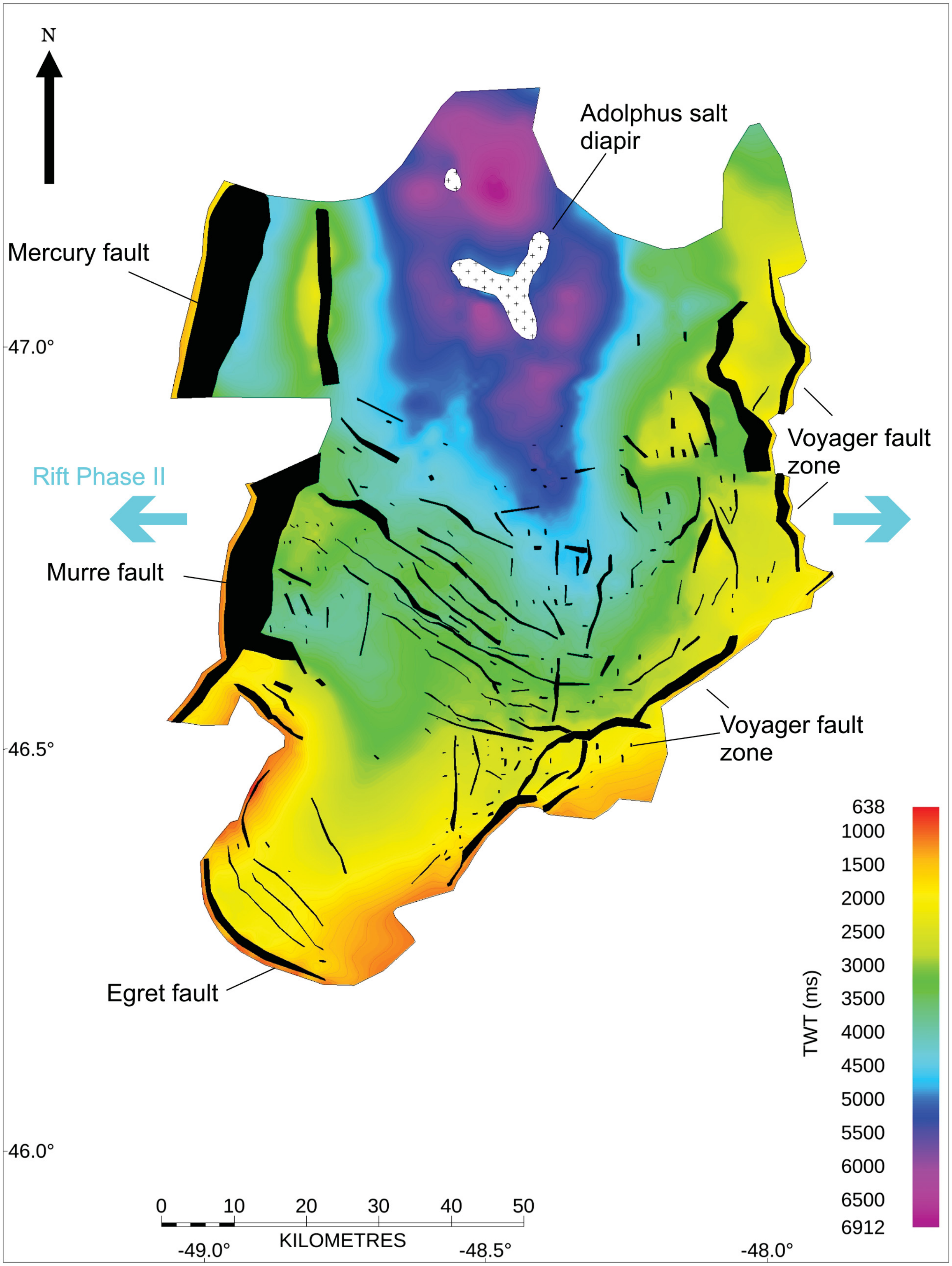

Figure 3.7: Time structure map of the Tithonian Unconformity. The fault gaps are shown in black.

II.

Fault mapping at the Tithonian Unconformity level using the Hebron 3D data illustrates that faults most active during rift phase II are predominantly north-south striking, suggesting an east-west extension direction (Fig. 3.8). There is debate as to the duration of rift phase II, with some authors suggesting a period of thermal subsidence between the "B" Marker limestone and the Mid Aptian Unconformity; this

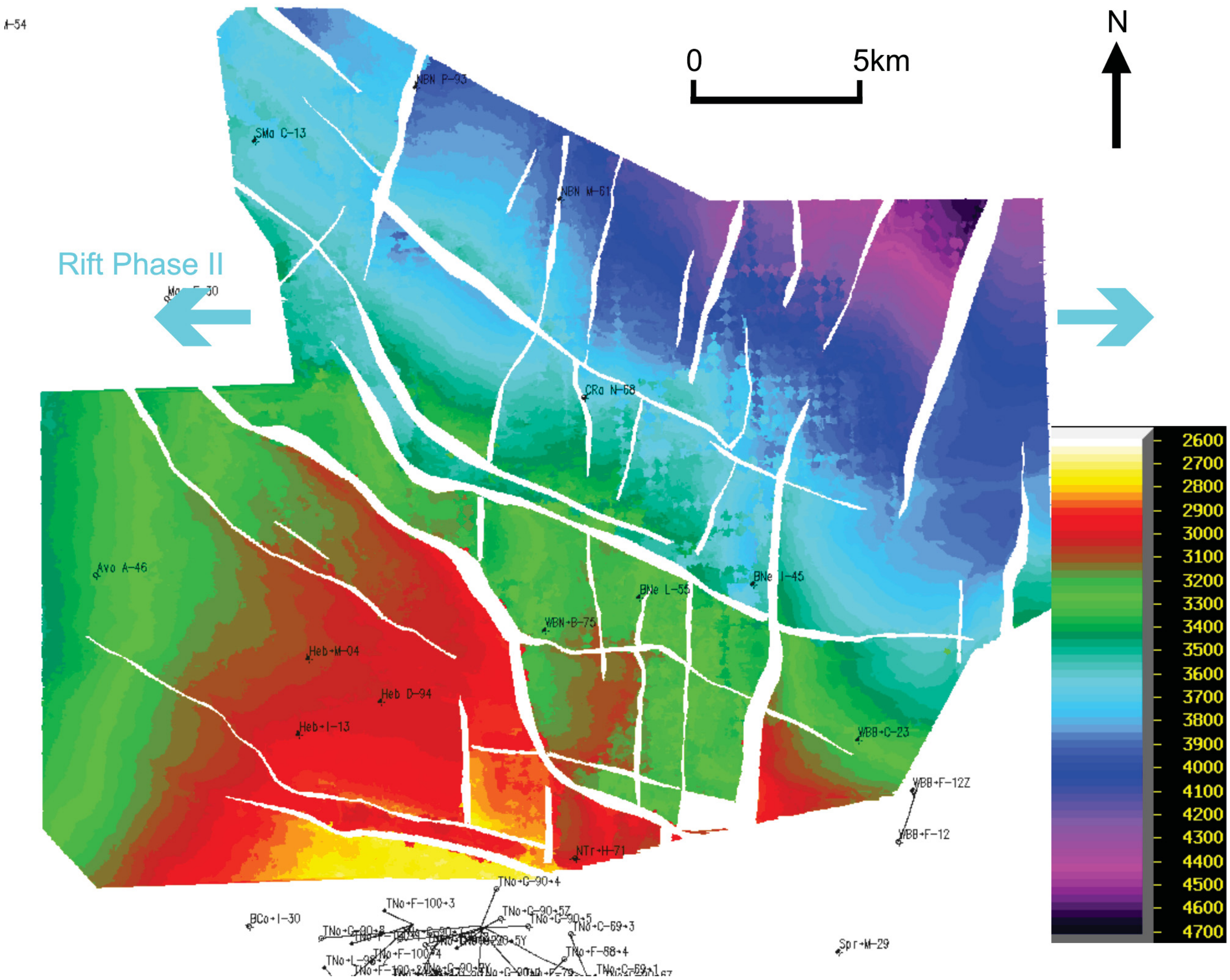

Figure 3.8: Time structure at the Tithonian Unconformity from the Hebron area 3D data. The fault gaps are shown in white. The faults active at this time are predominantly north-south striking. Data courtesy of Husky Energy.

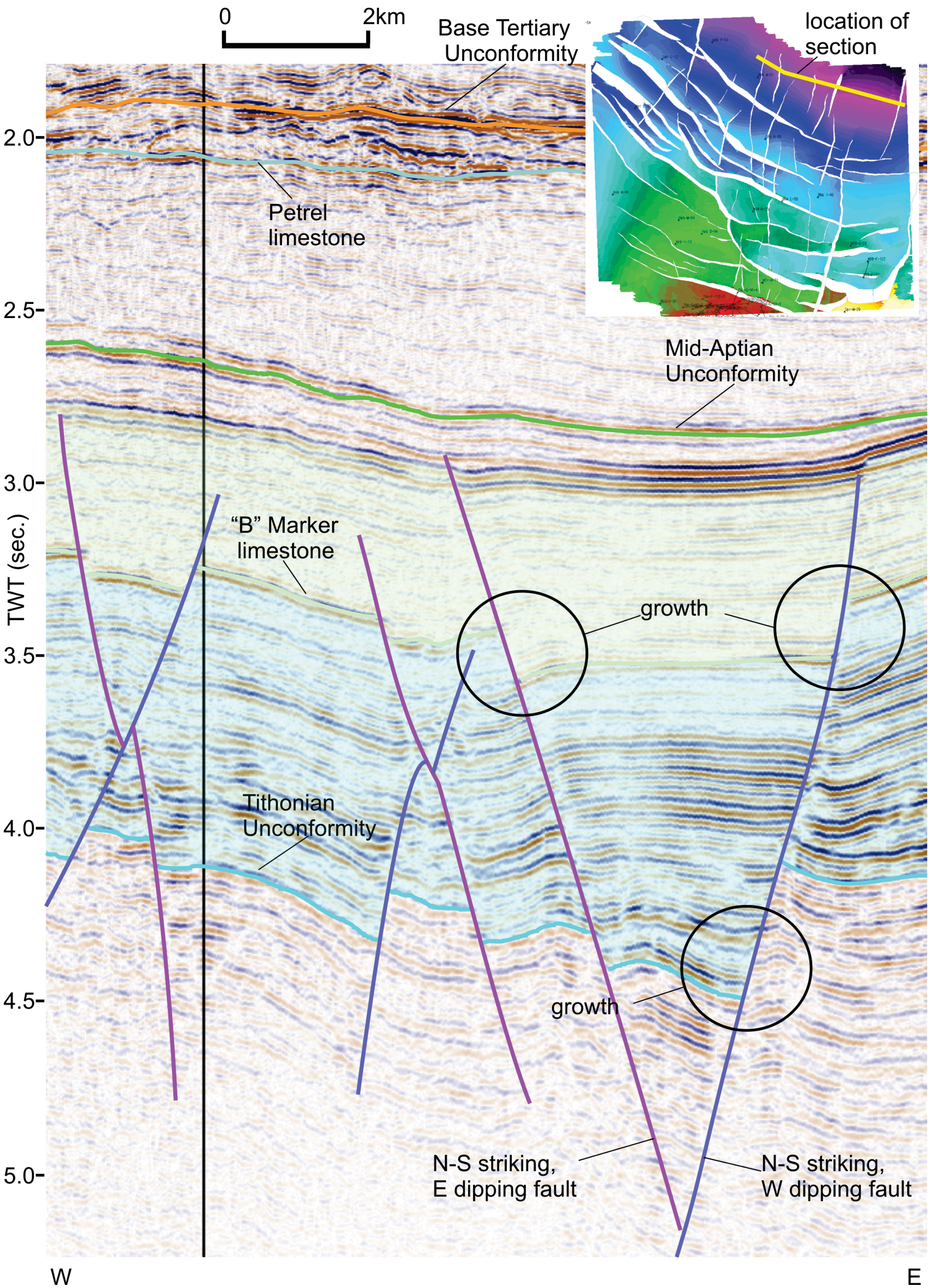

Figure 3.9: Interpreted east-west seismic profile across the Hebron area showing growth above the Tithonian Unconformity and above the "B" Marker limestone. Data courtesy of Husky Energy. The location of the section is shown on a time structure map at the"B" Marker Limestone from the Hebron area.

is summarized by Sinclair, 1993 [42]. Seismic data from the Hebron area show that, although some smaller north-south striking faults tip out just above the "B" Marker limestone, there is clear growth on the larger faults both above the Tithonian Unconformity and above the "B"Marker limestone (Fig. 3.9). This post "B" Marker growth is

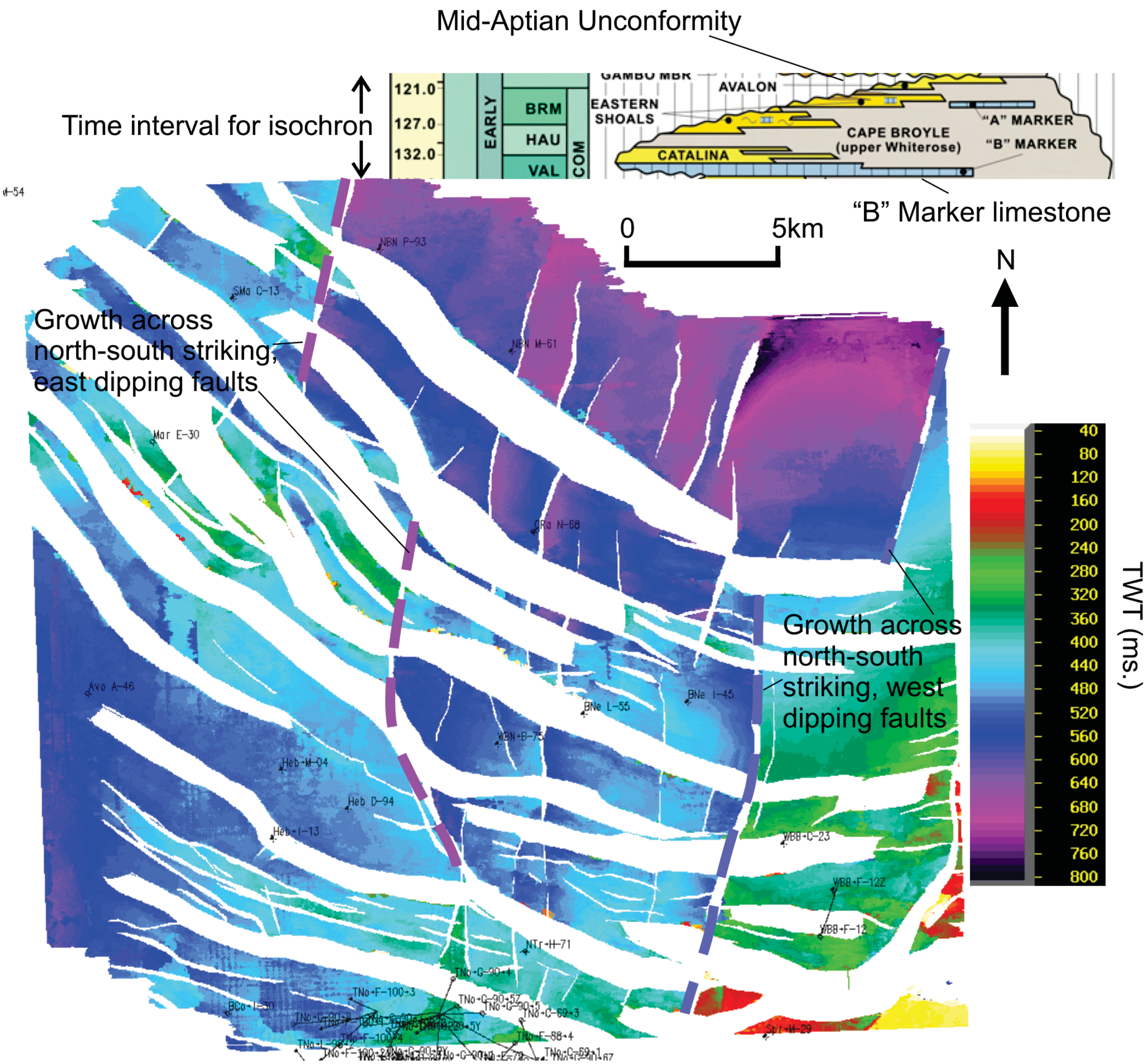

Figure 3.10: Isochron map between the Mid-Aptian Unconformity and the "B" Marker limestone from the Hebron area, showing growth across north-south faults during this time interval. Data courtesy of Husky Energy.

imaged across north-south striking faults on an isochron map between the Mid-Aptian Unconformity and the "B" Marker limestone (Fig. 3.10). There is up to 240 ms two way time thickness variation across the north-south faults in the "B"Marker limestone to Mid-Aptian Unconformity time interval indicating ongoing extension at this time. The time interval for rift phase II is therefore from the Tithonian Unconformity until the Mid-Aptian Unconformity (150 Ma - 112 Ma).

3.2.3 Faults at the Mid-Aptian Unconformity

The Mid-Aptian Unconformity is mapped over a range from around 1000 ms two way time in the south of the basin to 5000 ms two way time at the northern end of the basin (Fig. 3.11). This represents a depth range of approximately 0.95 km to 9.0 km. In the northwest of the basin the Mid-Aptian Unconformity is absent over the hinge of the Flying Foam fold. The Mid-Aptian Unconformity is cut by the Adolphus salt diapir and two smaller diapirs, and deepens around the salt.

The border faults were reactivated during rift phase III with oblique slip in a northeast-southwest direction (Section 3.4). Some of the internal north-south faults were reactivated with oblique slip, however most of the north-south faults tip out below the Mid-Aptian Unconformity. Across the basin interior there is a clear pattern of predominantly northwest-southeast striking faults on the whole basin map (Fig. 3.11) and on the map of the 3D Hebron area data (Fig. 3.12). Extension during rift phase III is assumed to be in a northeast-southwest direction, perpendicular to the fault trend. Significant growth across the northwest-southeast striking faults between the the Mid-Aptian Unconformity and the Petrel limestone is evident on the seismic data (Fig. 3.13). An isochron map between the Mid-Aptian Unconformity and the Petrel limestone shows up to 360 ms two way time thickness variation across the northwest-

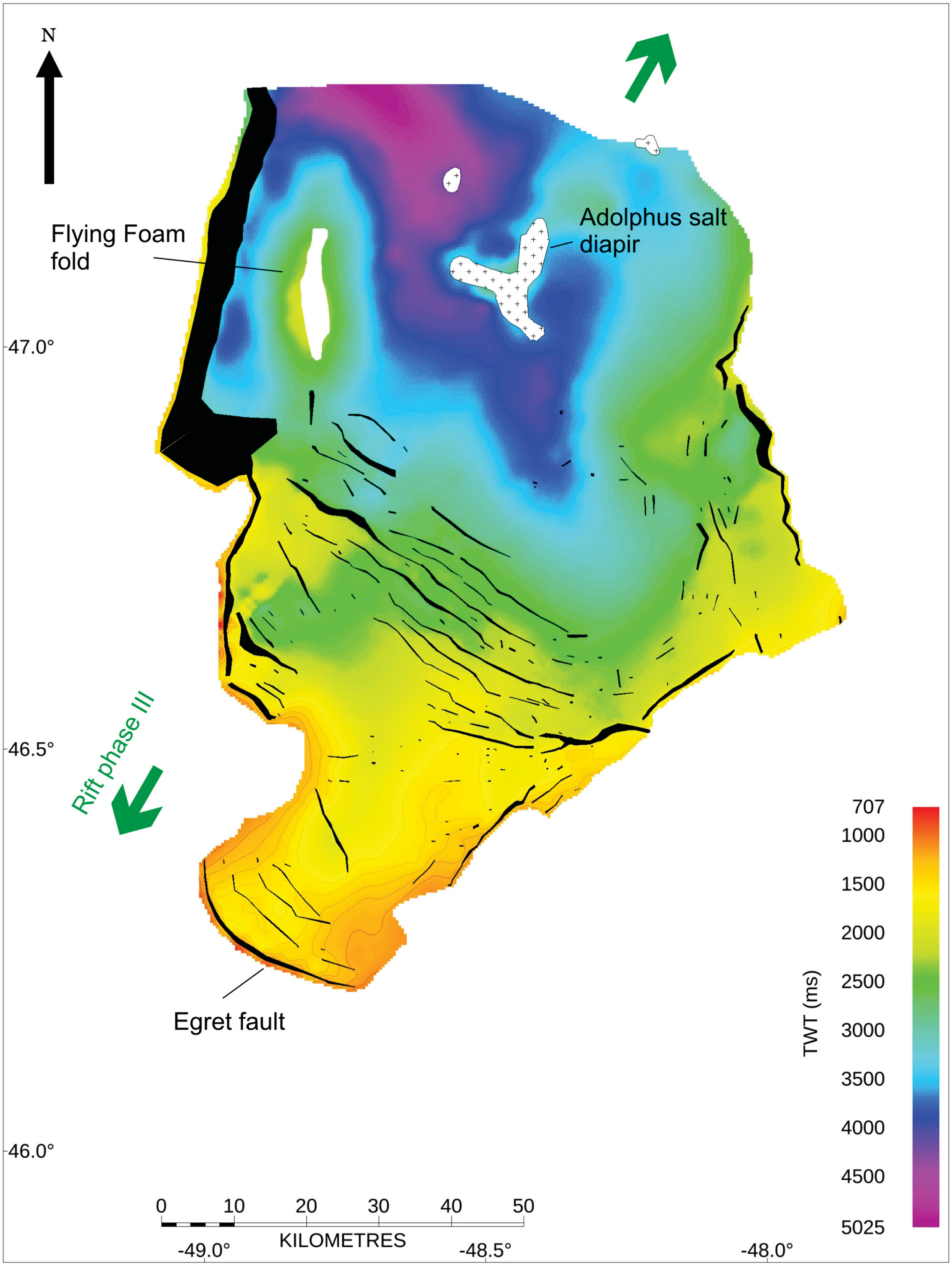

Figure 3.11: Time structure map of the Aptian Unconformity. The fault gaps are shown in black.

southeast striking faults during this time interval (Fig. 3.14). The time interval for rift phase III is from the Mid-Aptian Unconformity until the Cenomanian (112 Ma - 96 Ma).

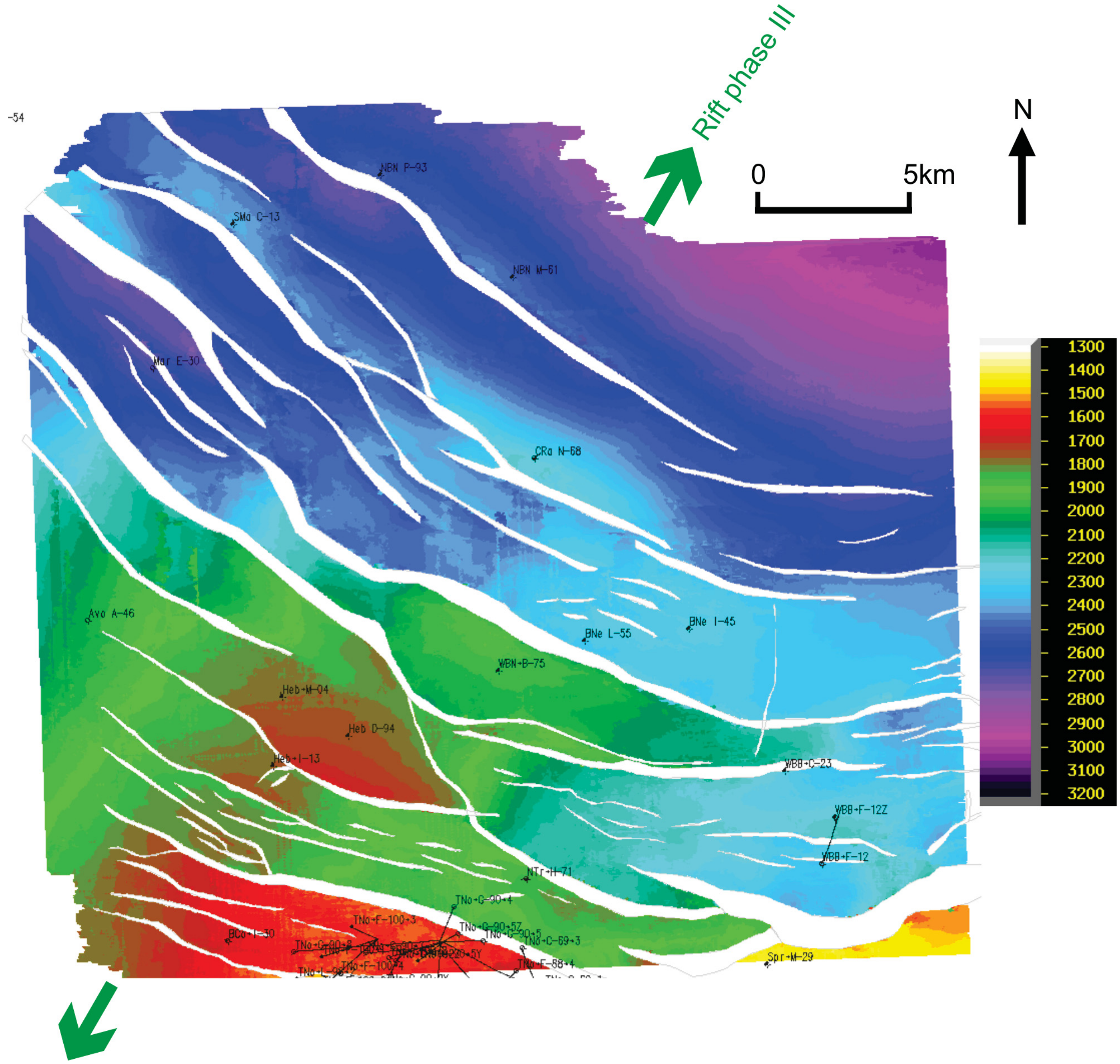

Figure 3.12: Time structure at the Mid-Aptian Unconformity from the Hebron area 3D data. The fault gaps are shown in white. The faults active at this time are predominantly northwest-southeast striking. Data courtesy of Husky Energy.

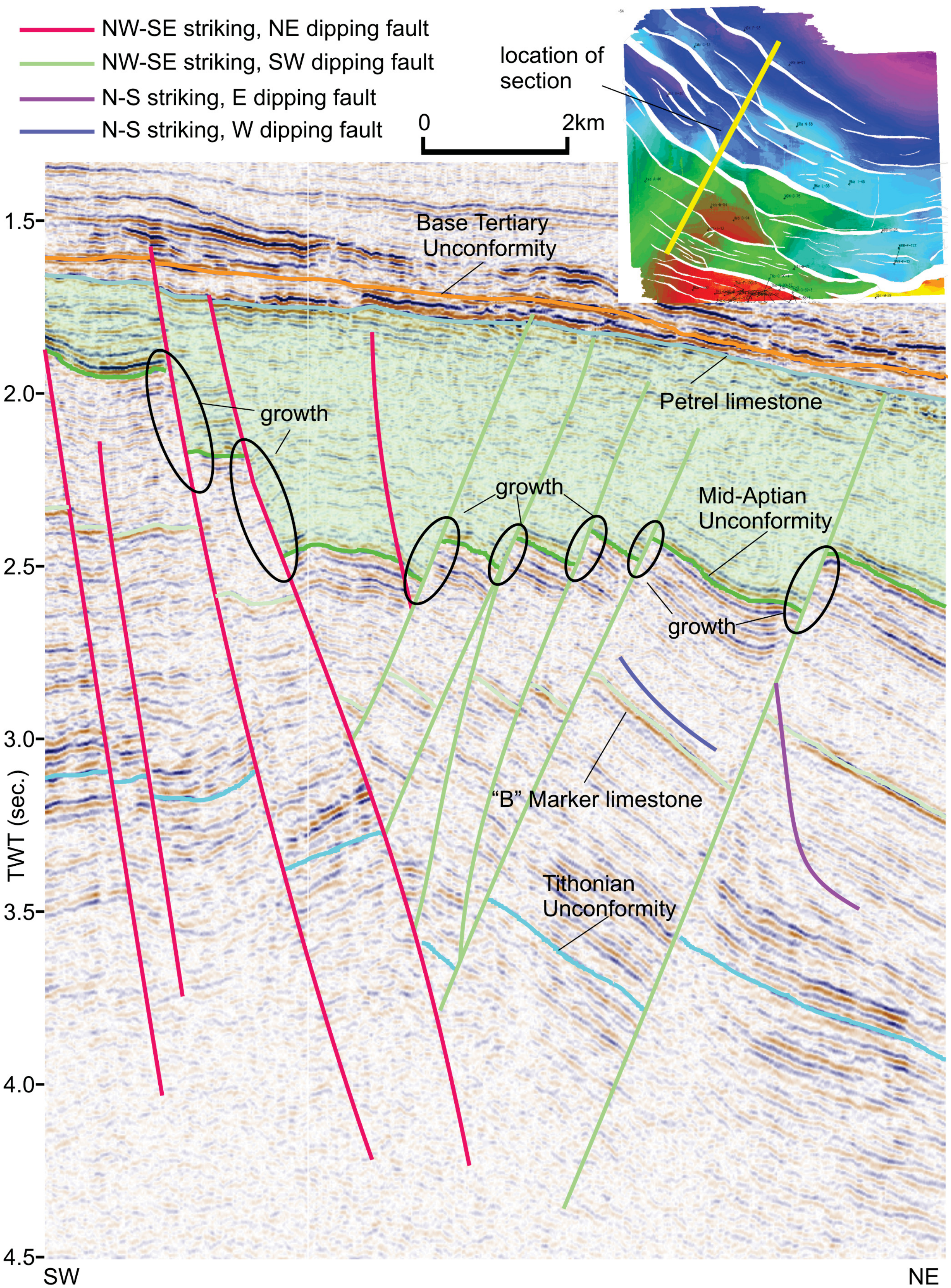

Figure 3.13: Interpreted northeast-southwest seismic profile across the Hebron area showing growth above the Mid-Aptian Unconformity. Data courtesy of Husky Energy. The location of the section is shown on a time structure map at the Mid-Aptian Unconformity from the Hebron area (see section 3.2.3).

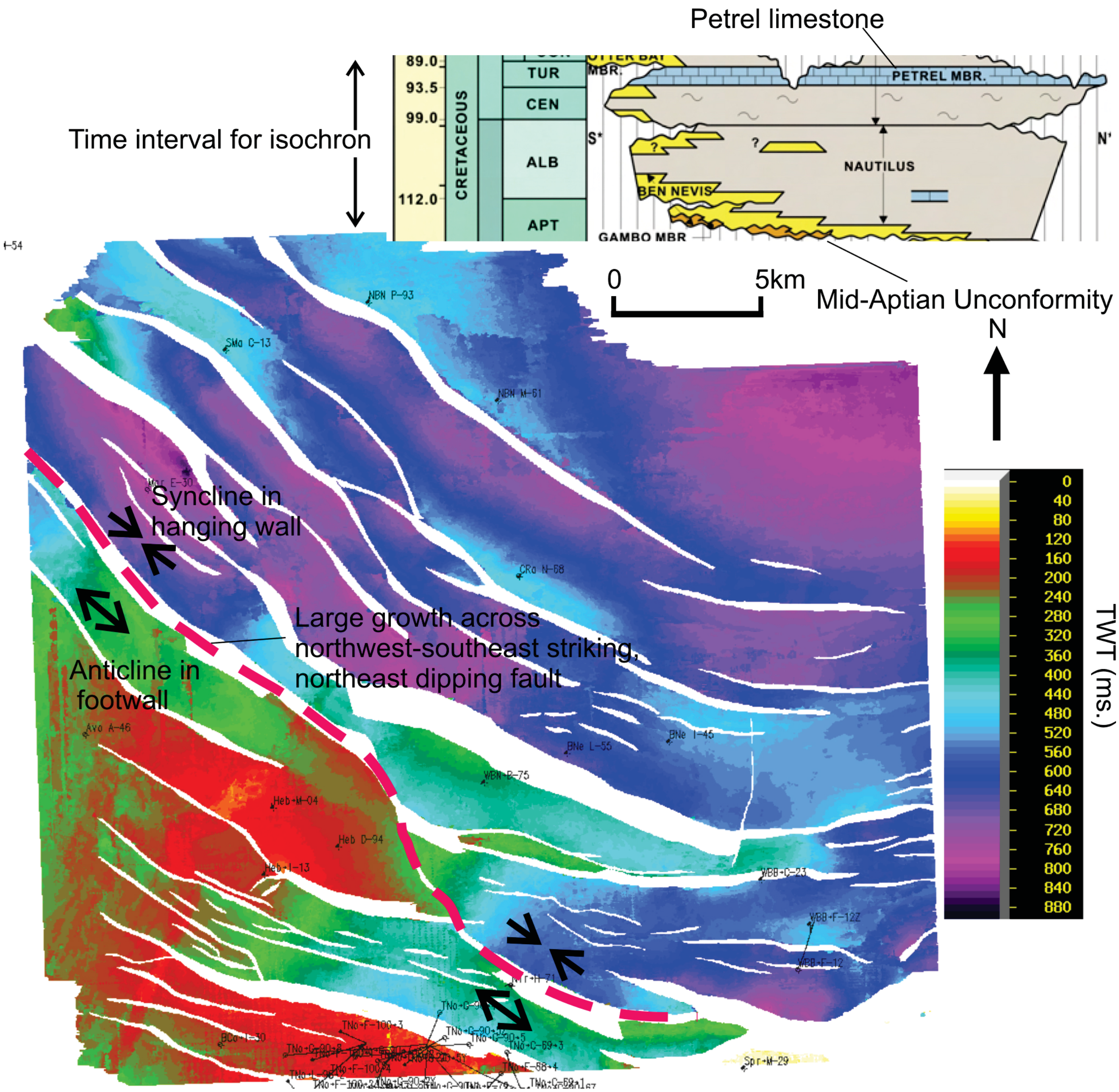

Figure 3.14: Isochron map between the Petrel limestone and the Mid-Aptian Unconformity from the Hebron area, showing growth across northwest-southeast faults during this time interval. Data courtesy of Husky Energy.

3.2.4 Faults at the Cenomanian Unconformity

The Cenomanian Unconformity is mapped over a range from around 700 ms two way time in the southwest of the basin to 3500 ms two way time at the northern end of the basin (Fig. 3.15). This represents a depth range of approximately 0.66 km to 4.6 km. The Cenomanian Unconformity is absent in an area over the Flying Foam fold and is cut by or displaced upwards over salt diapirs in the north of the basin. The larger faults in the basin, predominantly the border faults, are still evident at the Cenomanian Unconformity, with a minor amount of slip. Most of the basin interior faults tip out below the unconformity.

3.2.5 Faults at the Base Tertiary Unconformity

The Base Tertiary Unconformity is mapped over a range from around 400 ms two way time in the southwest of the basin to 3300 ms two way time at the northern end of the basin (Fig. 3.16). This represents a depth range of approximately 0.37 km to 4.5 km. The Base Tertiary Unconformity is pierced by or displaced upwards over salt diapirs in the north of the basin. A few faults, predominantly the larger border faults, propagate into the Cenozoic with a minor amount of slip. Time structure at the Base Tertiary Unconformity from the Hebron 3D area shows a few larger northwest-southeast faults still active at this time with a minor amount of slip (Fig. 3.17).

3.3 Crossing conjugate faults

Conjugate normal faults are normal faults with opposing dips. Conjugate faults commonly cross and intersect one another. Understanding and interpreting the fault intersection area is important for the oil industry, because the intersection area can trap hydrocarbons, create permeability anisotropy and reduce the effective thickness of seal and reservoir units (Ferrill et al., 2009 [12]). Crossing conjugate faults are common throughout the Jeanne d'Arc Basin and are observed in the Terra Nova,

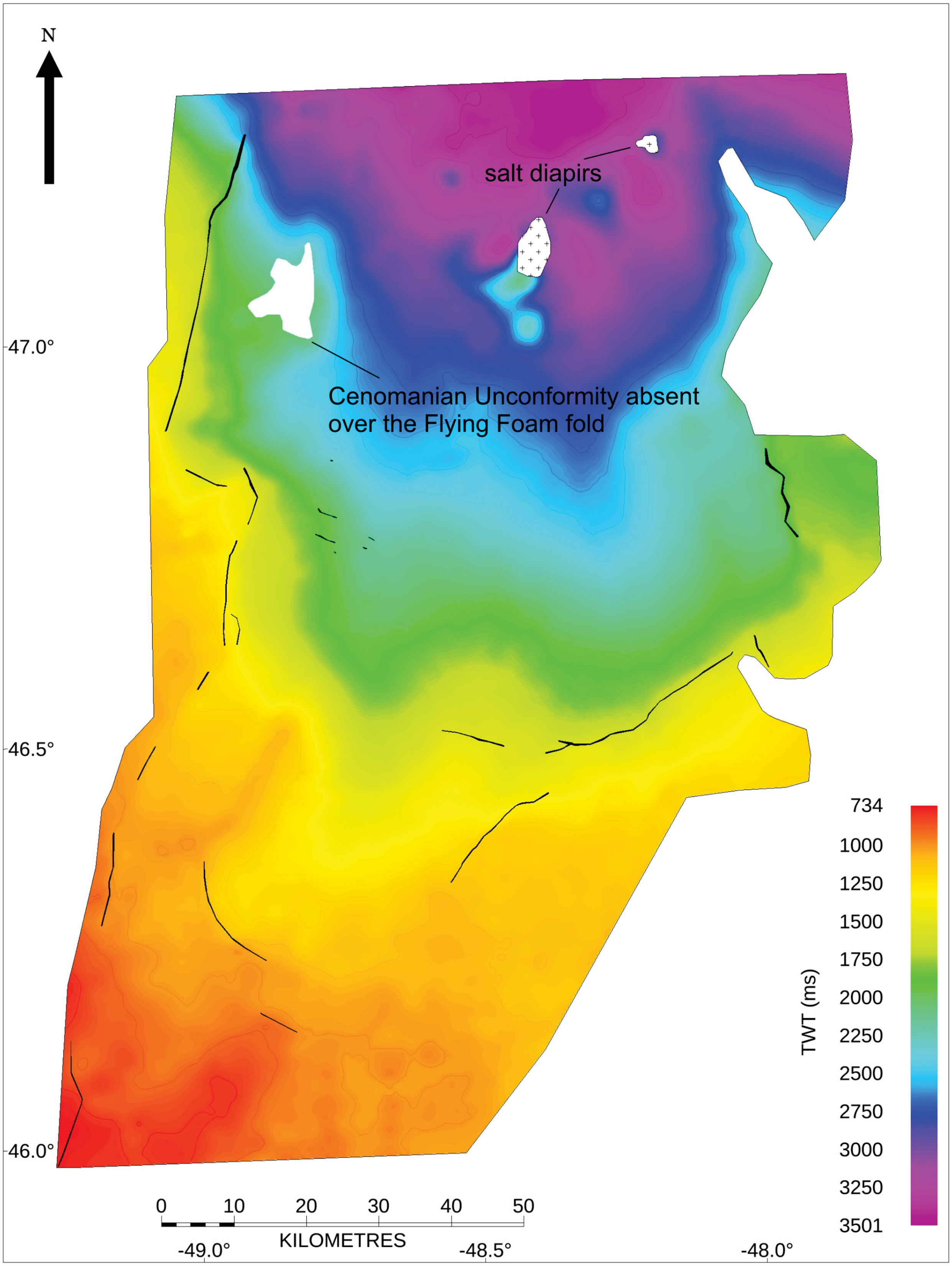

Figure 3.15: Time structure map of the Cenomanian Unconformity. The fault gaps are shown in black.

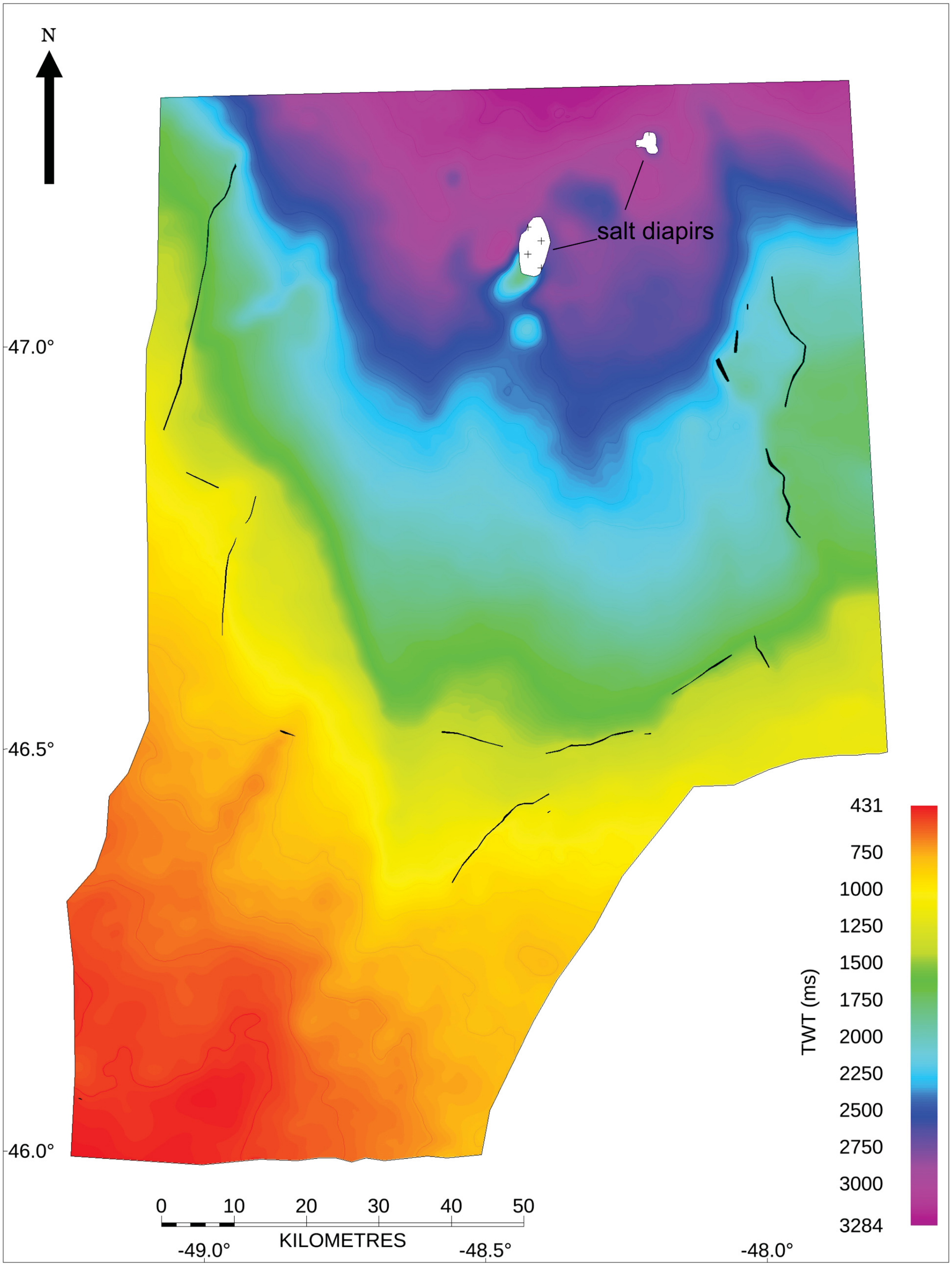

Figure 3.16: Time structure map of the Base Tertiary Unconformity. The fault gaps are shown in black.

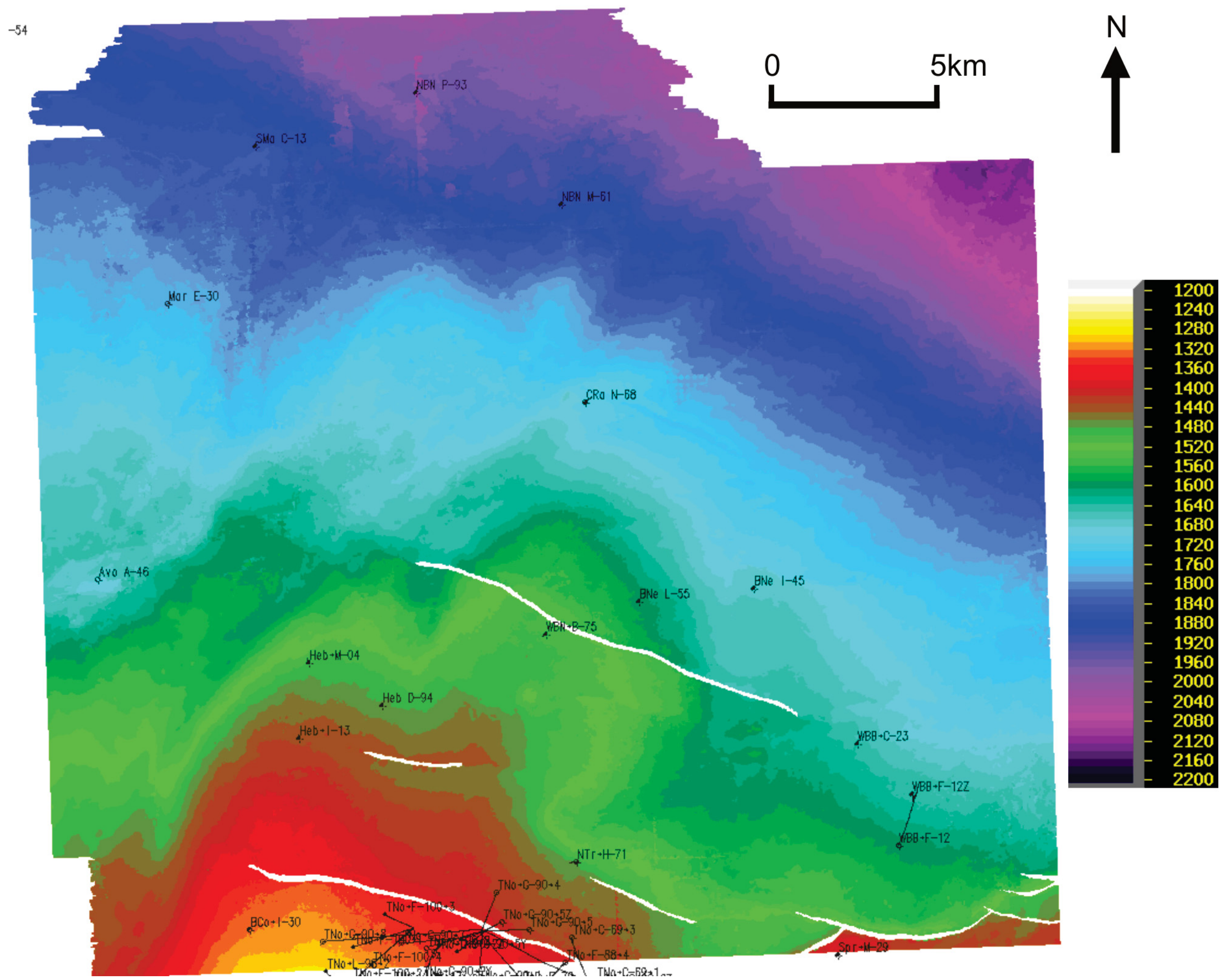

Figure 3.17: Time structure map of the Base Tertiary Unconformity from the Hebron area. The fault gaps are shown in white.

White Rose and Hibernia oil fields (Ferrill et al., 2009 [12]; (Fig. 1.5). In the Hebron area, crossing conjugate pairs are imaged using the 3D dataset in north-south striking fault pairs from rift phase II, in northwest-southeast striking fault pairs from rift phase III and in interacting north-south and northwest-southeast fault pairs. The 3D data is displayed as 2D snapshots (Figs. 3.18 to 3.21). A more comprehensive display of the 3D data is not possible due to confidentiality issues.

Figure 3.18 shows two north-south seismic segments from the Hebron area 3D dataset,

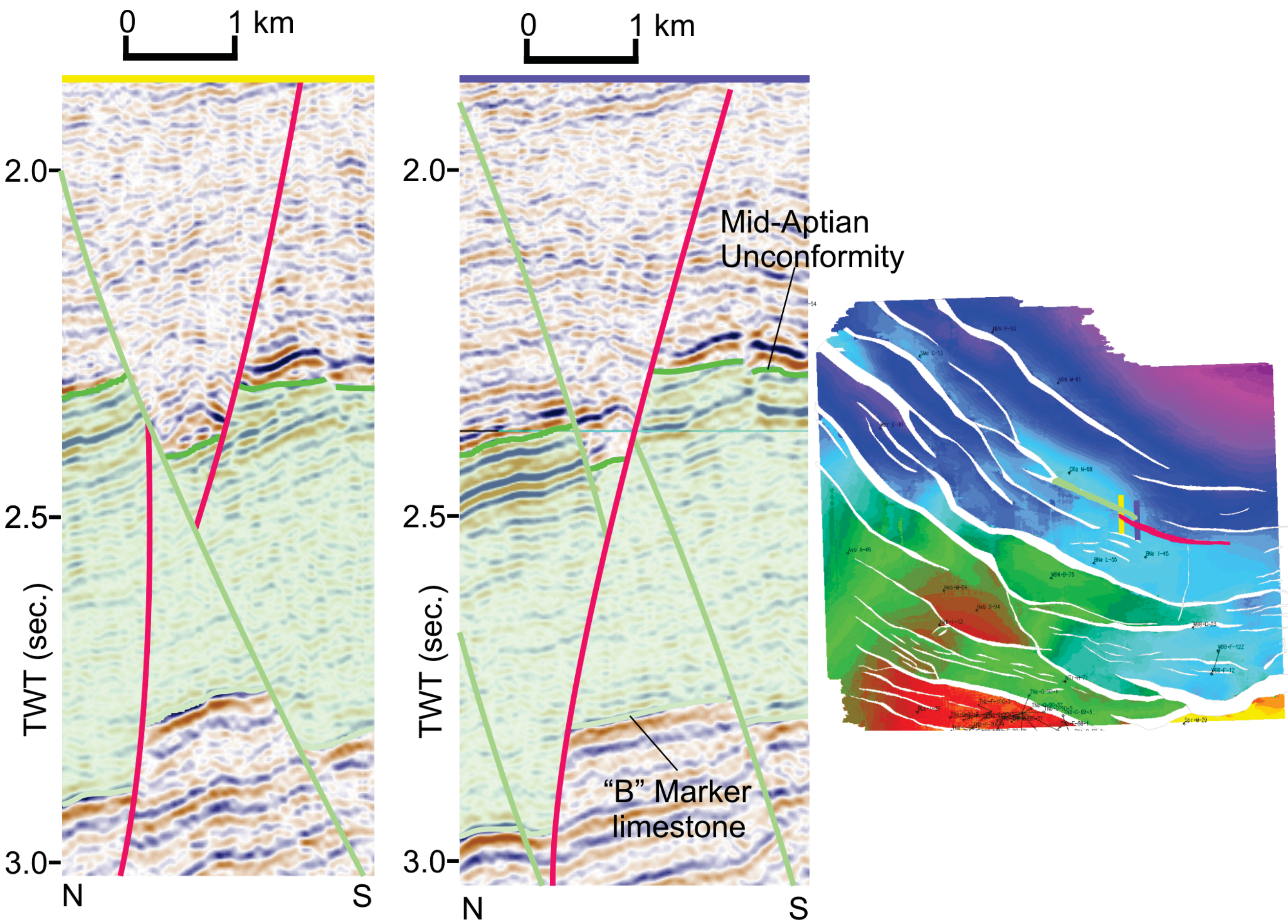

Figure 3.18: Interpreted north-south seismic profiles from the Hebron area showing northwest-southeast striking crossing conjugate faults. Data courtesy of Husky Energy. The location of the section is shown on a time structure map at the Mid-Aptian Unconformity from the Hebron area (Section 3.2.3).

illustrating northwest-southeast striking crossing conjugate faults. In the section to the west the green south-west dipping fault offsets the red north-east dipping fault whereas in the eastern section this reverses. This suggests lateral growth of the faults towards each other, with the faults becoming less dominant as they near their tip-out point and the dominant fault offsetting the less dominant fault. There is marked thinning of the strata in the intersection of the crossing conjugate faults between the Mid-Aptian Unconformity and the "B" Marker limestone from approximately 570 ms two way time to 370 ms two way time in the intersection area to produce a graben

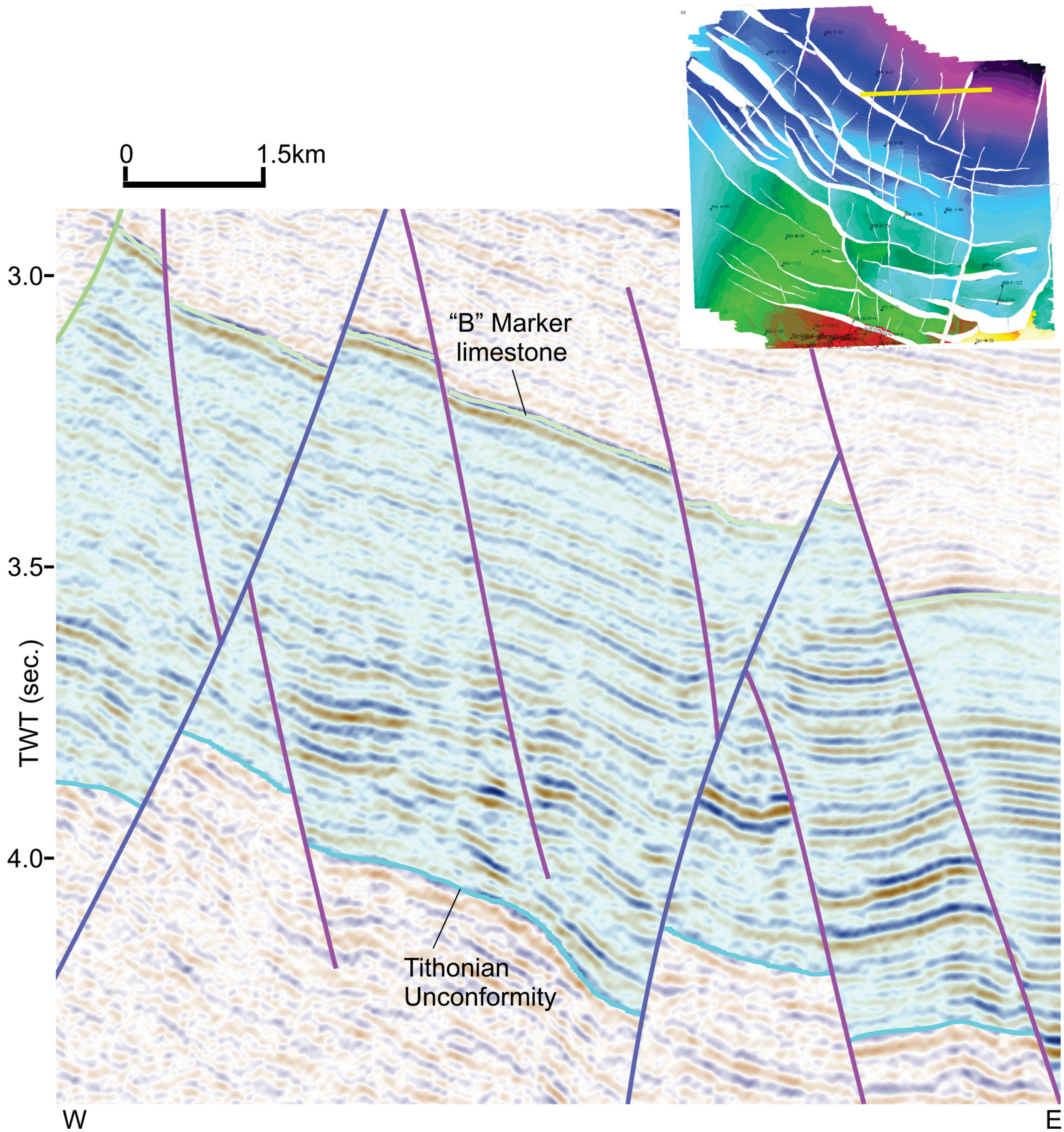

Figure 3.19: Interpreted east-west seismic profile from the Hebron area showing north-south striking crossing conjugate faults. Data courtesy of Husky Energy. The location of the section is shown on a time structure map at the"B" Marker Limestone from the Hebron area.

directly above a horst.

North-south crossing conjugate pairs can be best seen in the north of the Hebron area where there is no younger faulting to complicate the structures (Fig. 3.19). There is thinning of the strata in the fault intersection areas between the "B" Marker limestone and the Tithonian Unconformity from approximately 900 ms two way time to 700 ms two way time.

Across the centre of the Hebron area, the younger northwest-southeast faults (green) offset the earlier north-south faults (purple) (Fig. 3.20). Some of the large north-south faults are not offset, but cause an abrupt change in orientation of the northwest-

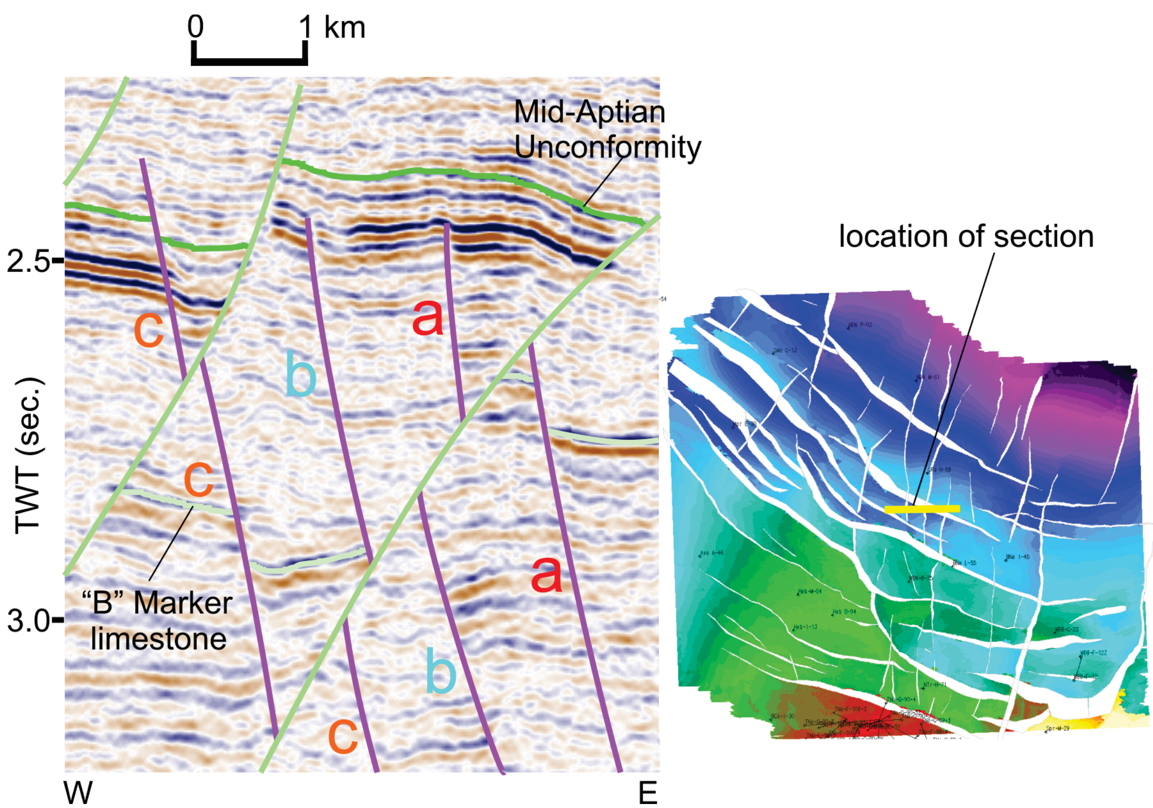

Figure 3.20: Interpreted east-west seismic profile from the Hebron area showing north-south striking faults offset by younger northwest-southeast striking faults. Data courtesy of Husky Energy. The location of the section is shown on a time structure map at the"B" Marker Limestone from the Hebron area.

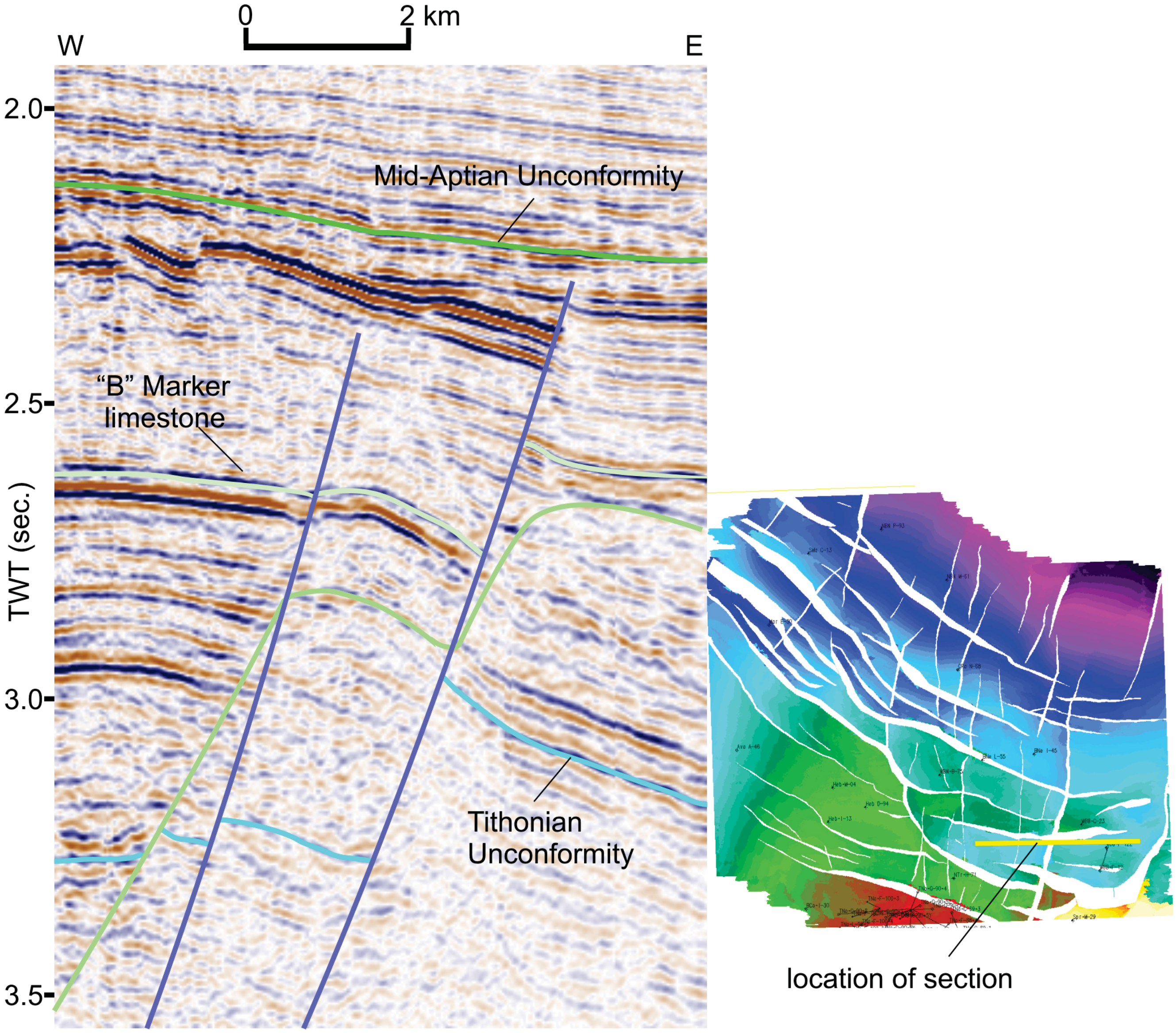

Figure 3.21: Interpreted east-west seismic profile across the Hebron area illustrating a change in trend of the later northwest-southeast striking faults(green) as they cross the earlier north-south striking faults(blue). Data courtesy of Husky Energy. The location of the section is shown on a time structure map at the"B" Marker Limestone from the Hebron area.

southeast faults (Fig. 3.21).

The interaction of faults from rift phase II and faults from rift phase III is complex, hence interpretation and mapping is difficult even with the continuity of the 3D data.

3.4 Transpressional structures associated with oblique slip

There is a strong association between anticlines in the Jeanne d'Arc Basin and oblique-slip fault reactivation of earlier northeast-southwest and north-south striking faults during rift phase III. Oblique slip at a restraining bend in the fault is inferred to cause the formation of compressional structures synchronous with extensional faulting. The recognition of oblique slip during rift phase III has a huge impact on the extension estimates for this rift phase. The pattern of transpressional structures associated with a restraining bend in the fault provides compelling evidence for oblique slip.

3.4.1 Hebron area anticline associated with oblique slip on the Voyager fault

There is a large anticline trending north-northeast-south-southwest across the Hebron area, visible on a time slice at 1828 ms two way time (Fig. 3.22). This is a continuation of the Terra Nova Arch to the south of the Hebron area (Sinclair, 1995 [43]). There is no thinning of strata between the Tithonian Unconformity and the Mid-Aptian Unconformity over the fold indicating that the fold post-dates the Mid-Aptian Unconformity (Fig. 3.23). Strata thin over the fold axis in the Mid-Aptian to Petrel interval inferring that this was the time of growth on the anticline, i.e. during rift phase III (Fig. 3.23). At this time there was extension in a northeast-southwest direction (Fig. 3.13), implying west-northwest-east-southeast compression synchronous with northeast-southwest extension. To the east of the fold the Voyager fault zone changes orientation from northeast-southwest striking to east-west striking. Figure 3.24 shows a series of short seismic profiles around the bend in the Voyager fault. At

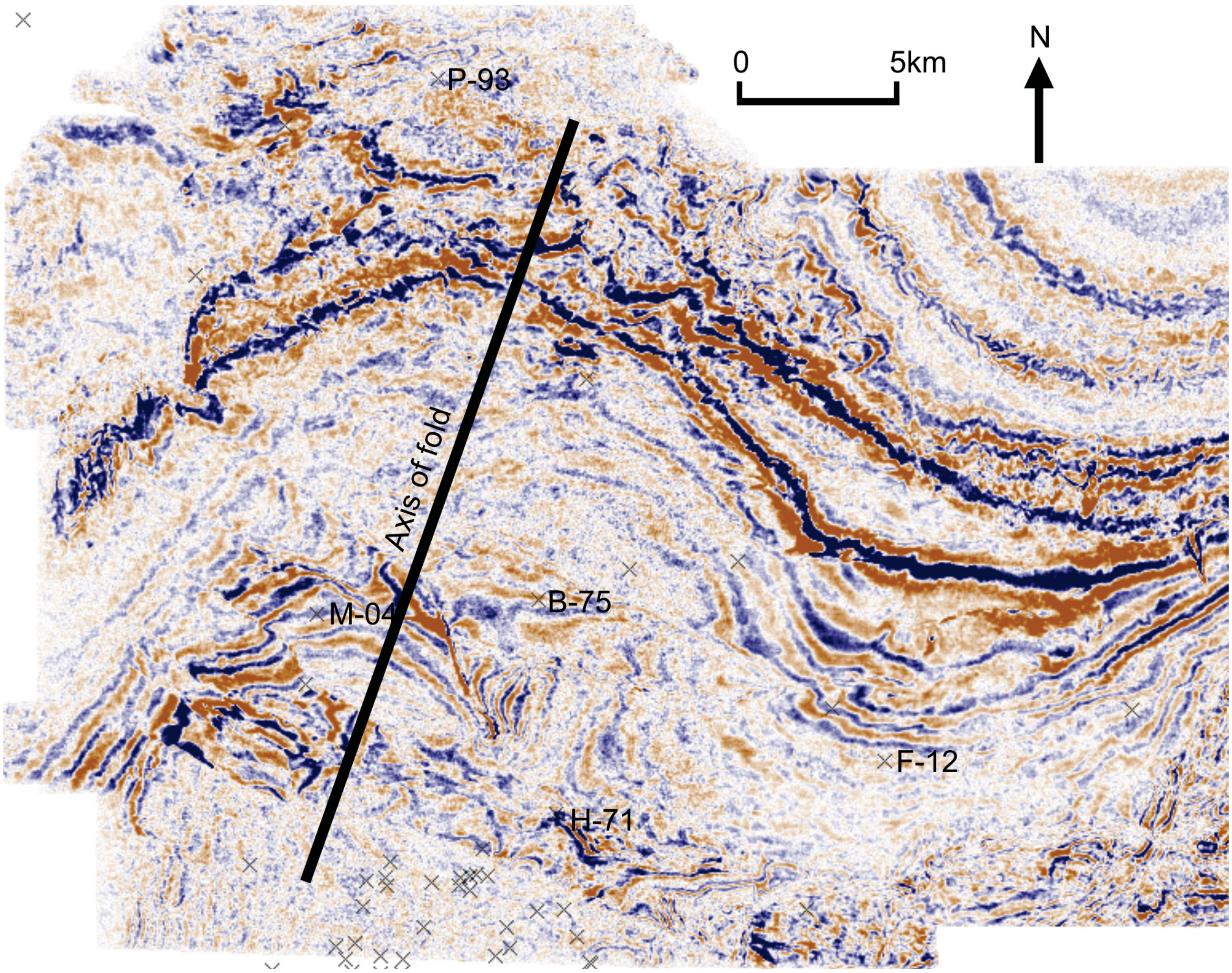

Figure 3.22: Time slice at 1828 ms two way time from the Hebron area, illustrating a large fold. Data courtesy of Husky Energy.

profile e.) the Voyager fault steps east and continues to strike northeast-southwest. There is a large amount of growth across the Voyager fault between the Mid-Aptian Unconformity and the Base Tertiary Unconformity on the east-west striking sections. As the fault changes orientation it is assumed that the rift phase III northeast directed extension was accommodated as dextral oblique slip along the northeast-southwest section of the fault. This created a restraining bend in the fault causing transpression (Fig. 3.25).

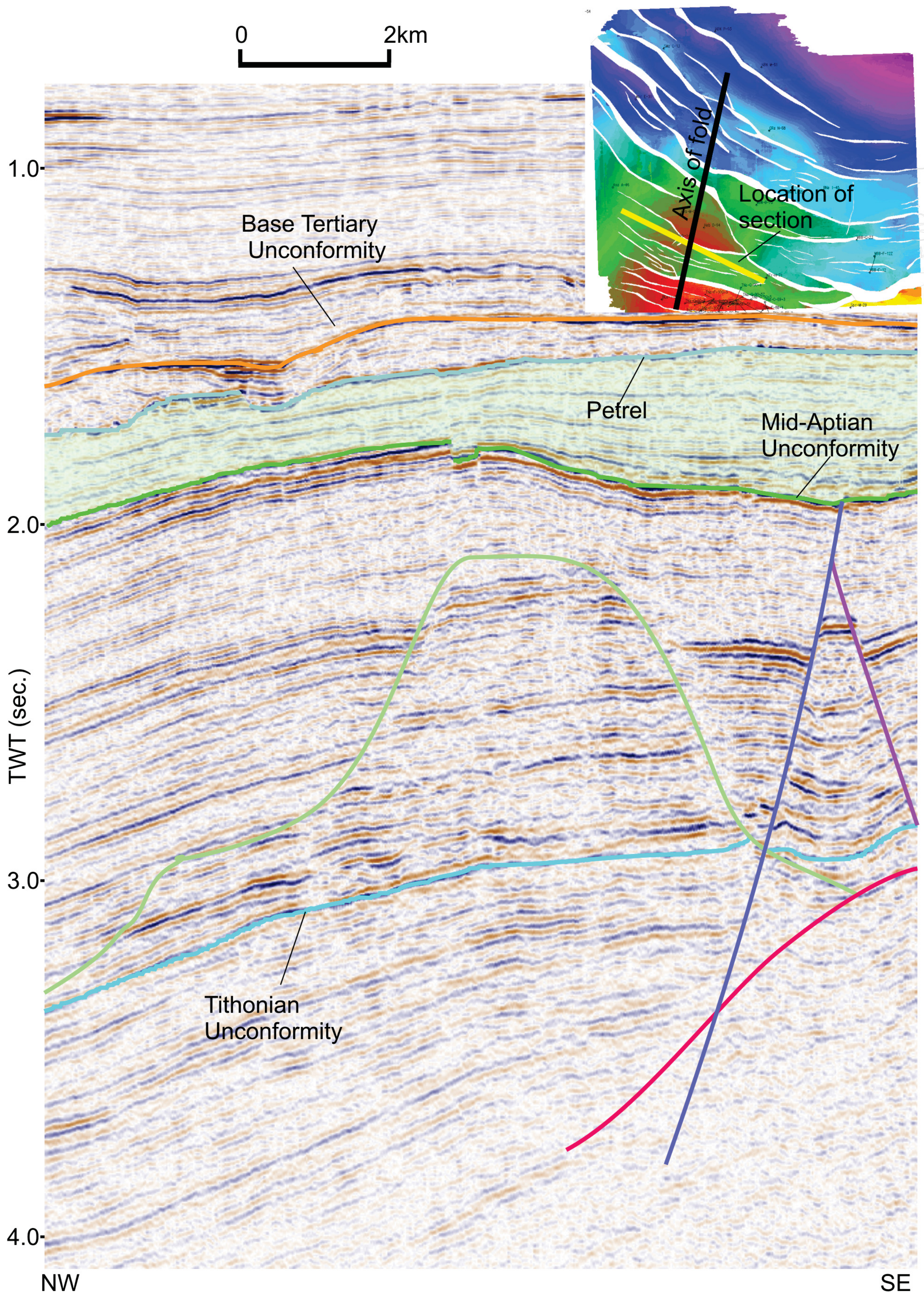

Figure 3.23: Interpreted northwest-southeast seismic profile from the Hebron area illustrating the timing of folding. Data courtesy of Husky Energy. The location of the section is shown on a time structure map at the Mid-Aptian Unconformity from the Hebron area (Section 3.2.3).

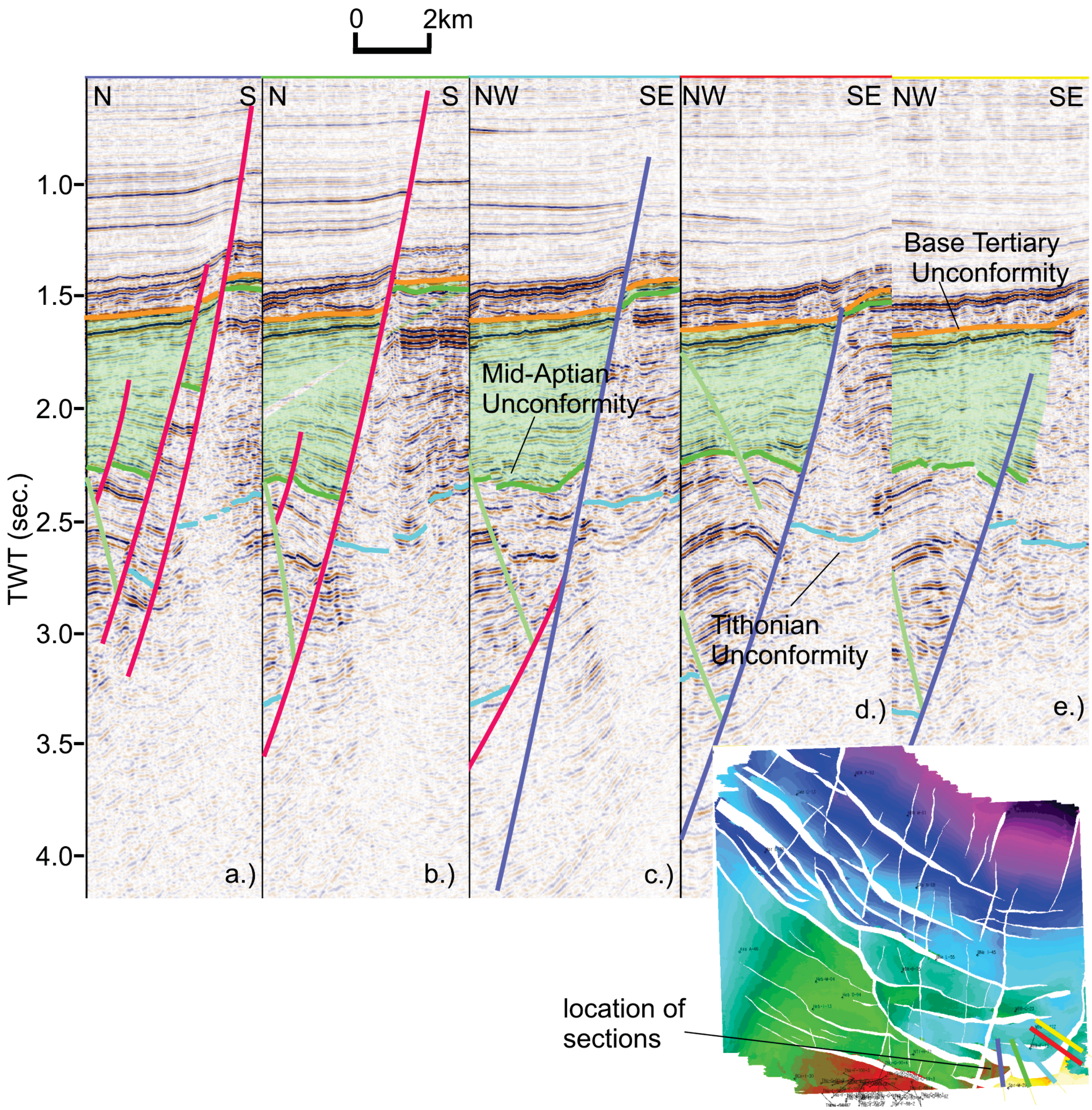

Figure 3.24: A series of short interpreted seismic profiles across the Voyager fault from the Hebron area around a bend in the Voyager fault. Data courtesy of Husky Energy. The location of the sections are shown on a time structure map at the"B" Marker Limestone from the Hebron area.

3.4.2 Hebron area anticline associated with oblique slip on a basin interior fault

There is a smaller anticline in the Hebron area, visible on a time slice at 2828 ms two way time (Fig. 3.26). There is no thinning of the strata over the fold before the

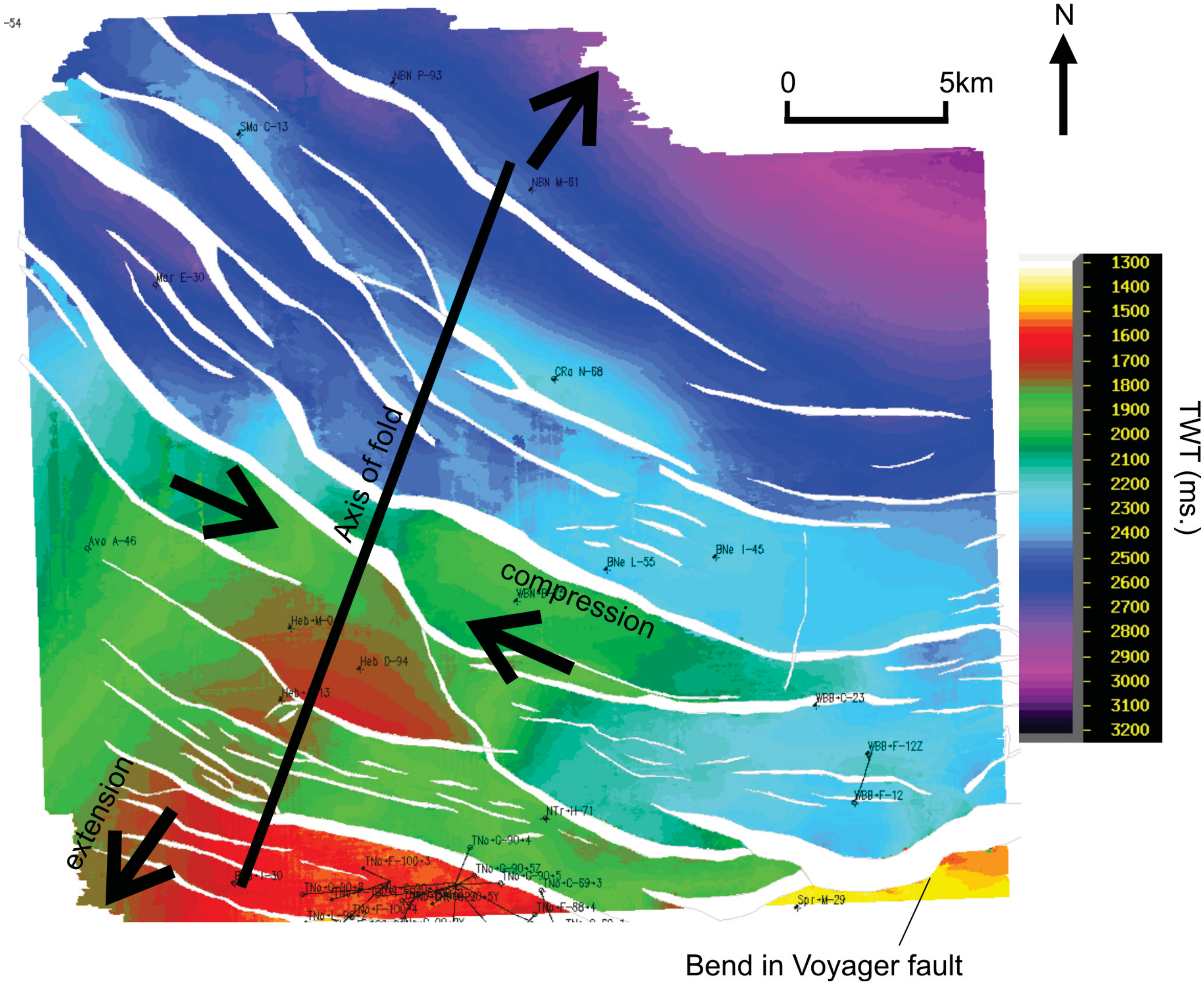

Figure 3.25: Timestructure at the Mid-Aptian Unconformity illustrating Aptian-Albian transpression. Data courtesy of Husky Energy.

Mid-Aptian Unconformity (Fig. 3.27) implying that the fold formed after the Mid-Aptian Unconformity. It is difficult to see growth over the fold after the Mid-Aptian Unconformity from the seismic section because of the interaction with northwest-southeast trending faults running parallel to the section. To the southwest of the anticline there is a kink in one of the major northwest-southeast striking faults, with a segment of the fault trending north-south. Figure 3.28 illustrates a seismic profile

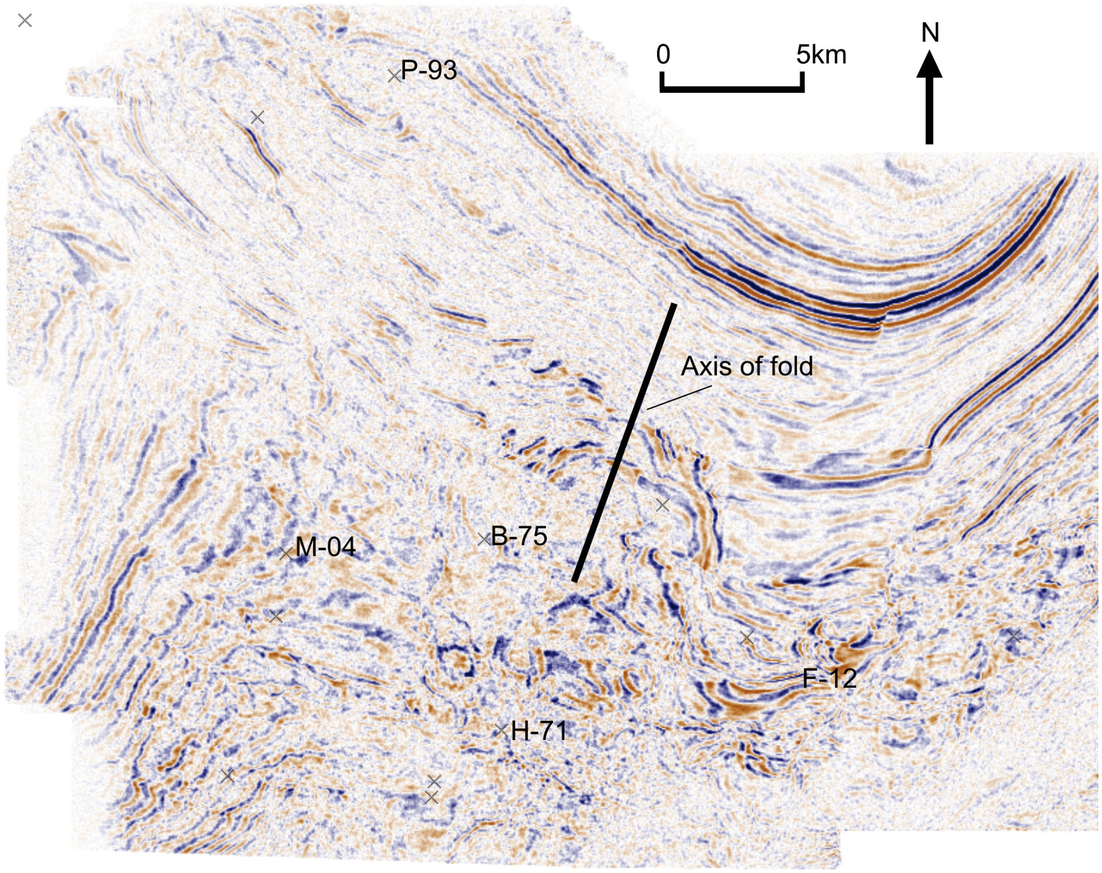

Figure 3.26: Time slice at 2828 ms two way time from the Hebron area, showing a subsidiary fold. Data courtesy of Husky Energy.

through the north-south segment of the fault, showing growth between the Tithonian Unconformity and the "B" Marker limestone and between the "B" Marker and the Mid-Aptian. There is a small amount of growth between the Mid-Aptian and the Petrel, but more of the extension is taken up on an east-west striking fault. The time structure maps show that the fault is north-south striking at the Tithonian level and becomes north-northwest-south-southeast striking at the Mid-Aptian level. It is proposed that the north-south segment of the predominantly northwest-southeast fault was a rift phase II fault reactivated with oblique slip during rift phase III. This caused transpression and formation of the anticline synchronous with northeast-southwest extension during rift phase III (Fig. 3.29). The stratigraphy drapes over

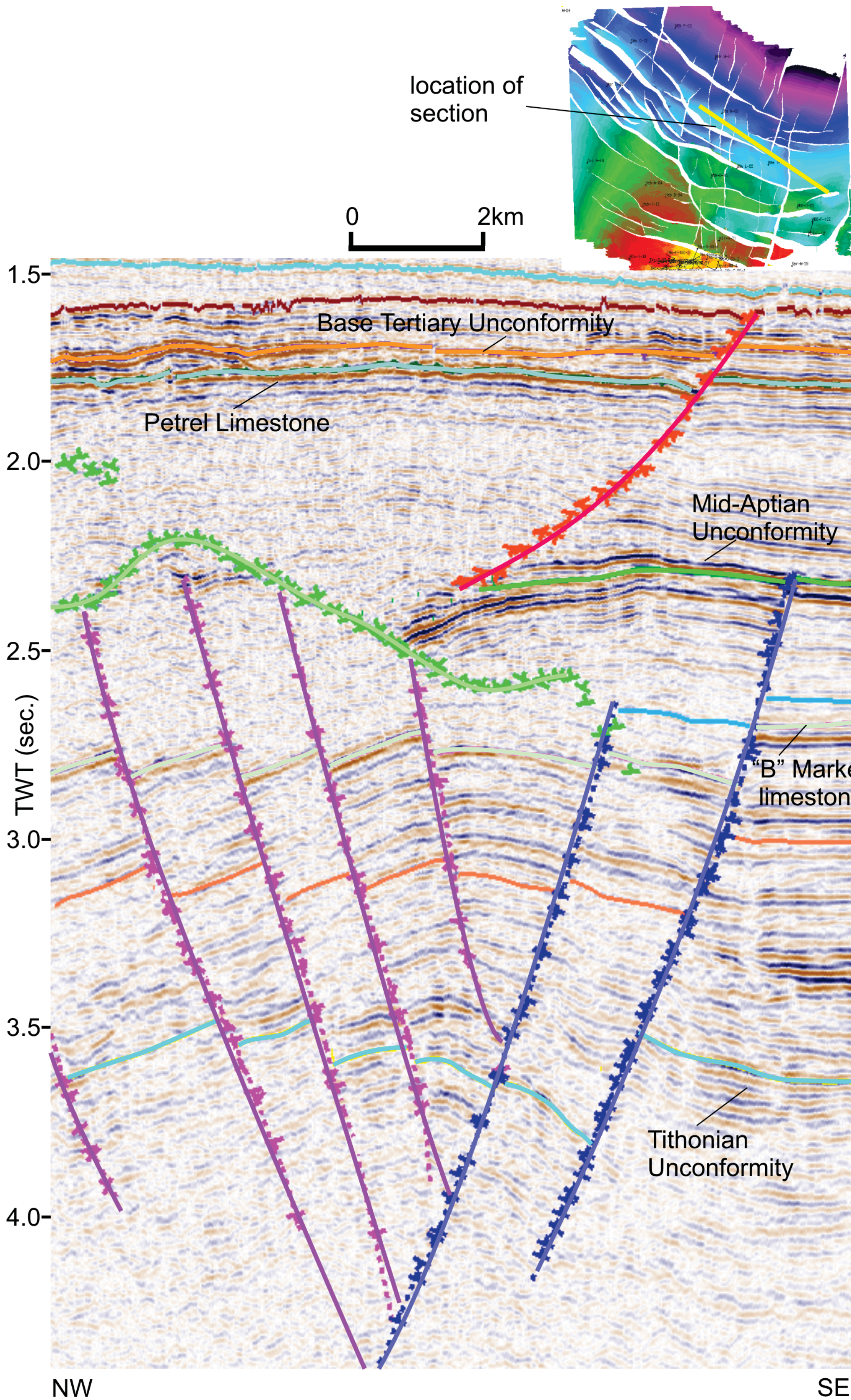

Figure 3.27: Northwest-southeast seismic profile from the Hebron area showing a subsidiary fold. Data courtesy of Husky Energy. The location of the section is shown on a time structure map at the"B" Marker Limestone from the Hebron area. (Note that the Seisworks fault intersections are visible underneath the interpreted faults.)

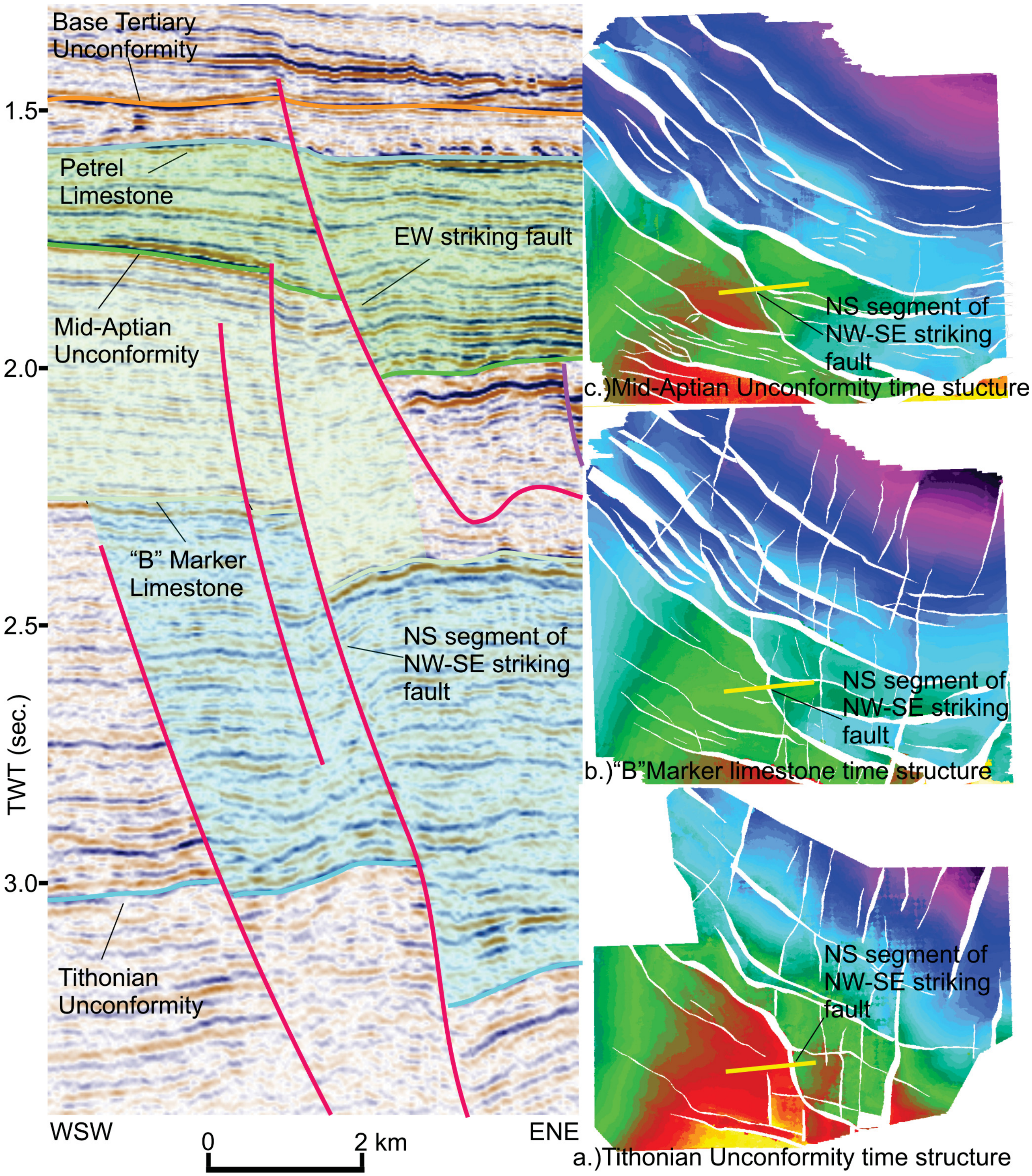

Figure 3.28: West-southwest-east-northeast seismic profile from the Hebron area illustrating growth on a north-south segment of a northwest-southeast striking fault. The time structure maps show that the fault is north-south striking at the Tithonian level and becomes north-northwest-south-southeast striking at the Mid-Aptian level. Data courtesy of Husky Energy.

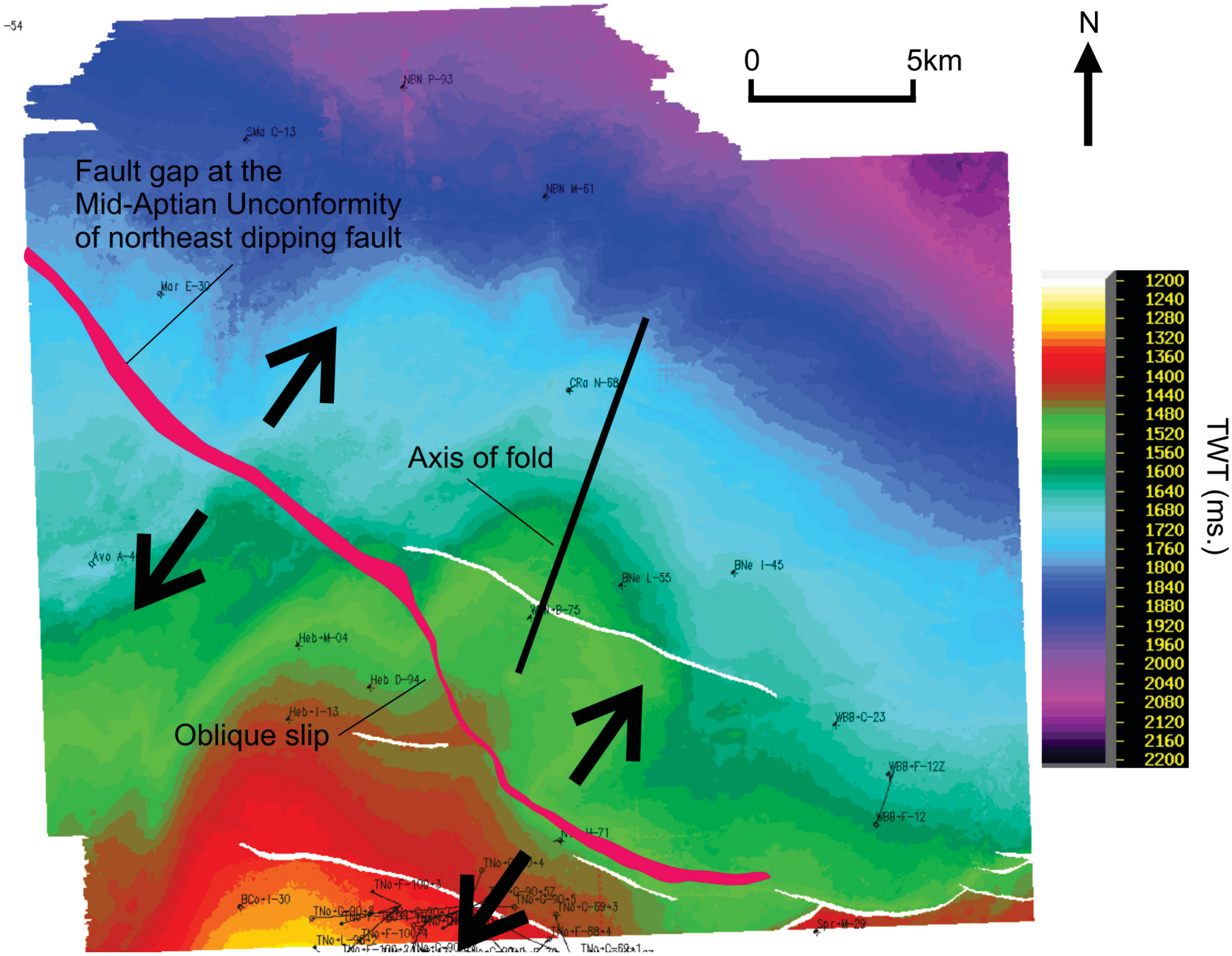

Figure 3.29: Time structure at the Base Tertiary Unconformity from the Hebron area illustrating the relationship of a subsidiary fold to a kink in a large northwest-southeast fault. Data courtesy of Husky Energy.

the fold at the Base Tertiary Unconformity level (Fig. 3.29).

3.4.3 Flying Foam anticline associated with oblique slip on the Mercury fault

The Flying Foam fold is a huge structure dominating the northwest of the Jeanne d'Arc Basin, illustrated on a time slice at 3392 ms two way time from the Flying

Foam 3D dataset (Fig. 3.30). The Flying Foam fold is variously suggested to be an anticline above ramp flat geometry in the footwall of the Mercury fault (Tankard et al., 1989 [50]; McClay, 1989 [29]), an immature salt diapir (Enachescu, 1987 [11]) and an extensional forced fold above a sub-salt normal fault (Withjack and Callaway, 2000 [61]).

On an east-west profile across the Flying Foam anticline, the stratigraphy between the Tithonian Unconformity and the Mid-Aptian Unconformity is fairly uniform in

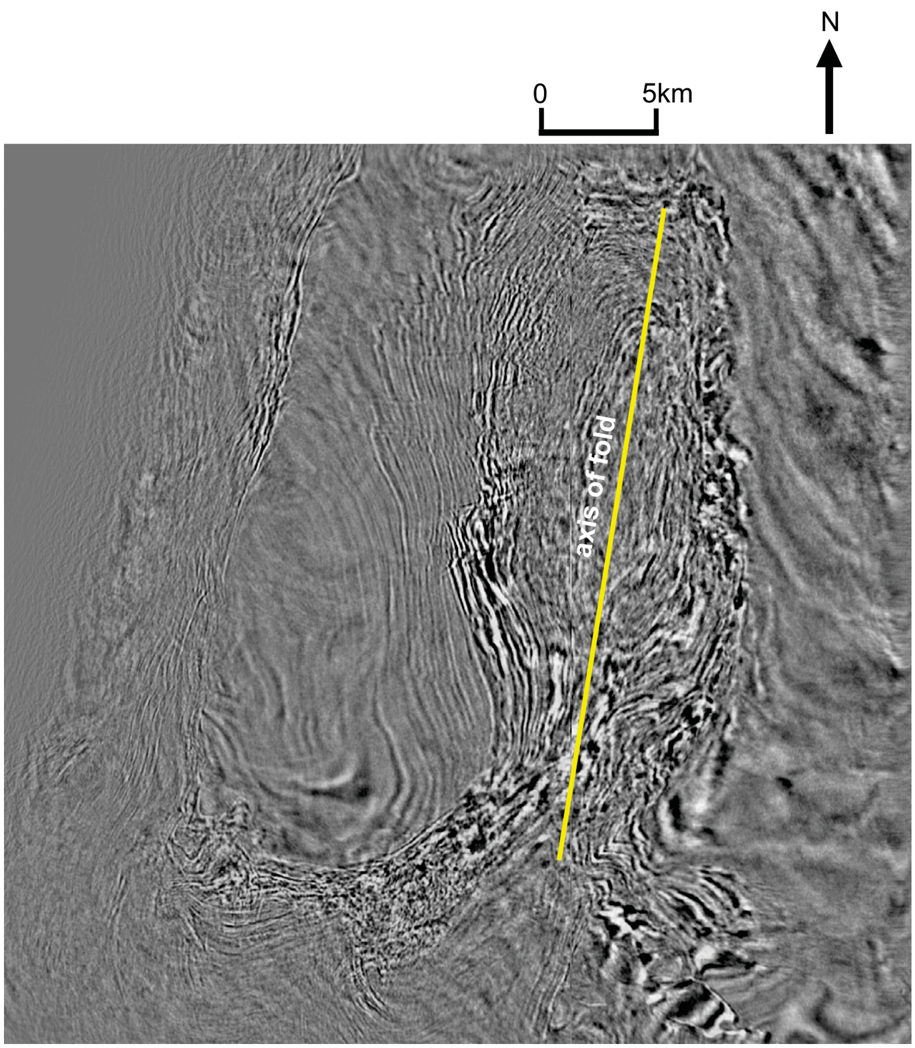

Figure 3.30: Time slice at 3392 ms two way time from the Flying Foam area, illustrating the Flying Foam fold. Data courtesy of WesternGeco.

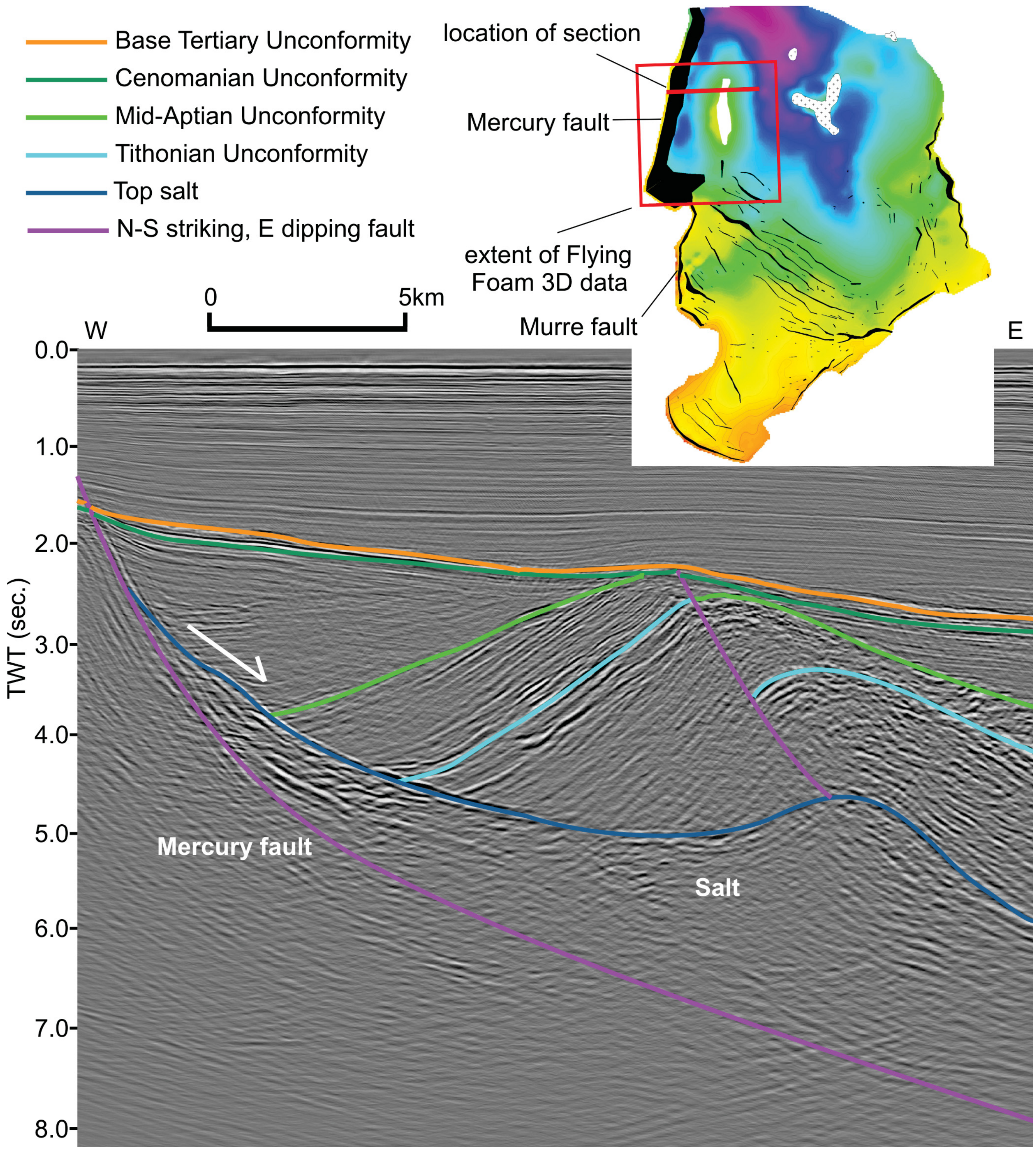

Figure 3.31: East-west seismic profile from the Flying Foam 3D survey, illustrating the Flying Foam fold. Data courtesy of WesternGeco. The location of the section is shown on a time structure map at the Mid-Aptian Unconformity (Section 3.2.3).

thickness on the west side of the fold except over the apex where it is cut, possibly by multiple unconformities (Fig. 3.31). On the east limb of the fold the Mid-Aptian Unconformity cuts into the underlying strata, thinning the Tithonian Unconformity to Mid-Aptian Unconformity interval away from the fold apex. The stratigraphy between the Mid-Aptian Unconformity and the Cenomanian Unconformity thins over the fold with onlap onto the Mid-Aptian Unconformity on the east limb of the fold. The apex of the fold is cut by a north-south trending fault which soles in the salt. There is a large amount of growth above the Mid-Aptian Unconformity across the Mercury fault with a fanning geometry into the fault.

The Murre and Mercury basin boundary faults formed as a series of en echelon faults

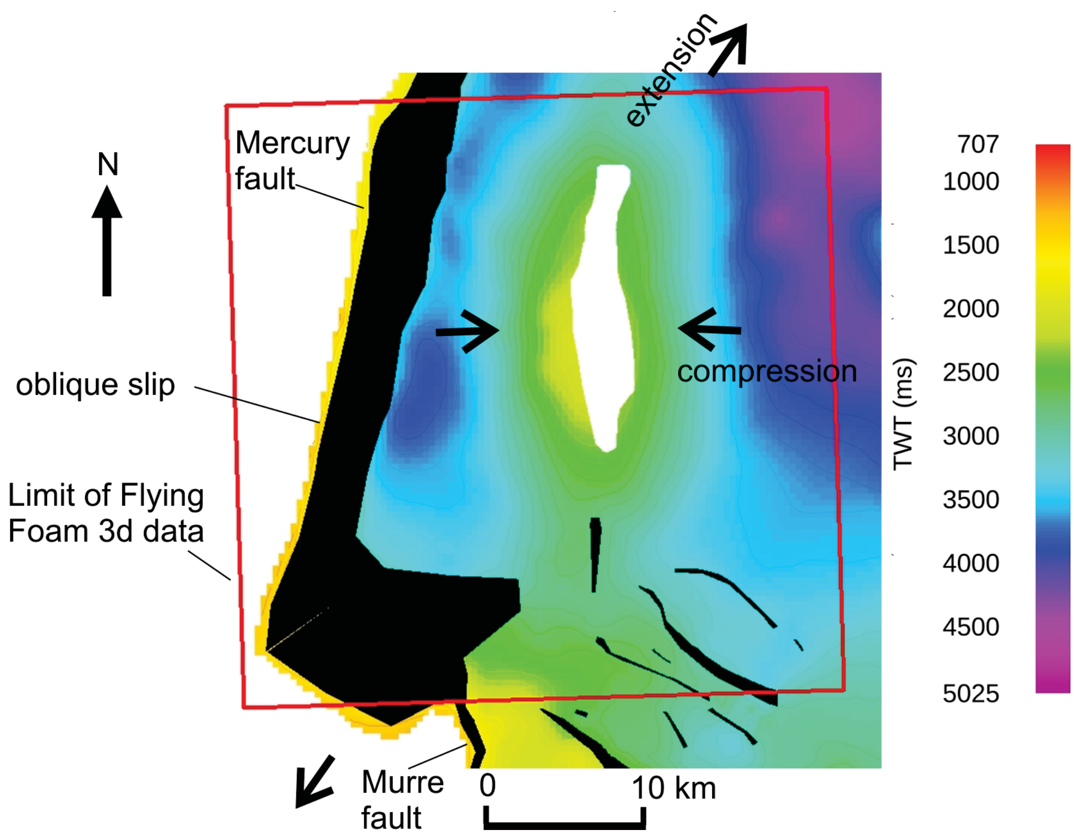

Figure 3.32: Time structure at the Mid-Aptian Unconformity, illustrating the relationship between the Flying Foam fold, oblique slip on the Mercury fault and a major bend in the Murre/Mercury fault.

separated by tilted relay ramps (Sinclair, 1995 [43]; Tankard et al., 1989 [50]). To the southwest of the Flying Foam anticline the Murre fault is offset approximately 11 km to the east of the Mercury fault (Fig. 3.32). It is proposed that the two faults were separated by a tilted relay ramp during the first two rift phases, but with the

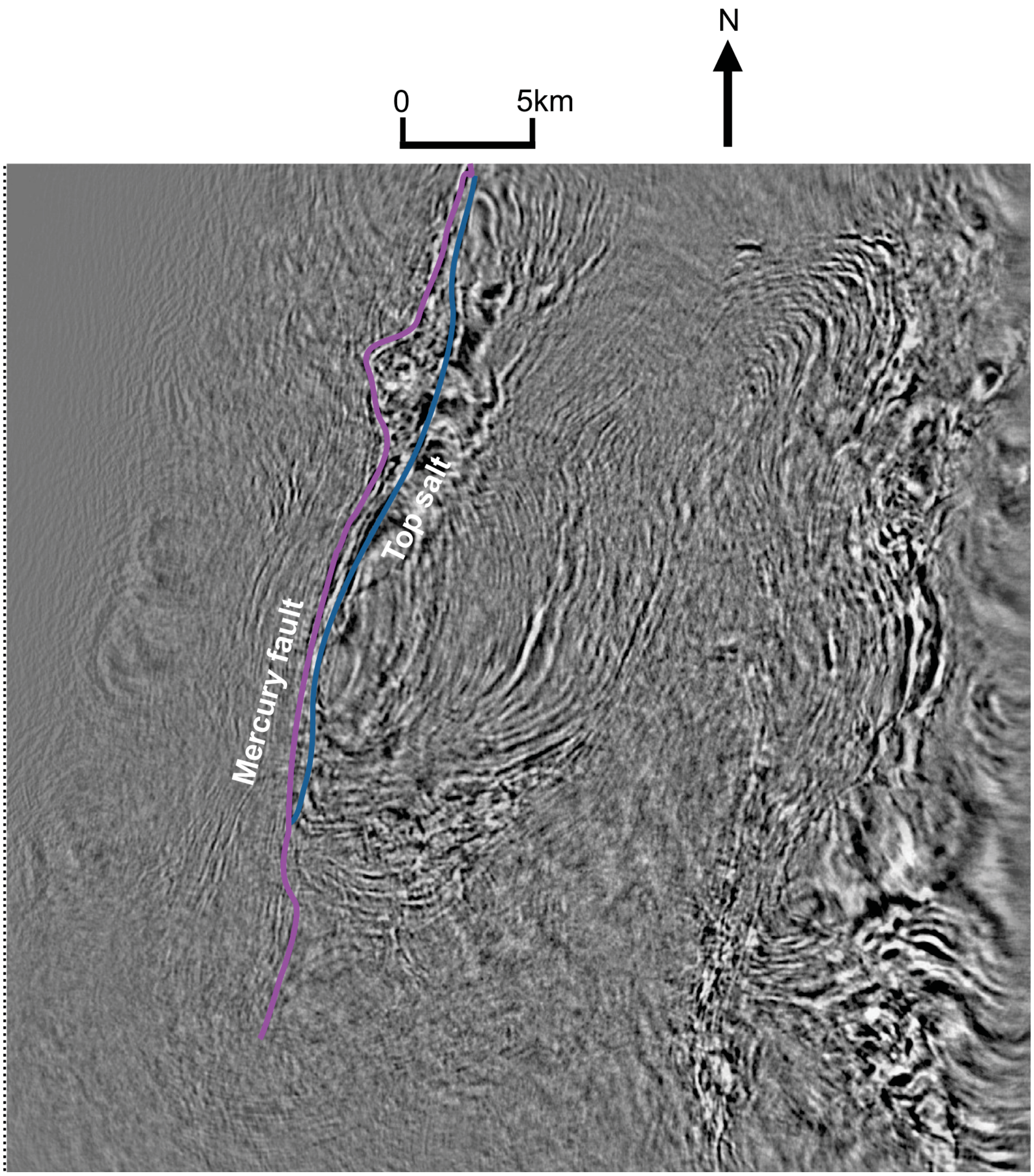

Figure 3.33: Time slice at 4416 ms two way time from the Flying Foam area illustrating a salt wedge along the Mercury fault. Data courtesy of WesternGeco.

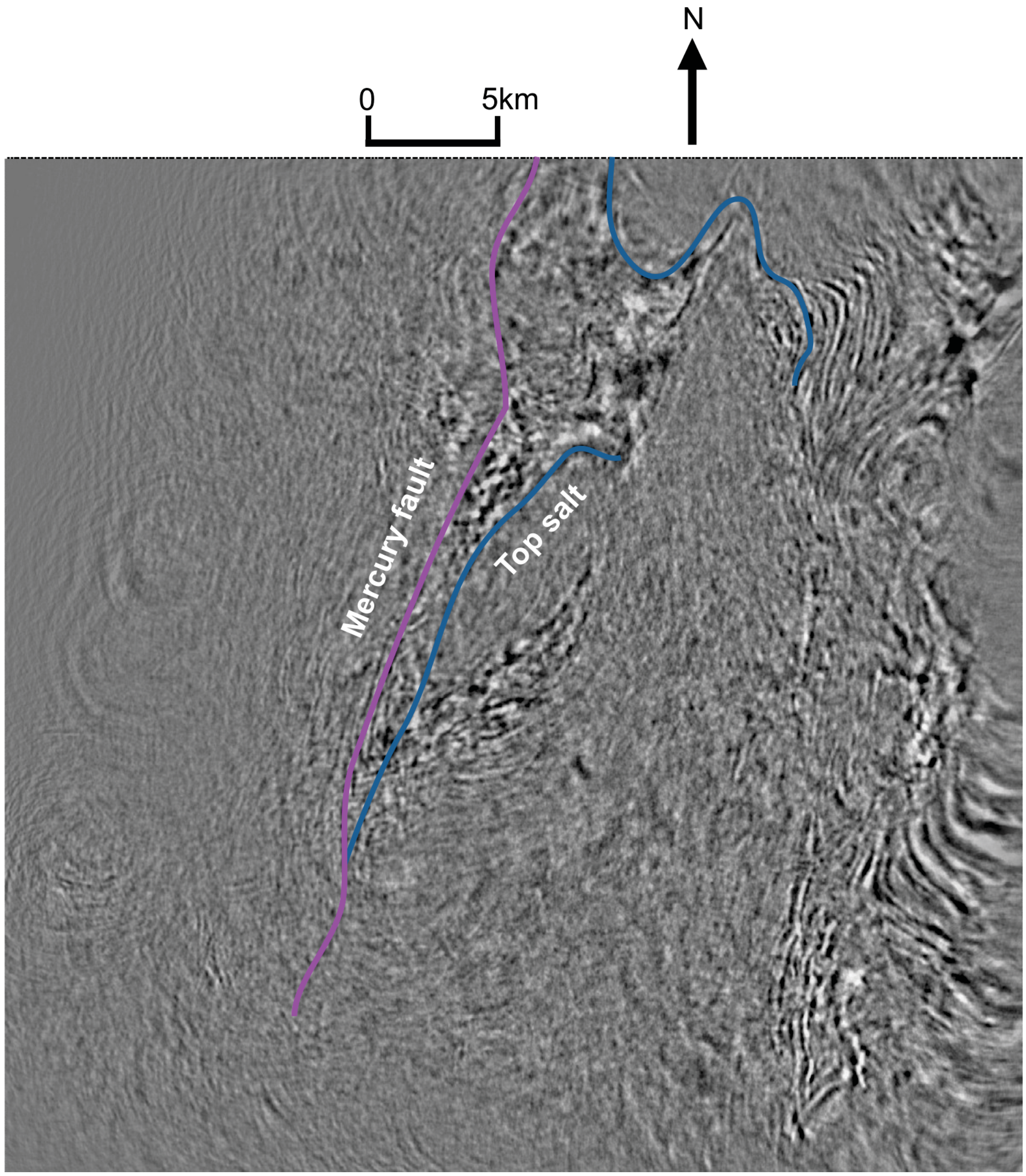

Figure 3.34: Time slice at 5200 ms two way time from the Flying Foam area illustrating a salt wedge along the Mercury fault. Data courtesy of WesternGeco.

onset of northeast-southwest oriented extension the relay structure broke down and a northeast dipping normal fault formed (Fig. 2.16). The Mercury fault formed the boundary between the northeast extending basin and the stable Bonavista Platform, and it is inferred to have been reactivated with oblique slip during rift phase III, causing transpression at the bend in the Murre/Mercury fault and the formation of the Flying Foam fold (Fig. 3.32).

A wedge of salt is interpreted along the Mercury fault on the seismic section (Fig. 3.31), and on time slices at 4416 ms two way time (Fig. 3.33) and 5200 ms two way time (Fig. 3.34) by interpolation of salt along the Murre fault in the Hibernia I-46 wel (Sinclair et al., 1999 [44])l. The salt acted as a detachment surface aiding deformation.

3.5 Salt tectonics

Salt acts as a detachment surface in gravity-driven and basement involved extension, hence basins containing salt deform more easily (Vendeville et al., 1995 [54]).

Evaporites were deposited in the Jeanne d'Arc Basin during the Late Triassic to Early Jurassic and locally exceed 2 km in thickness (Holser et al., 1988 [15]). The evaporites consist of halite interbedded with shale, minor dolomitic mudstones and siltstones in the lower part of the section and massive halite at the top of the section (McAlpine, 1990 [28]). In the south of the basin the salt appears to be in-situ bedded layers, whereas throughout the remainder of the basin there is evidence for salt mobilization (Fig. 3.35 - 3.37). In the north of the basin the Adolphus diapir reaches the water bottom (Fig. 3.36). Salt is weak and incompressible making it inherently unstable.

Bouyancy was originally thought to be an important mechanism for salt diapirism, but it is likely to be secondary to other driving forces. There is a close correlation between crustal extension and salt mobilization, with the onset of salt tectonics frequently coinciding with the onset of a rift phase (Jackson and Vendeville, 1994 [19]). Diapir evolution can progress from reactive growth, through an active phase to pas-

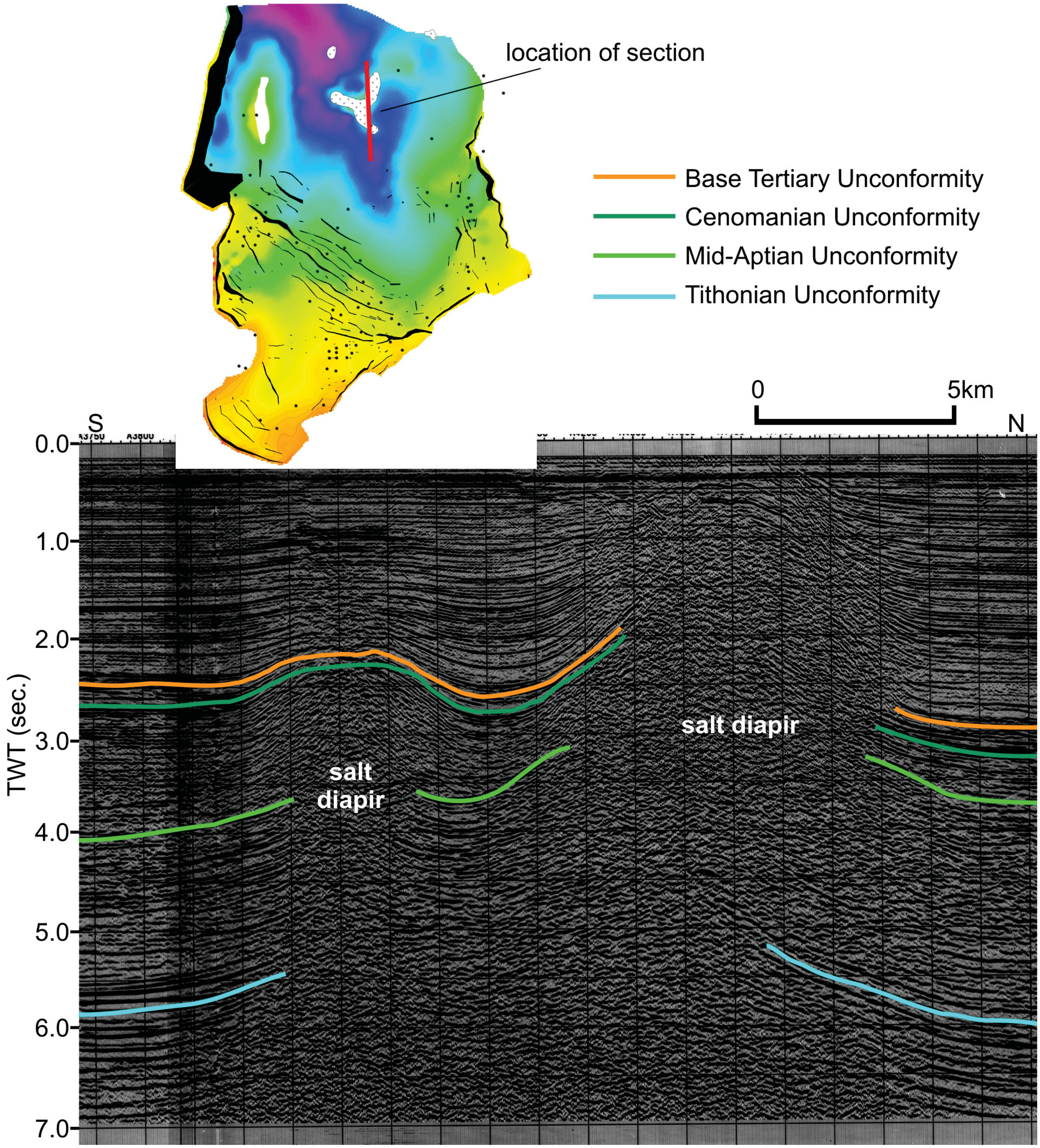

Figure 3.35: Interpreted north-south seismic profile from the SOQUIP survey across the Adolphus salt diapir. Data courtesy of CNLOPB. The location of the section is shown on a time structure map at the Mid-Aptian Unconformity (Section 3.2.3).

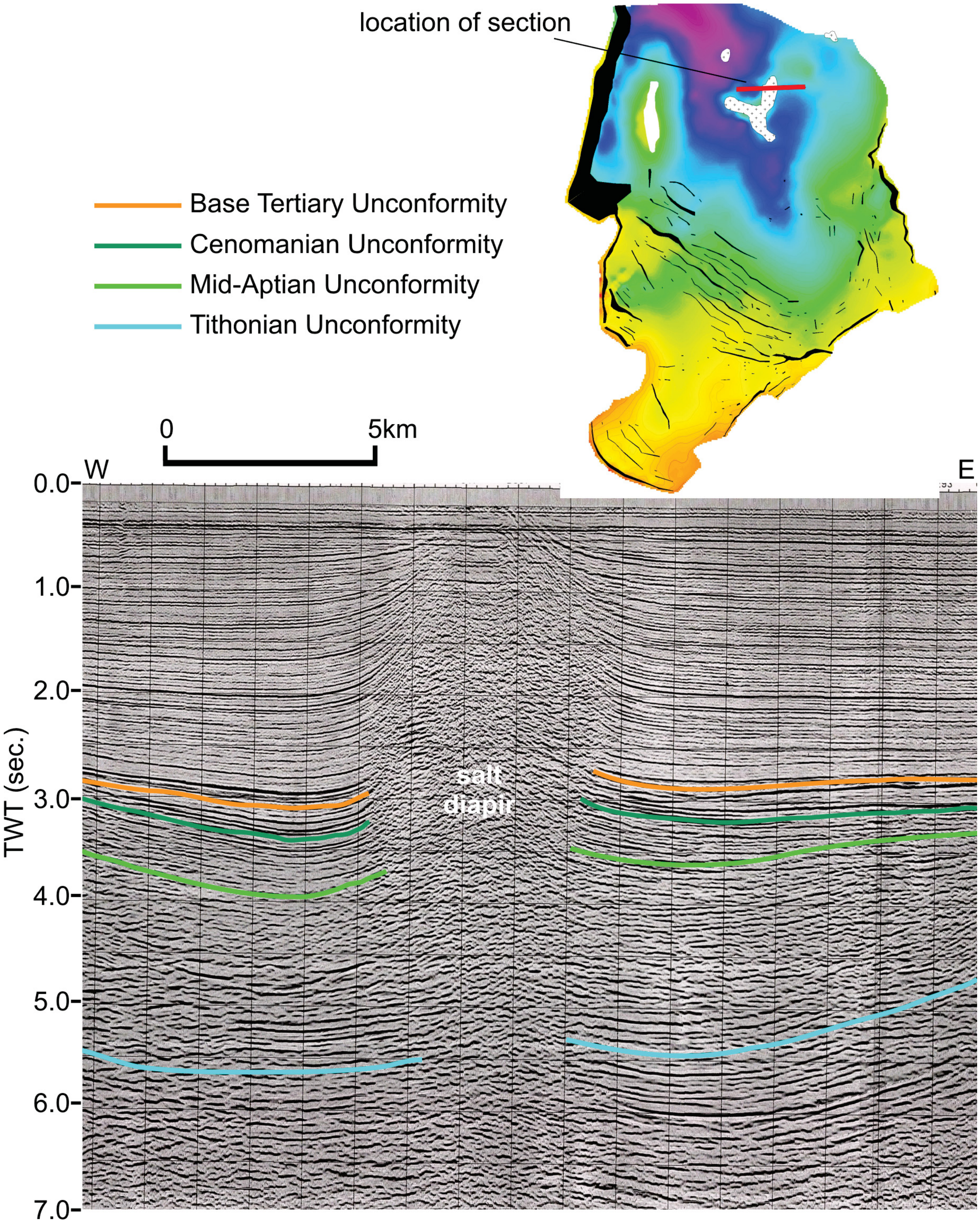

Figure 3.36: Interpreted east-west profile from the SOQUIP survey across the Adolphus salt diapir. Data courtesy of CNLOPB. The location of the section is shown on a time structure map at the Mid-Aptian Unconformity (Section 3.2.3).

sive diapirism (Hudec and Jackson, 2007 [17]). During the reactive phase salt rise is controlled by extension; salt using the space created by fault movement to be emplaced in the overburden (Vendeville and Jackson, 1992 [55]). After extension, salt can continue to be emplaced actively if the salt is less dense than overburden. Active diapirs quickly break through to the sediment surface, where they can grow passively. Sediments thin over the crest of salt features and thicken in basins around the salt.

The most important factor governing diapir growth during extension is the supply of salt. In the Jeanne d'Arc Basin the abundant salt allowed the dramatic Adolphus salt diapir to grow (Figs. 3.35 and 3.36). It is likely that piercement of the Adolphus diapir began as reactive growth during extension at the start of rift phase II. There is indication that the Adolphus diapir subsequently grew actively because the reflectors next to the diapir are arched upwards from the Mid-Aptian Unconformity onwards. If the growth had reached the passive phase the reflectors abutting the diapir would be relatively undeformed. Salt withdrawal basins can be seen on the seismic sections (Figs. 3.35 and 3.36) and as deepening around the Adolphus diapir on the time structure maps (Figs. 4.3 and 4.5). Another example of a salt feature is the Egret salt wall in the south of the basin (Fig. 3.37).

In places there is a sliver of salt along the Murre or Mercury fault (Figs. 3.31, 3.33, 3.34 and 3.38). In the Hibernia area this is present in the Hibernia I-46 well as a wedge of the Eurydice red clastics, the Argo salt, and dolomites and evaporites of the Iroquios Formation (Fig. 1.6) next to the Murre fault (Fig. 3.38). The stacking pattern is not consistent with that found in other wells and slickenslides are common in the dolomites, inferring that slices of the salt, evaporites, clastics and dolomites were sheared and dragged along the fault (Sinclair et al., 1999 [44]). The salt acted as a detachment with slip along the upper surface of the salt, or the salt, clastic,

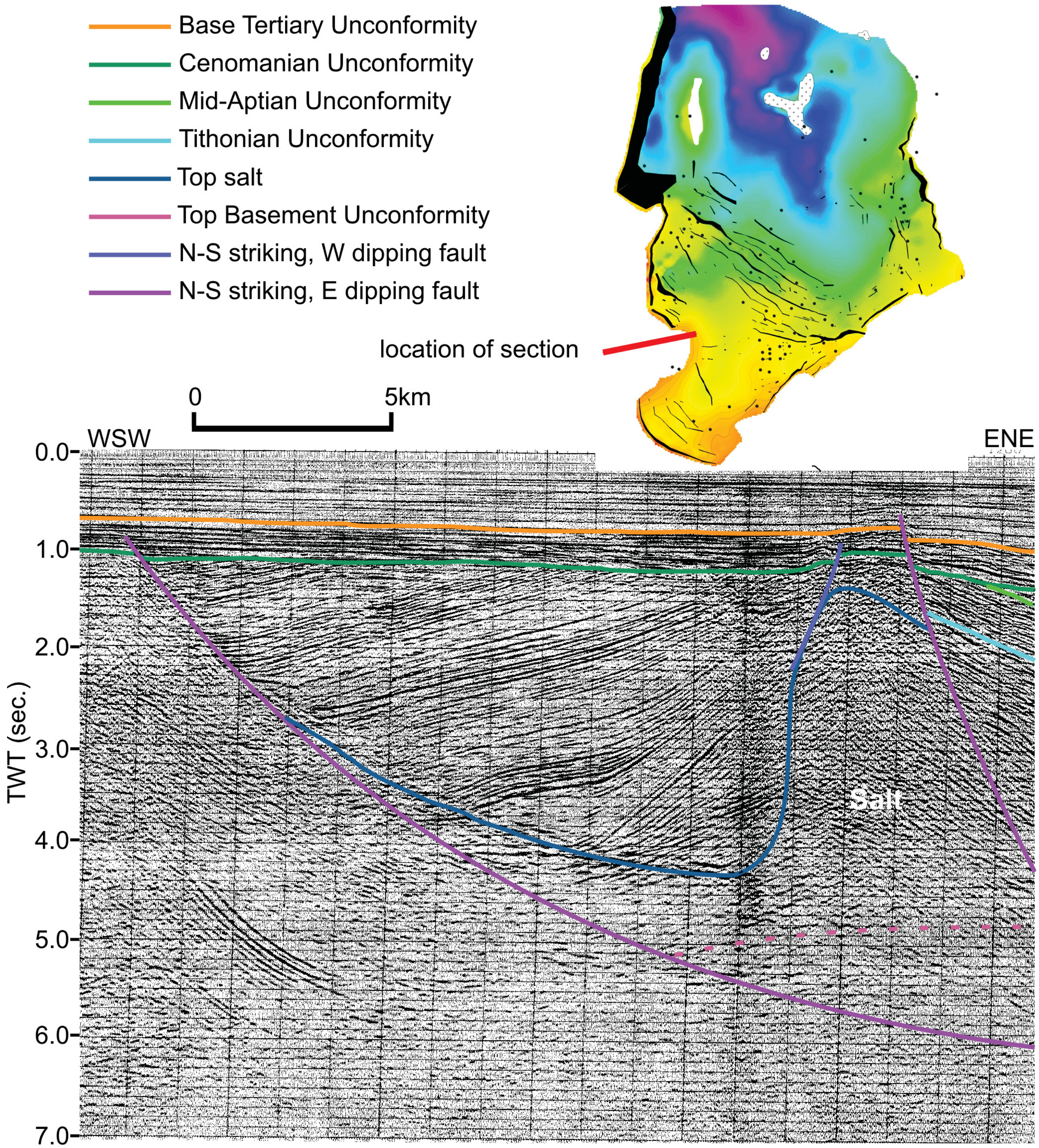

Figure 3.37: Interpreted west-southwest-east-northeast profile from the HBV survey illustrating the Egret salt wall. Data courtesy of CNLOPB. The location of the section is shown on a time structure map at the Mid-Aptian Unconformity (Section 3.2.3).

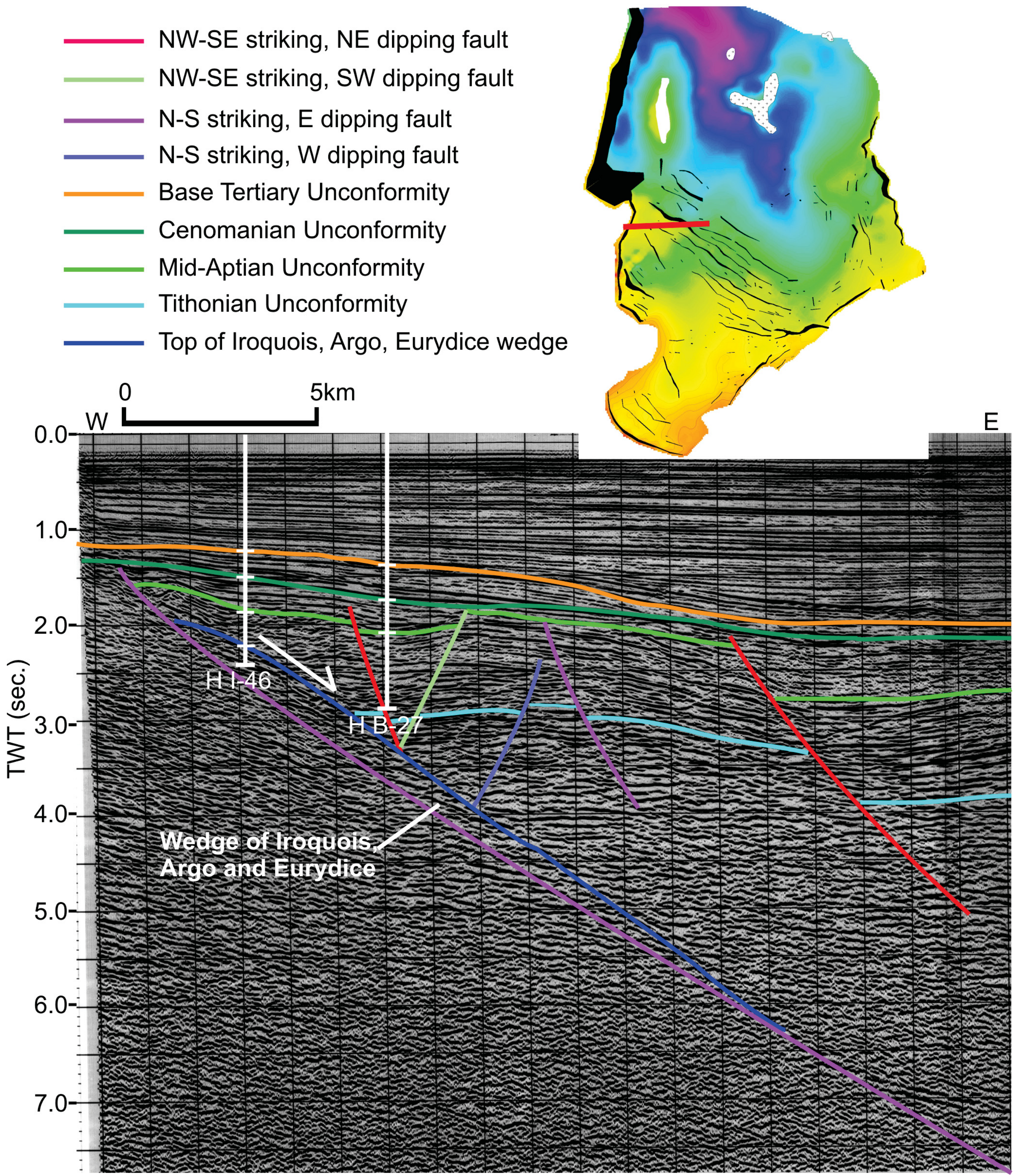

Figure 3.38: Interpreted east-west profile from the SOQUIP survey showing a sliver of salt along the Murre fault. Data courtesy of CNLOPB. The location of the section is shown on a time structure map at the Mid-Aptian Unconformity (Section 3.2.3).

dolomite and evaporite mix. Despite evidence for salt movement within the basin, it has not been possible to clarify the role of salt tectonics on faulting within the basin due to poor imaging at the depth of the salt.

3.6 Summary of the timing and direction of extension in the Jeanne d'Arc Basin

The Jeanne d'Arc Basin formed during rift phase I in the Late Triassic to Early Jurassic (228 Ma - 186 Ma). The border faults trend northeast-southwest indicating northwest-southeast oriented extension direction during rift phase I. The border faults were reactivated during rift phase II and a new set of north-south striking internal basin faults formed. The extension direction during rift phase II is assumed to be east-west perpendicular to the predominant fault trend. Rift phase II commenced at the Tithonian Unconformity and continued until just before the Mid-Aptain Unconformity (150 Ma - 112 Ma). Most north-south faults tip out below the Mid-Aptian Unconformity and a new set of northwest-southeast oriented internal basin faults formed during the Aptian to Albian rift phase III (112 Ma - 96 Ma), indicating a northeast-southwest extension direction. There is a pattern of folding synchronous with extension during rift phase III. Transpressional structures are inferred to have been caused by oblique slip at a restraining bend in the fault. Northeast-southwest oriented oblique slip reactivation of border faults and some segments of north-south internal basin faults during the rift phase III is assumed. There was minor slip on large faults during the Late Cretaceous and into the Cenozoic.

Unravelling the interaction between crossing conjugate faults is complex with the continuity of the 3D data. Imaging and interpreting cross cutting faults using 2D data leads to an underestimation of extension (Fig. 2.21 and Fig. 2.22).

Salt deposited during rift phase I was mobilized during and subsequent to rift phase II. Salt withdrawal basins formed around huge salt diapirs in the North of the basin resulting in a marked deepening of the basin. Salt acted as a detachment surface aiding deformation. There was slip on the upper surface of salt wedges along the Murre and Mercury faults during extension.

Chapter 4

Extension and reconstruction through time of the Jeanne d'Arc Basin

4.1 Introduction

Chapter 3 established the timing and direction of extension in the Jeanne d'Arc Basin. This chapter shows the incremental extension for each rift phase obtained by summing fault heaves along measurement lines across the basin (Section 2.2.3). The extension estimates are displayed on the time structure maps introduced in Chapter 3. Fault heave measurements were used to create beta grids for each rift phase (Section 2.2.4). The beta grids were used to restore the time structure maps to their position before each rift phase using GeoArctic's proprietary PlateDEF software (GeoArctic Ltd. website [13]), which models deformable plate margins (Chapter 5). The GeoArctic plate model is derived from work funded jointly by the Irish Shelf Petroleum Studies

Group (ISPSG) of the Petroleum Infrastructure Programme (PIP) and Nalcor Energy.

4.2 Time structure maps illustrating extension during each rift phase

The following time structure maps illustrate the extension during each rift phase (Figs. 4.1 - 4.8). Each rift phase has two maps: 1.) showing the basic extension values and 2.) showing values based on double extension on the internal faults (Section 2.2.6) to account for the extension discrepancy between the 2D data and the 3D data (Section 2.2.5).

4.2.1 Rift phase I

The extension measurements for rift phase I were obtained by measuring the component of heave (Fig. 2.14) in the measurement direction across each fault at the Top Basement Unconformity level, and subtracting the component of heave on that fault at the Tithonian Unconformity level (Fig. 2.15). Dip slip motion was assumed. Figure 4.1 shows the extension across the basin for rift phase I produced by summing the extension measurements from each fault along the measurement lines. Figure 4.2 shows the extension across the basin using the double extension measurements (Section 2.2.6).

Extension during rift phase I increases from approximately 8 km across the south of the basin to around 16 km across the centre of the basin and then decreases to about 7 km further north (Fig. 4.1). Some of the extension is probably missing from the estimates in the north of the basin where mapping of the Top Basement is limited

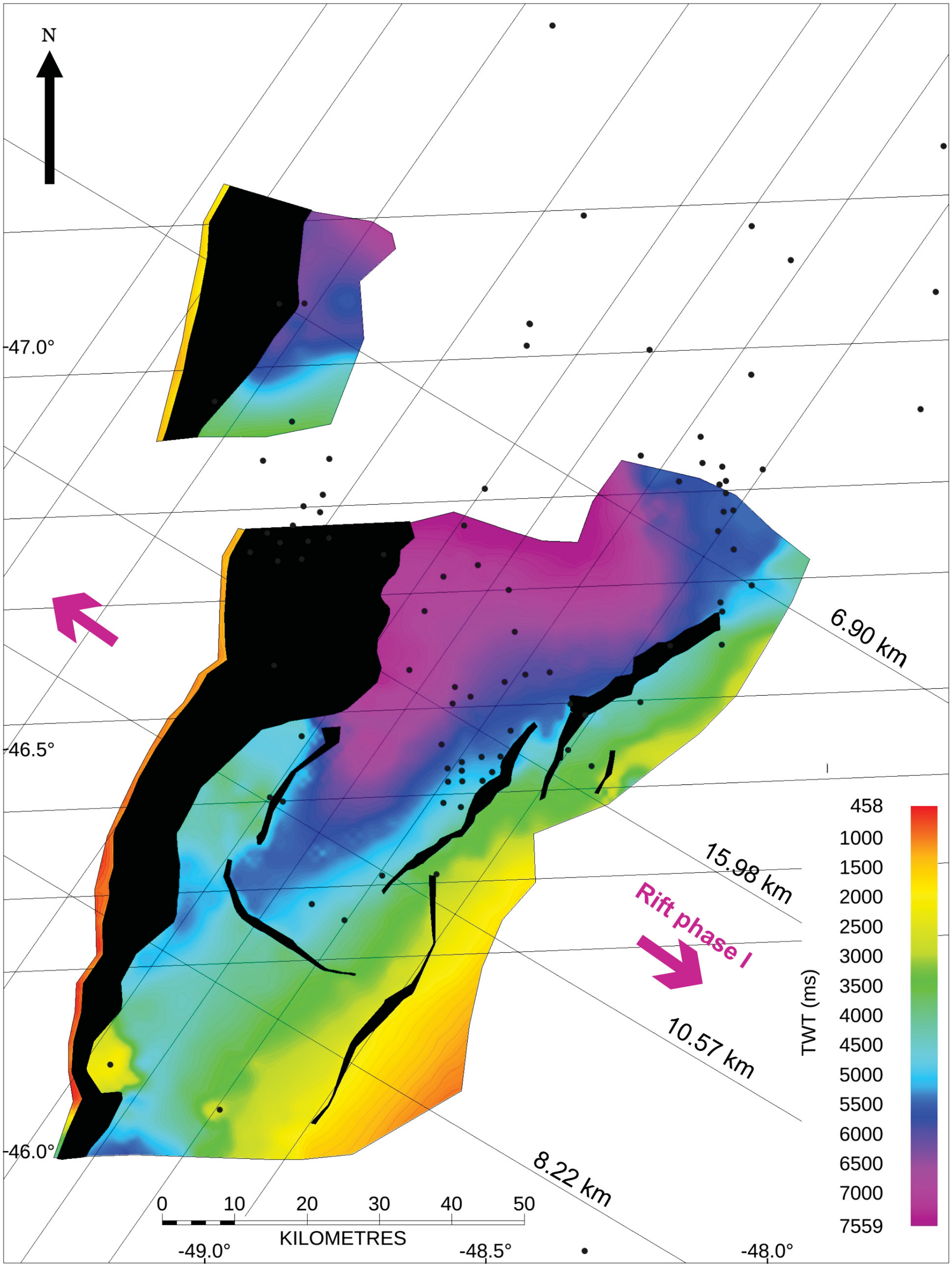

Figure 4.1: Time structure map of the Top Basement Unconformity showing extension estimates across the basin during rift phase I in a northwest-southeast direction.

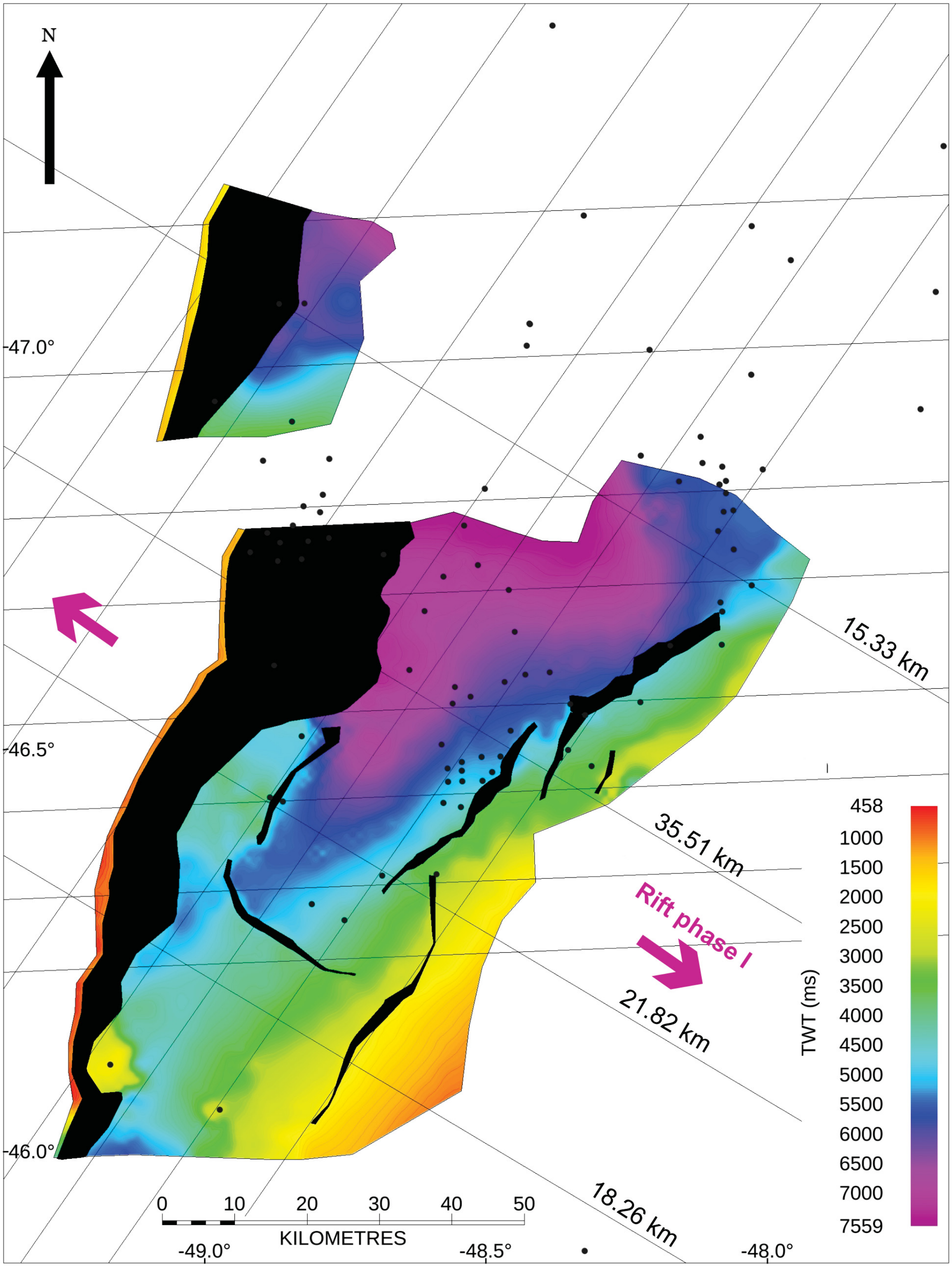

Figure 4.2: Time structure map of the Top Basement Unconformity showing double extension estimates across the basin during rift phase I in a northwest-southeast direction.

by the depth extent of the seismic (Fig. 3.5). Using the double extension estimates (Section 2.2.6), extension during rift phase I increases from around 18 km across the south of the basin to 35 km across the centre and decreases to about 15 km further north (Fig. 4.2).

4.2.2 Rift phase II

The extension measurements for rift phase II were obtained by measuring the component of heave (Fig. 2.14) in the measurement direction across each fault at the Tithonian Unconformity level, and subtracting the component of heave on that fault at the Mid-Aptian Unconformity level (Fig. 2.15). Dip slip motion was assumed. Figure 4.3 shows the extension across the basin for rift phase II produced by summing the extension measurements from each fault along the measurement lines. Figure 4.4 shows the extension across the basin using the double extension measurements (Section 2.2.6).

Extension during rift phase II increases from 0.72 km across the south of the basin to 8.6 km across the centre of the basin and then decreases to 5.0 km across the north of the basin (Fig. 4.3). Using the double extension estimates (Section 2.2.6), extension during rift phase II increases from around 0.14 km across the south of the basin to about 12 km across the centre and decreases to about 7 km across the north of the basin (Fig. 4.4)

4.2.3 Rift phase III

The extension measurements for rift phase III were obtained by measuring the component of heave (Fig. 2.14) in the measurement direction across each fault at the

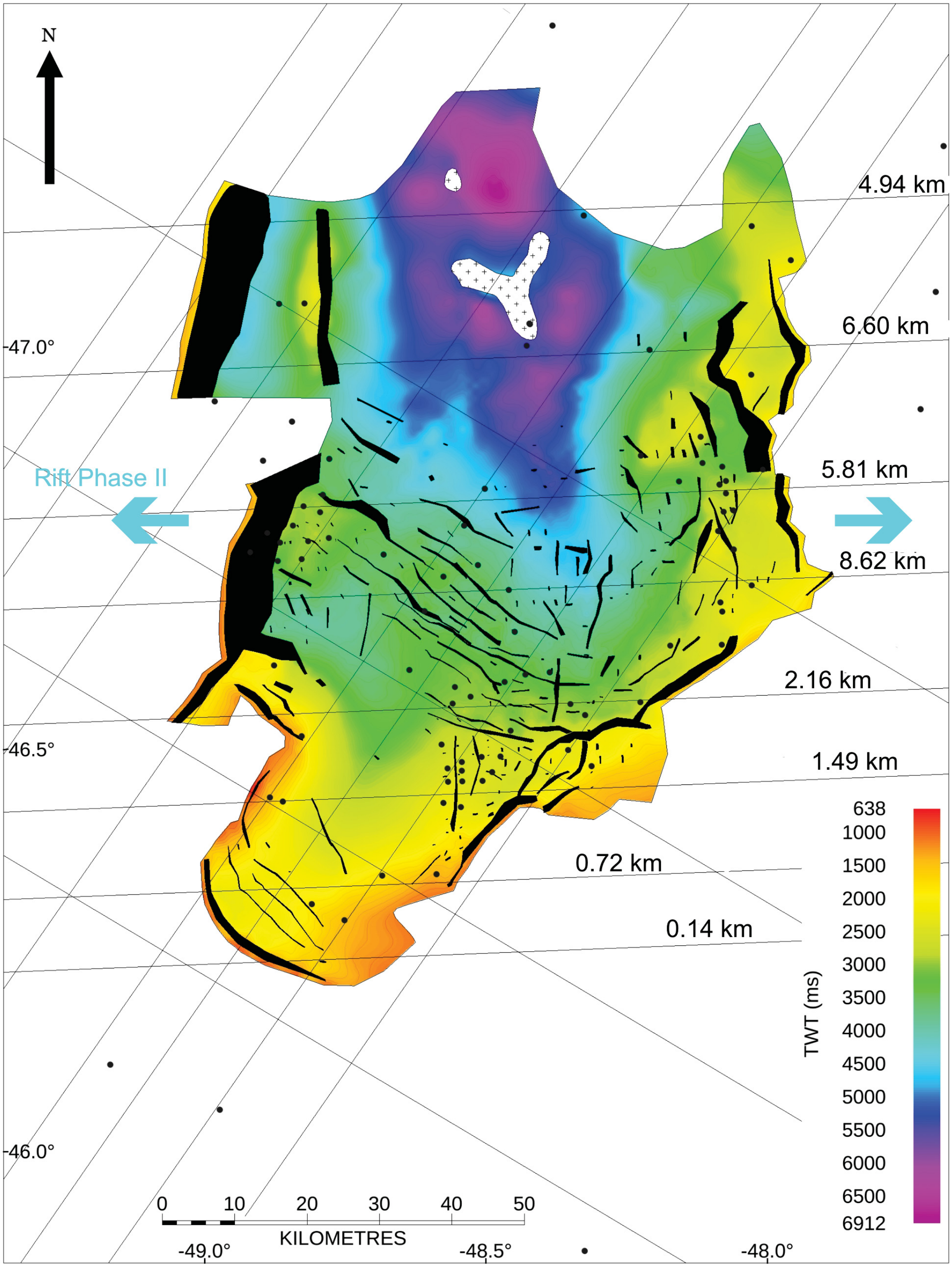

Figure 4.3: Time structure map of the Tithonian Unconformity showing extension estimates across the basin during rift phase II in an east-west direction.

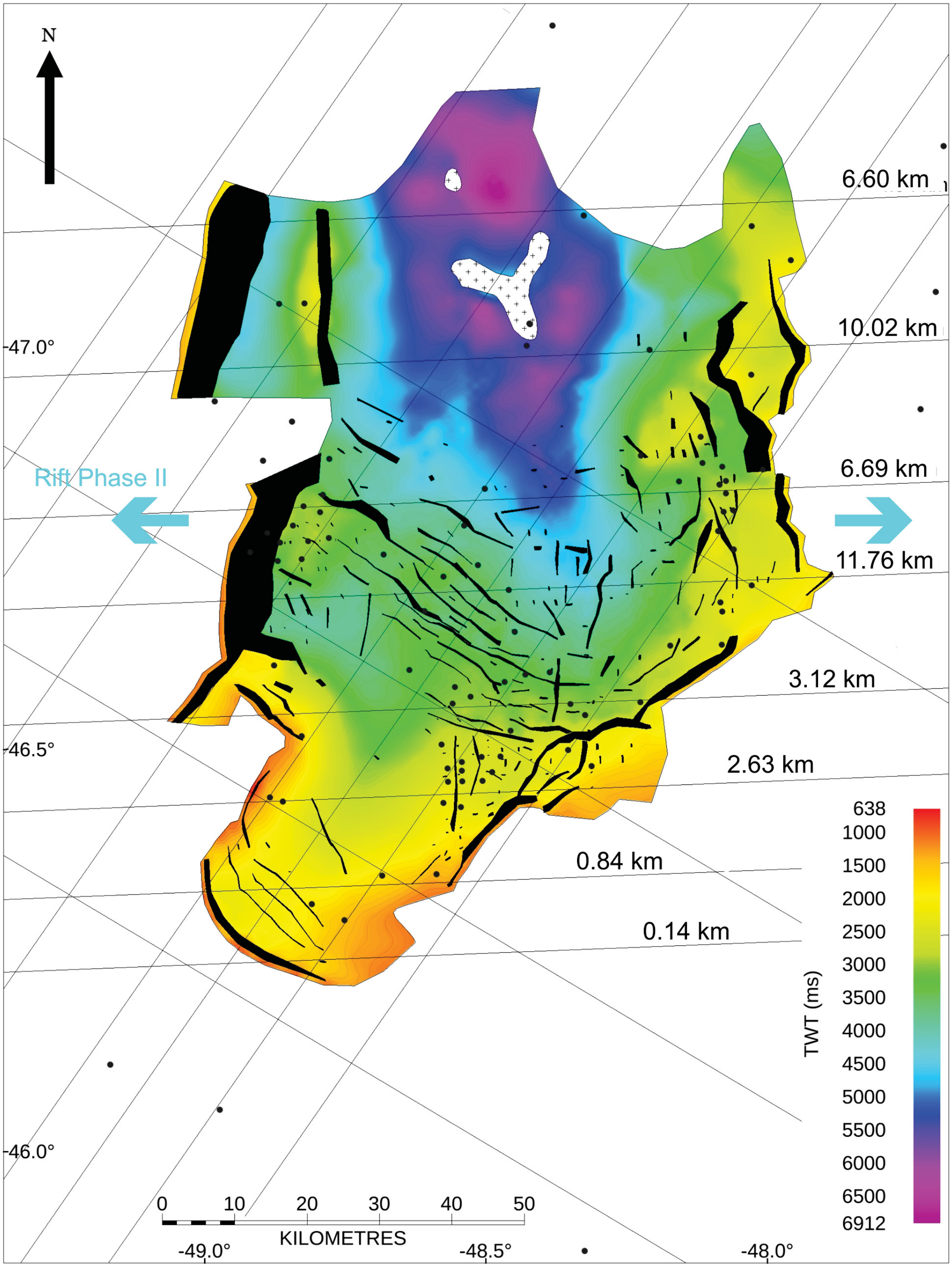

Figure 4.4: Time structure map of the Tithonian Unconformity showing double extension estimates across the basin during rift phase II in an east-west direction.

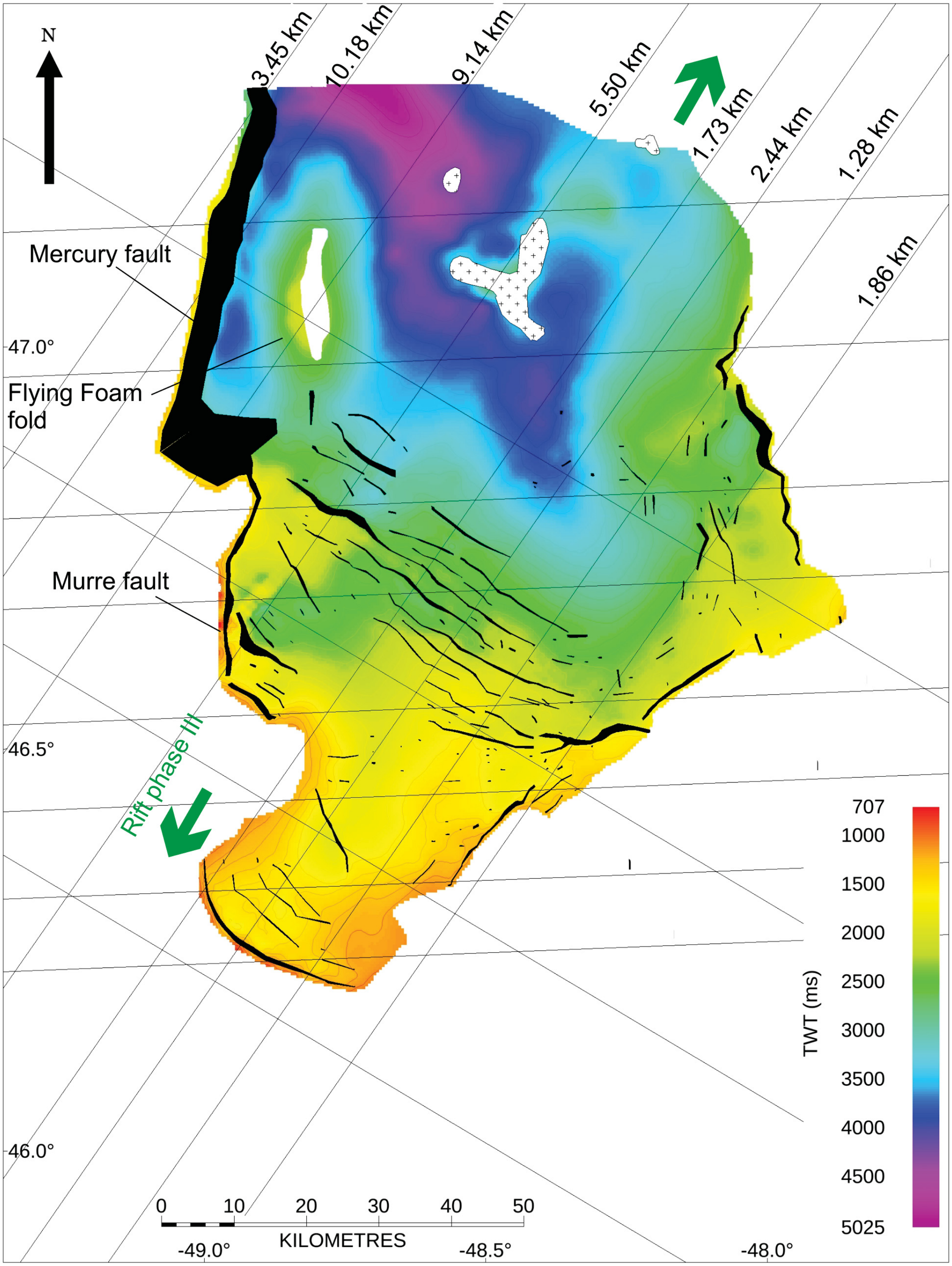

Figure 4.5: Time structure map of the Aptian Unconformity showing extension estimates across the basin during rift phase III in an northeast-southwest direction.

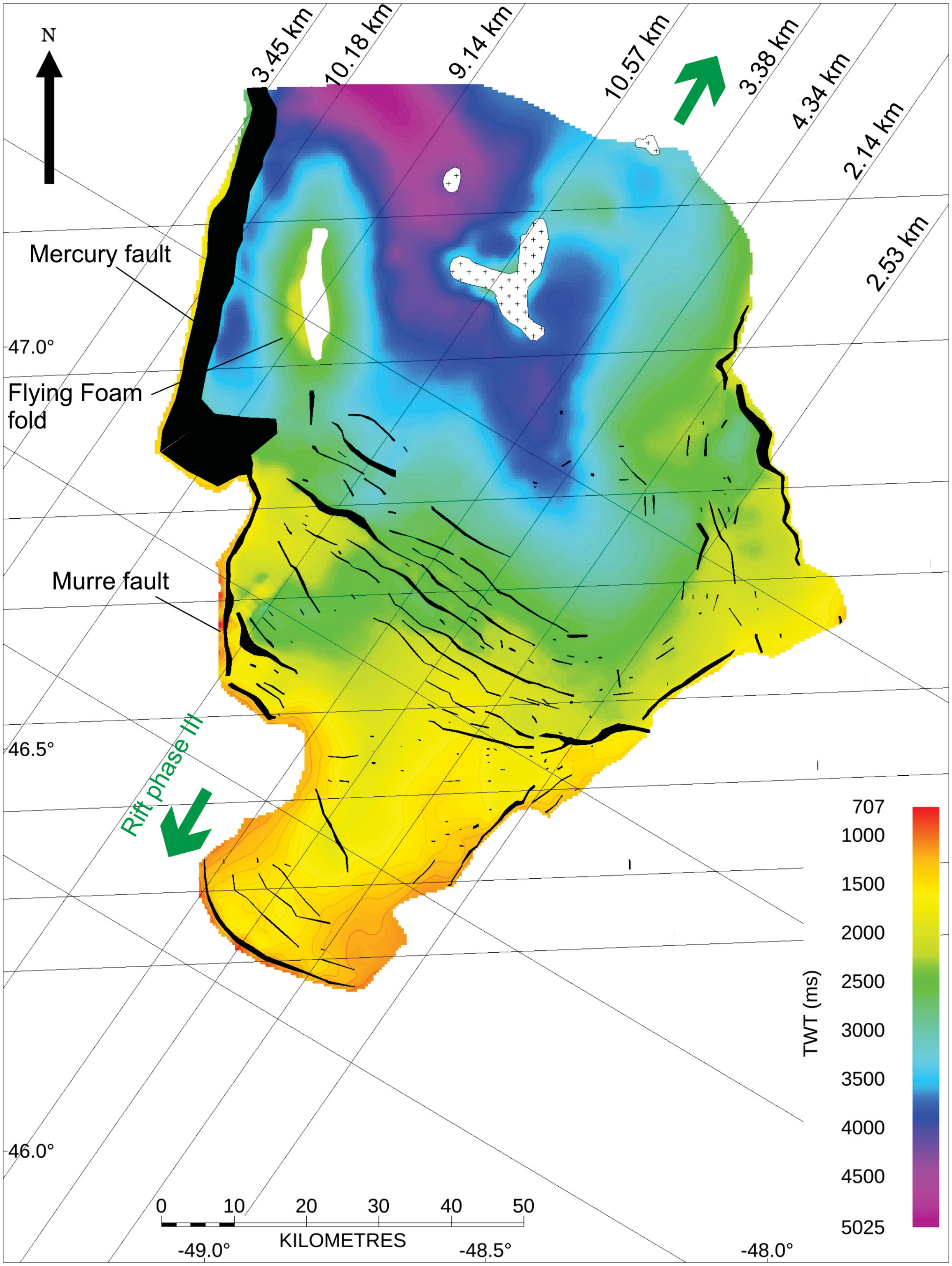

Figure 4.6: Time structure map of the Aptian Unconformity showing double extension estimates across the basin during rift phase III in an northeast-southwest direction.

Mid-Aptian Unconformity level, and subtracting the component of heave on that fault at the Cenomanian Unconformity level (Fig. 2.15). Figure 4.5 shows the extension across the basin for rift phase III produced by summing the extension measurements from each fault along the measurement lines. Figure 4.6 shows the extension across the basin using the double extension measurements (Section 2.2.6).

Extension across the basin during rift phase III ranges from 1.28 km to 2.44 km along the measurement lines that do not cross the Murre or Mercury faults. Extension across the basin is 5.5 km along the line that crosses the Murre fault and up to 10.2 km along the lines that cross the Mercury fault (Fig. 4.5). Using the double extension estimates (Section 2.2.6), extension during rift phase III ranges from 2.1 km to 4.3 km along the measurement lines that do not cross the Murre or Mercury faults and up to 10.6 km along lines that cross the Murre or Mercury faults (Fig. 4.6). In the Flying Foam area the extension is all taken up on the border faults, whereas to the south and east of the Flying Foam the extension is spread across numerous smaller faults.

4.2.4 Late Cretaceous extension

The extension measurements for the Late Cretaceous were obtained by measuring the component of heave (Fig. 2.14) in the measurement direction across each fault at the Cenomanian Unconformity level, and subtracting the component of heave on that fault at the Base Tertiary Unconformity level (Fig. 2.15). It is not possible to establish an extension direction during the Late Cretaceous, hence extension was measured in each of the earlier extension directions by summing the extension measurements from each fault along the measurement lines (Fig. 4.7).

There is a small amount of heave on the bigger faults at the Cenomanian level, re-

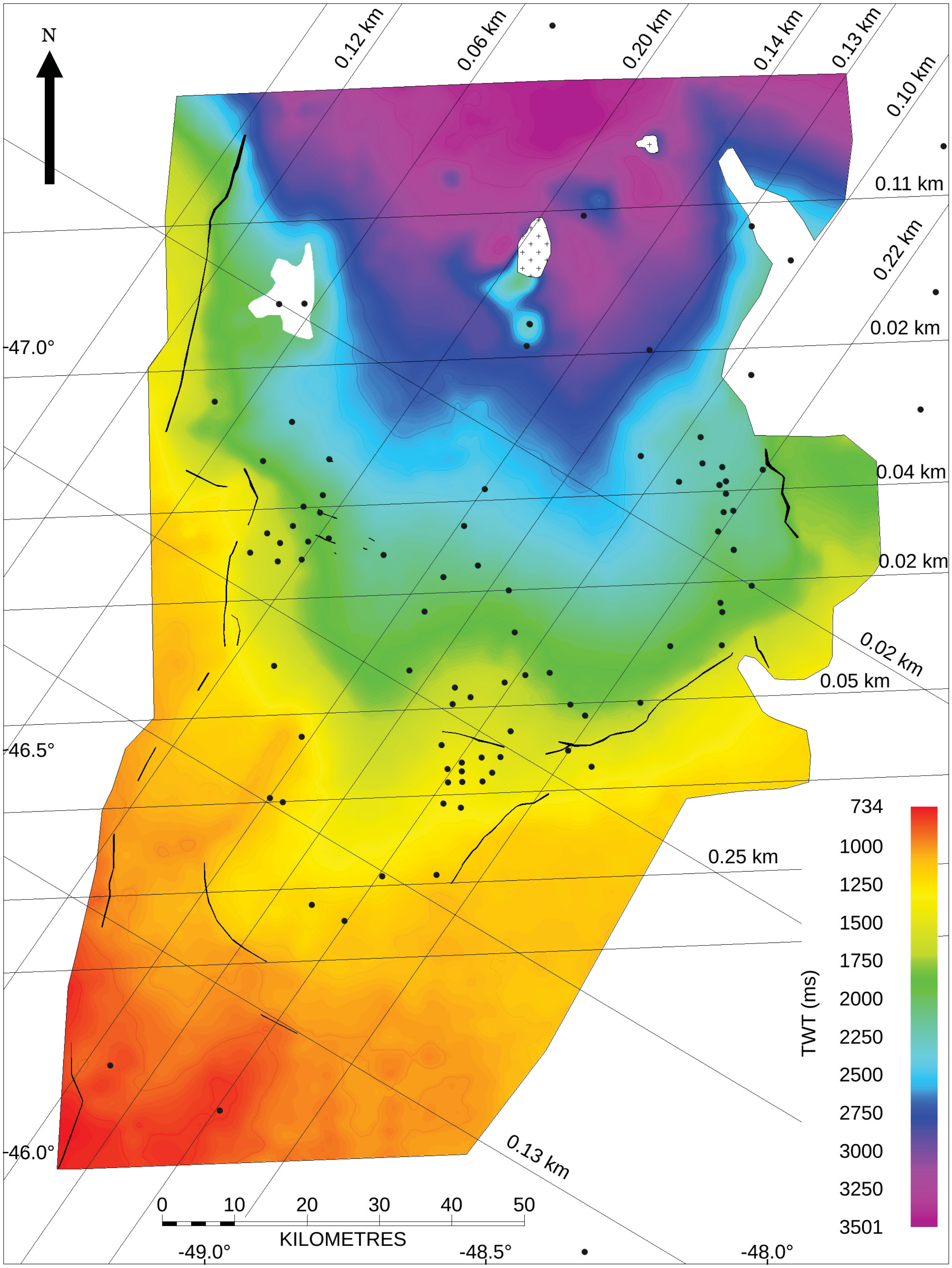

Figure 4.7: Time structure map of the Cenomanian Unconformity showing extension estimates along the measurement lines during the Late Cretaceous.

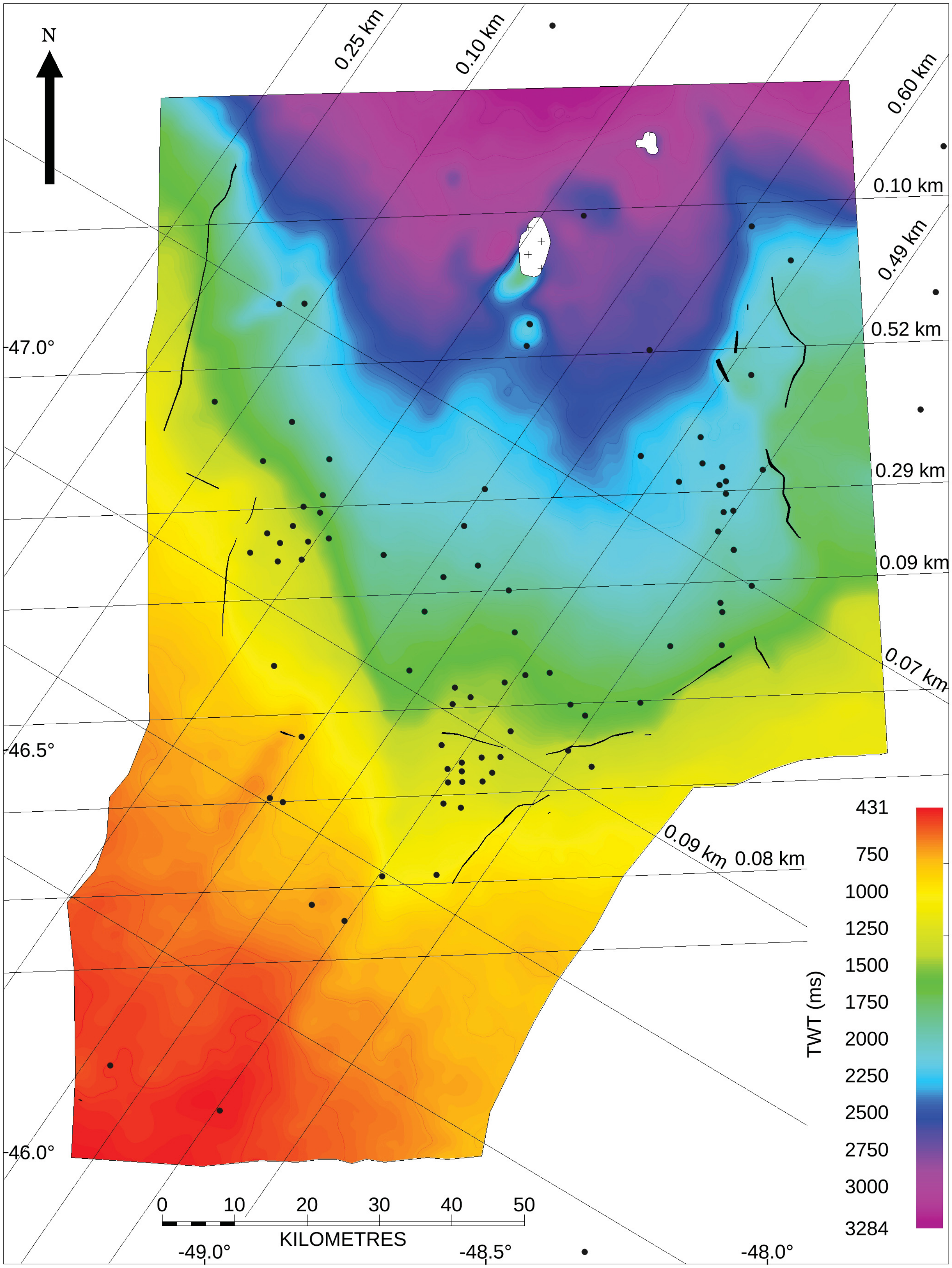

Figure 4.8: Time structure map of the Base Tertiary Unconformity showing extension estimates along the measurement lines during the Cenozoic.

sulting in extension values along the lines ranging from zero to 0.25 km.

4.2.5 Cenozoic extension

The extension measurements for the Cenozoic were obtained by measuring the component of heave (Fig. 2.14) in the measurement direction across each fault at the Base Tertiary Unconformity level. It is not possible to establish an extension direction during the Cenozoic, hence extension was measured in each of the earlier extension directions by summing the extension measurements from each fault along the measurement lines (Fig. 4.8).

There is a small amount of heave across the bigger faults in the basin at the Base Tertiary level, but this mostly contributes insignificant extension when compared to the total extension through time. In the northeast corner across the Voyager fault zone there is a larger amount of extension resulting in 0.52 km of extension on the northernmost east-west line and 0.6 km of extension on the northernmost northeast-southwest line.

4.2.6 Summary of the temporal and spatial variation in extension across the Jeanne d'Arc Basin

The extension across the basin is summarized in Figure 4.9 using the original extension estimates and in Figure 4.10 using the double extension estimates (Section 2.2.6). The length of the coloured bars represents the amount of extension in that direction according to the scale at the bottom. The coloured bars are placed along the Murre and Mercury faults on the northwest-southeast lines and the east-west lines and across the centre of the basin on the northwest-southeast lines, however they represent ex-

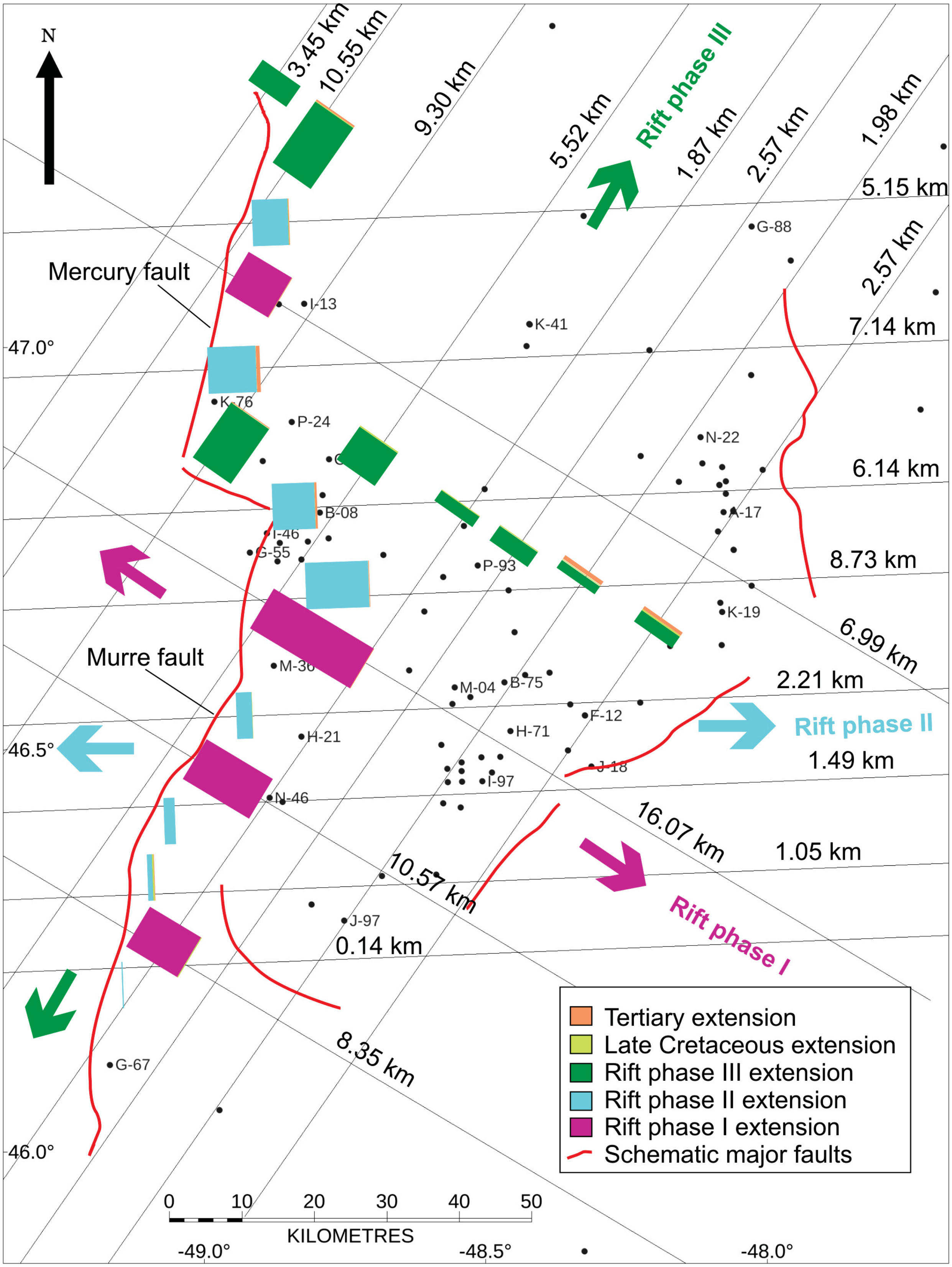

Figure 4.9: Summary of the temporal and spatial variation in extension across the Jeanne d'Arc Basin using the origanial extension estimates.

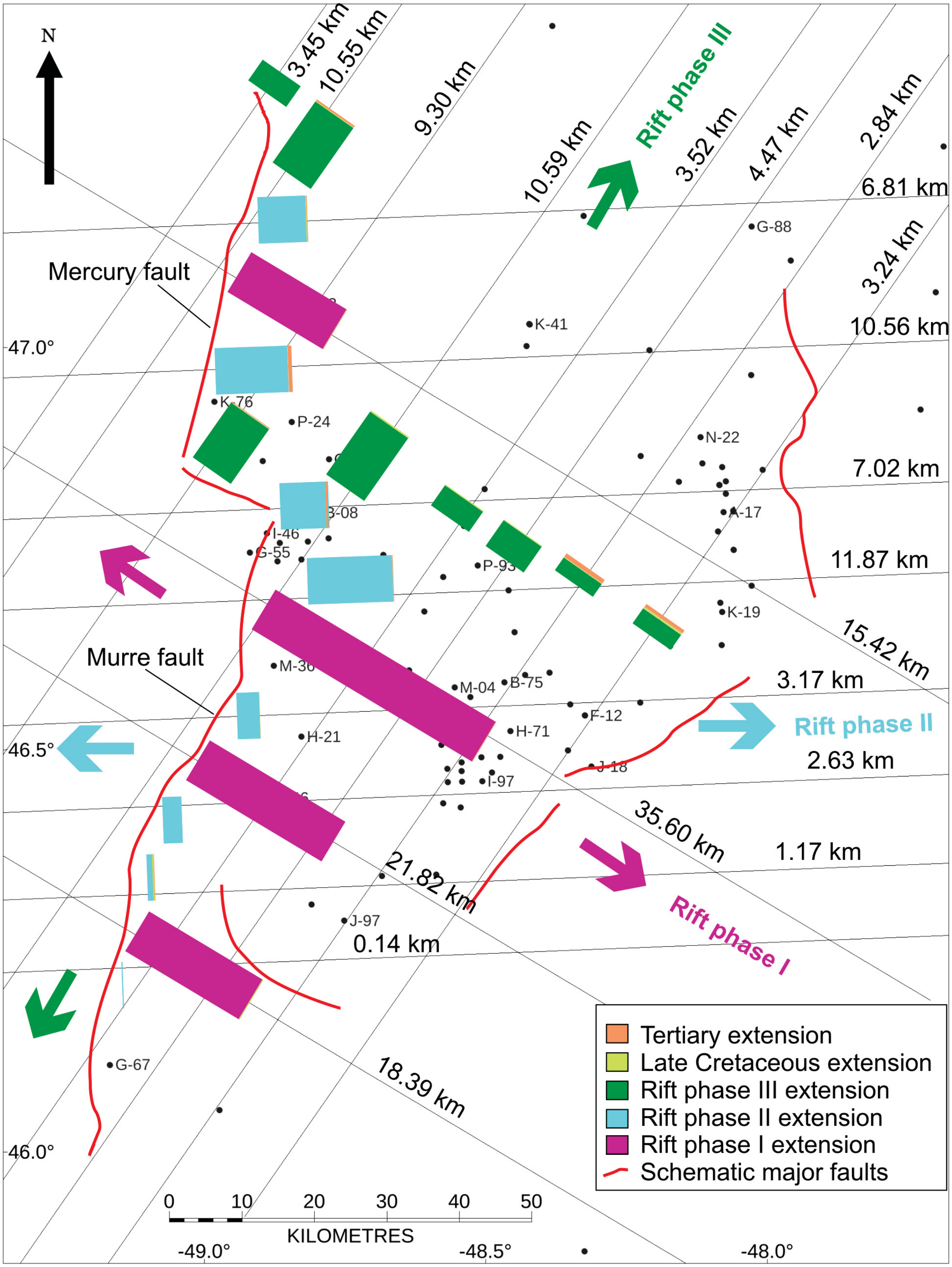

Figure 4.10: Summary of the temporal and spatial variation in extension across the Jeanne d'Arc basin using the double extension estimates

tension along the entire line. Looking at the general pattern, rift phase I (pink bars) dominates the southern half of the basin using the original extension estimates (Fig. 4.9) and throughout the basin using the double extension estimates (Fig. 4.10). The extension increases northwards to the centre of the basin during rift phase I (pink bars) and rift phase II (cyan bars) using both the original (Fig. 4.9) and the double (Fig. 4.10) extension estimates. Further north the extension from rift phase I (pink bars) and rift phase II (cyan bars) decreases slightly. However, there is a lack of data from rift phase I in the north of the basin where the Top Basement Unconformity becomes deeper than the depth extent of the seismic. On the northeast-southwest lines extension is predominantly from rift phase III (dark green bars) and is greater on the lines which cross the Murre and Mercury faults. There is insignificant extension after the Early Cretaceous as indicated by the scarcity of light green and orange bars.

4.3 Restored time structure maps

Beta grids were created for each rift phase (Section 2.2.4) from the components of heave (Fig. 2.14) in the extension direction. The beta grids were used as input into GeoArctic's proprietary PlateDEF software (GeoArctic Ltd. website [13]), which models deformable plate margins (Chapter 5), to restore the time structure maps to their position before each rift phase. Figures 4.11 - 4.16 show the outlines of the time structure maps and their restored positions before each rift phase. Each unconformity time structure map has two restorations: 1.) using the basic extension values and 2.) using values based on double extension on the internal faults (Section 2.2.6) to account for the extension discrepancy between the 2D data and the 3D data (Section 2.2.5). The restorations to 112 Ma (green line) show only a small reduction in area from the present day, indicating a small quantity of extension during rift phase III (Fig.

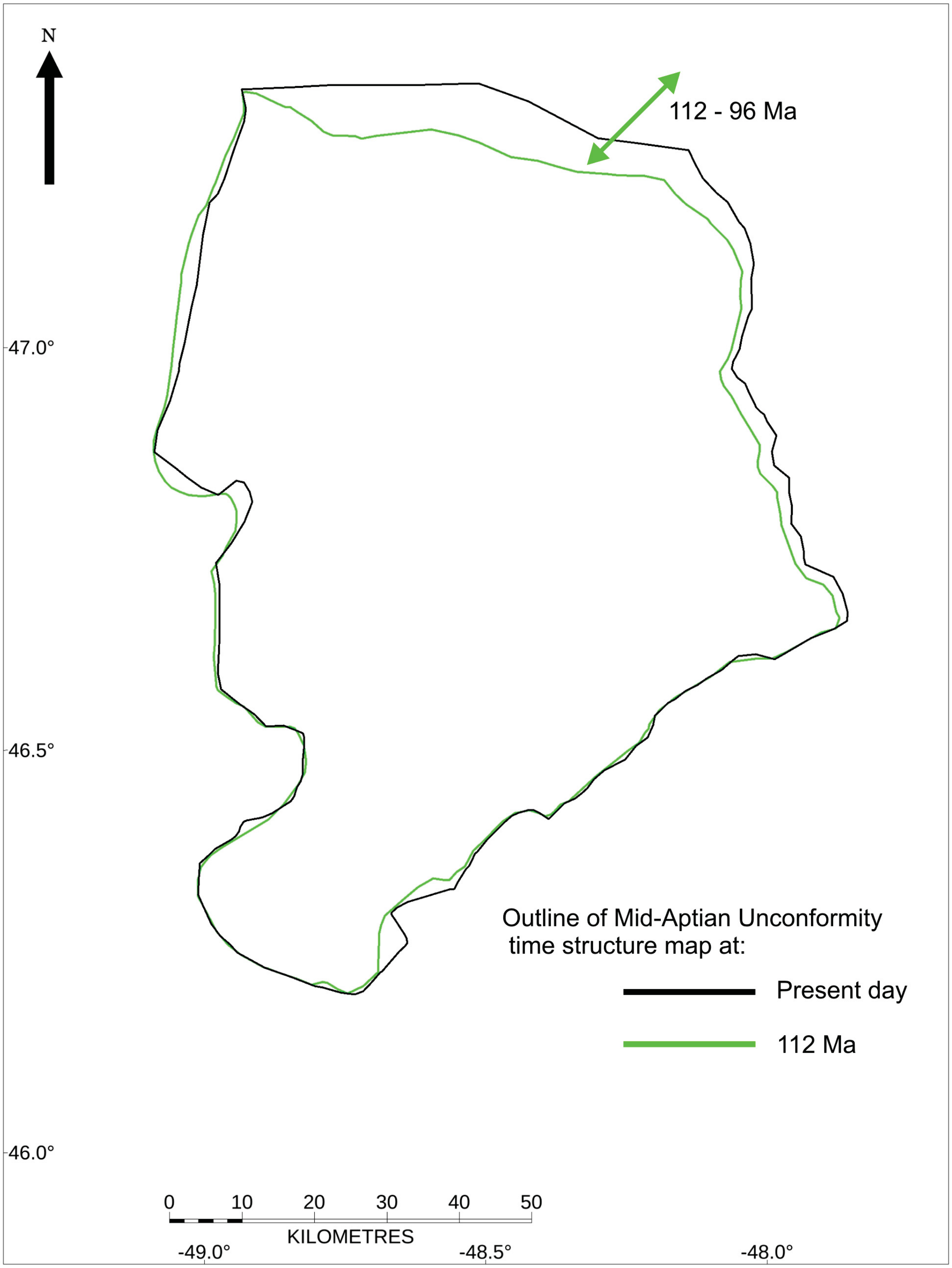

Figure 4.11: Outline of the Mid-Aptian Unconformity time structure map at present day and restored to before rift phase III. The green arrow illustrates the extension direction during rift phase III

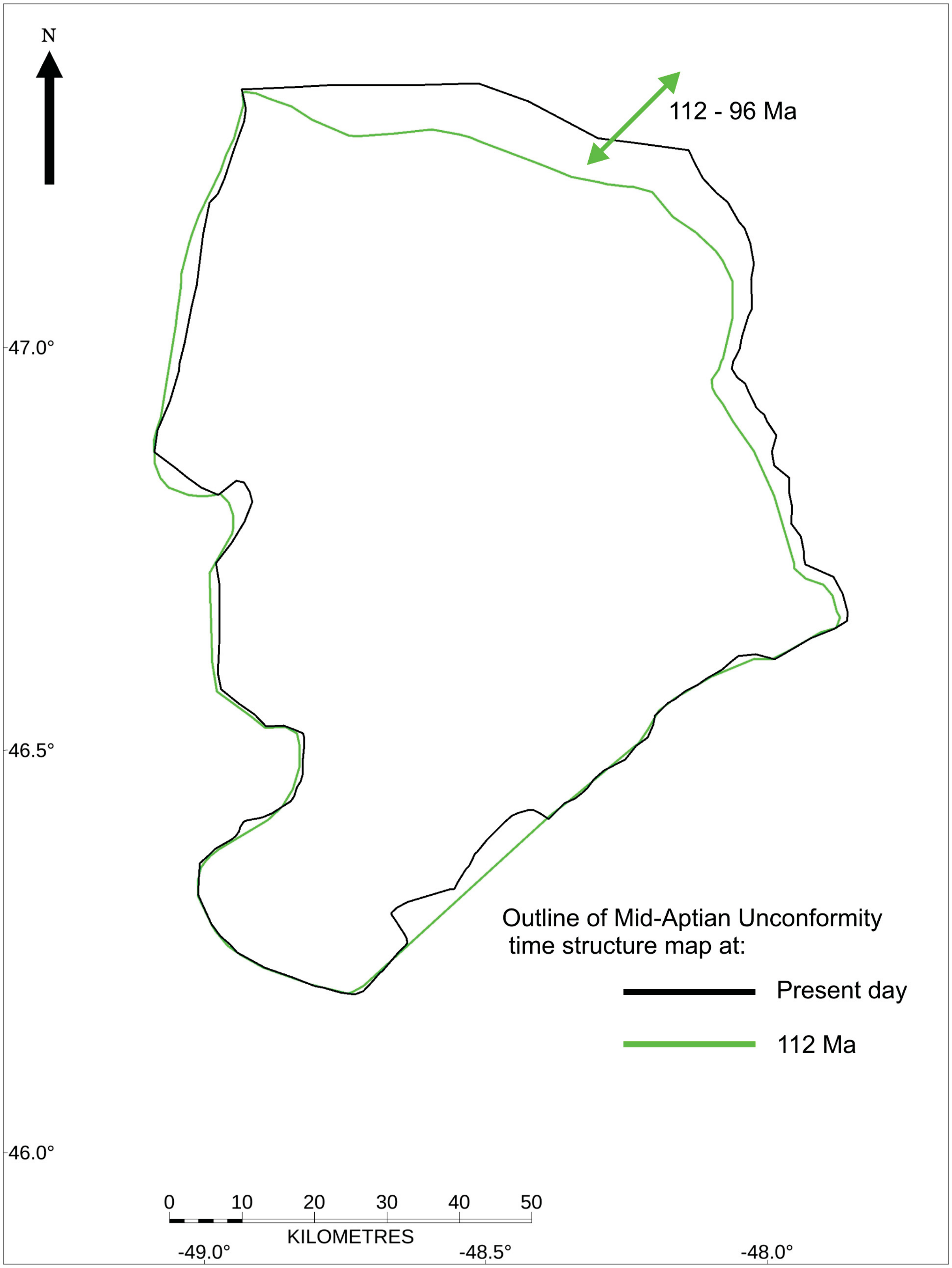

Figure 4.12: Outline of the Mid-Aptian Unconformity time structure map at present day and restored to before rift phase III using double extension values. The green arrow illustrates the extension direction during rift phase III

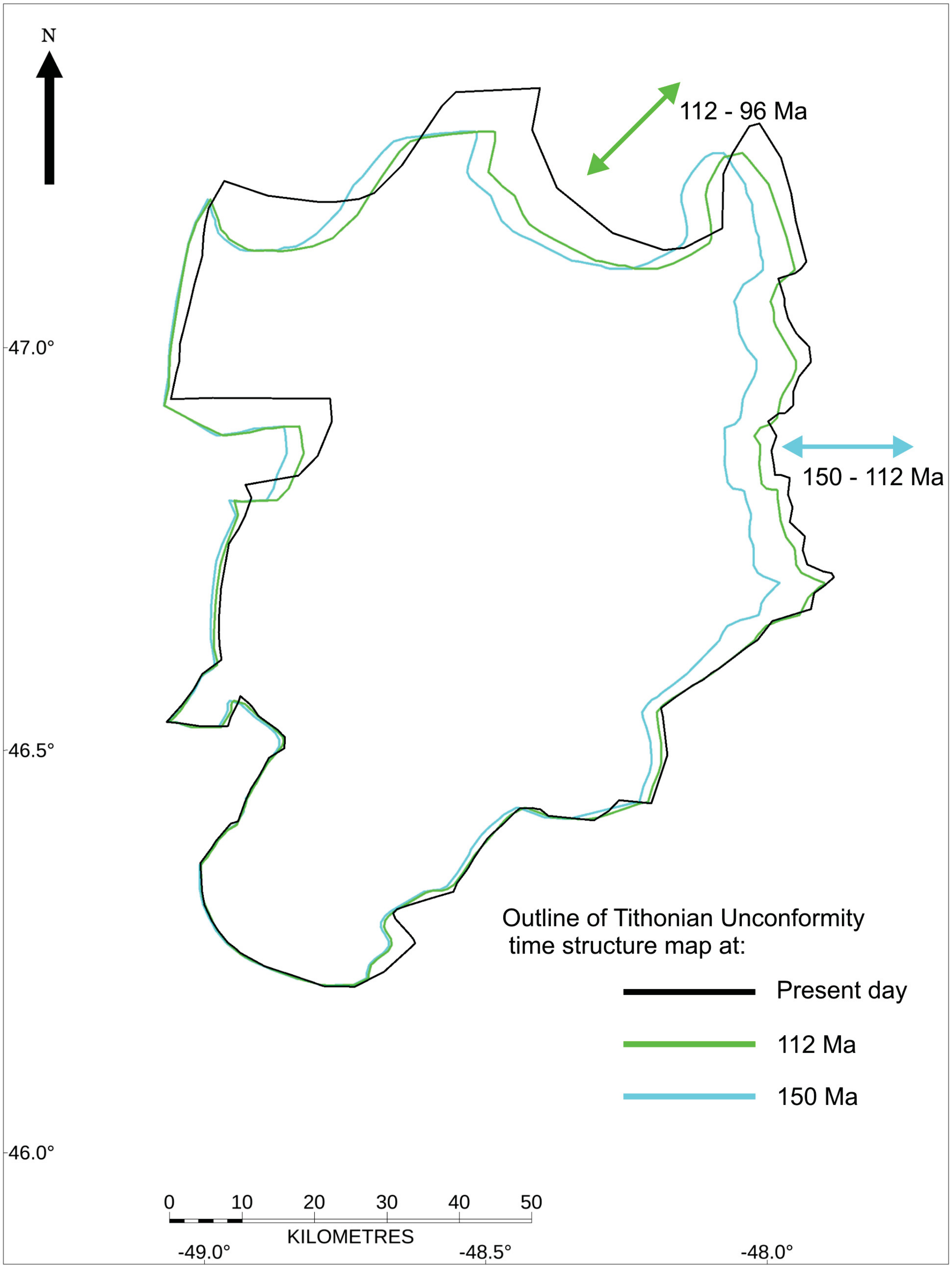

Figure 4.13: Outline of the Tithonian Unconformity time structure map at present day and restored to before rift phases II and III. The cyan and green arrows illustrate the extension directions during rift phases II and III respectively.

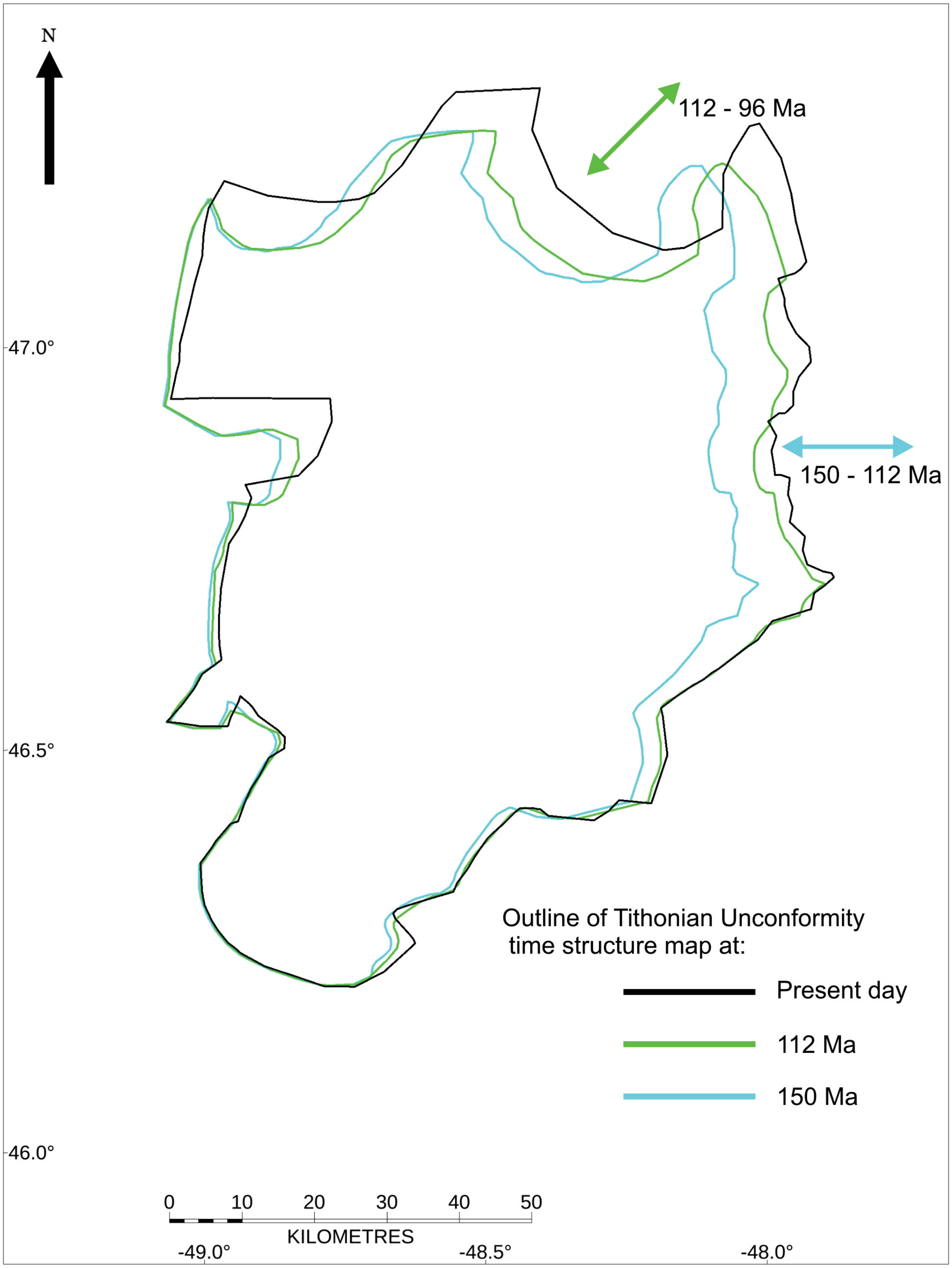

Figure 4.14: Outline of the Tithonian Unconformity time structure map at present day and restored to before rift phases II and III using double extension values. The cyan and green arrows illustrate the extension directions during rift phases II and III respectively.

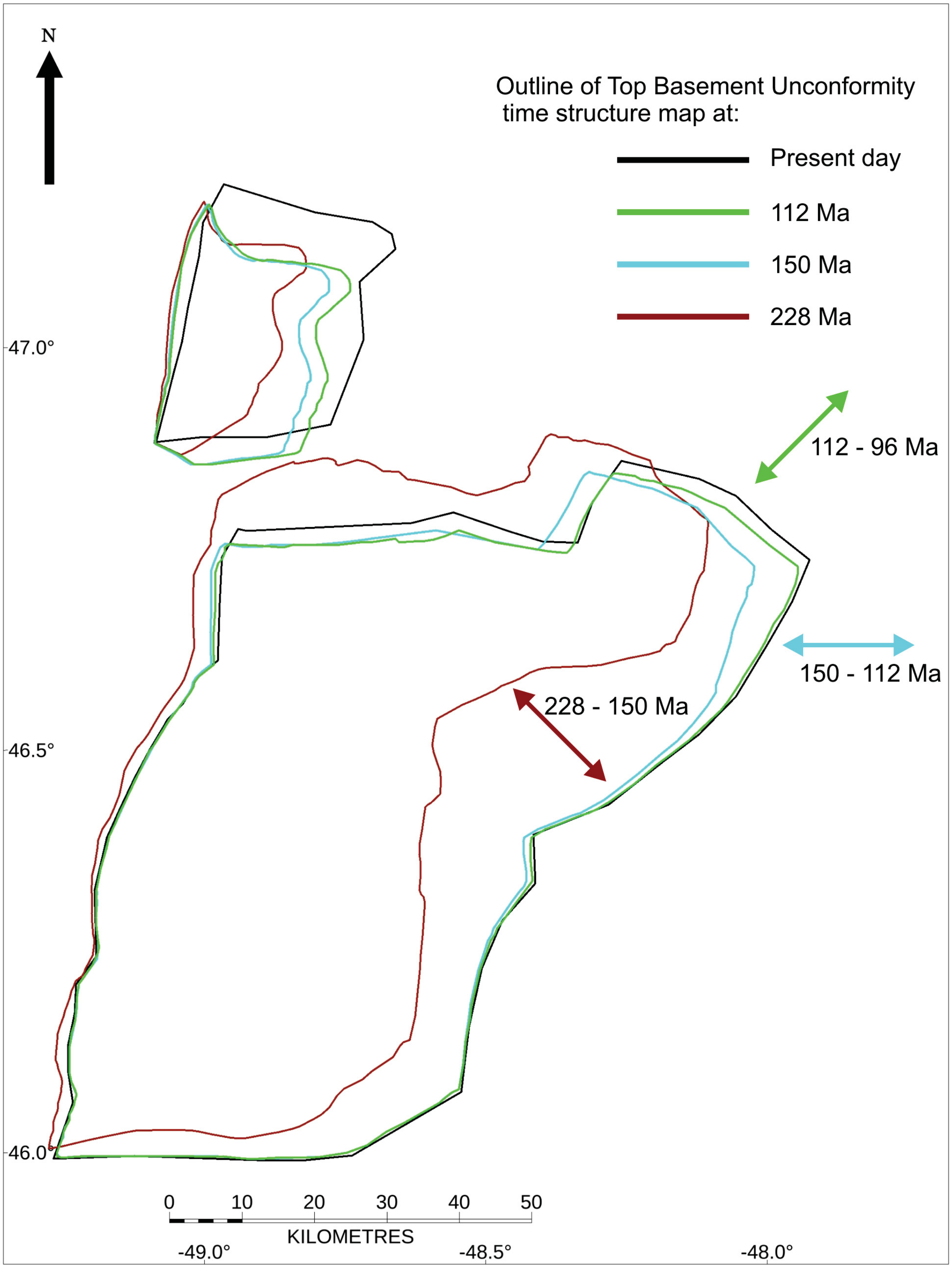

Figure 4.15: Outline of the Top Basement Unconformity time structure map at present day and restored to before rift phases I, II and III. The red, cyan and green arrows illustrate the extension directions during rift phases I, II and III respectively.

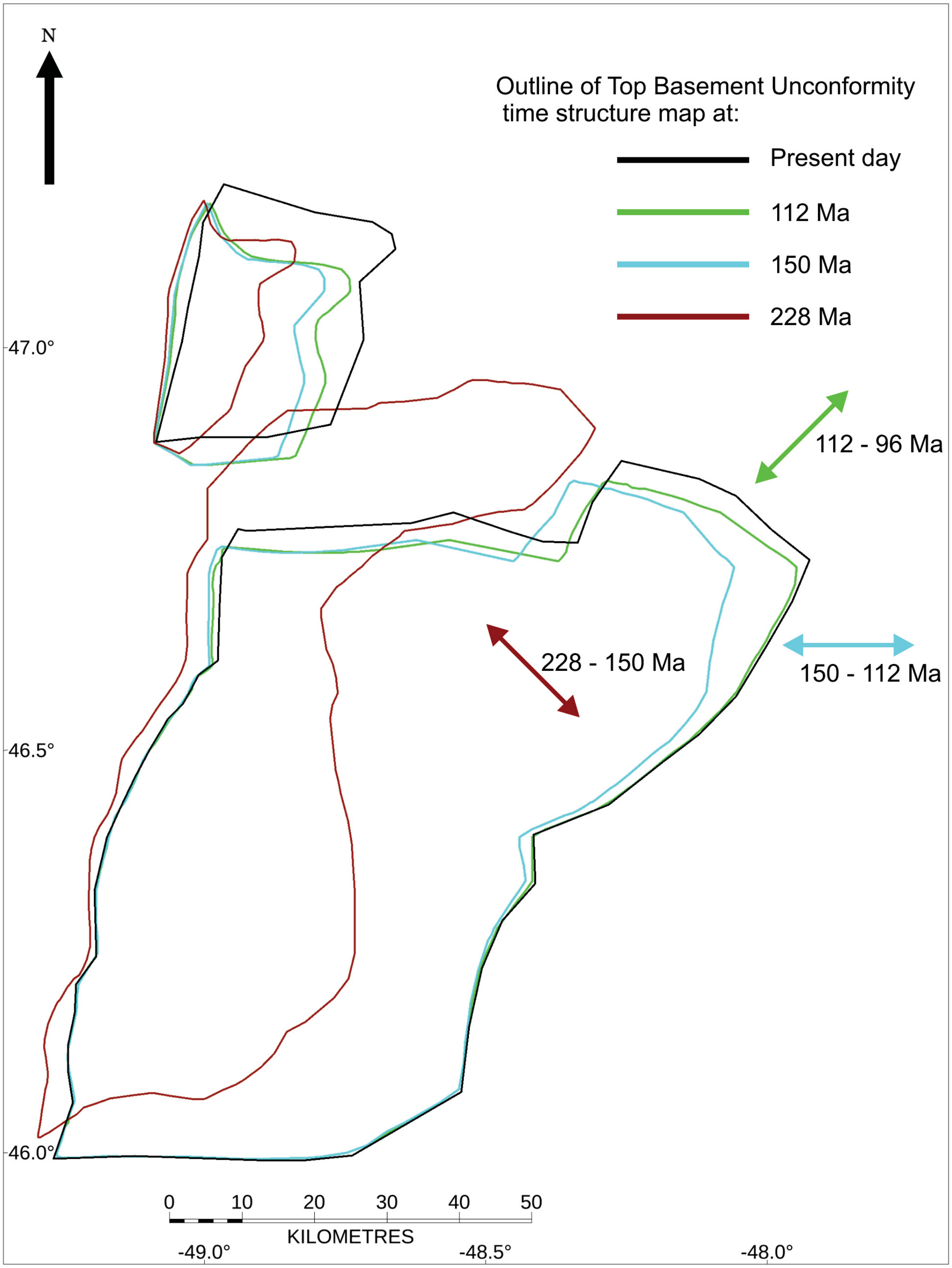

Figure 4.16: Outline of the Top Basement Unconformity time structure map at present day and restored to before rift phases I, II and III using double extension values. The red, cyan and green arrows illustrate the extension directions during rift phases I, II and III respectively.

4.11). The difference between the first set of maps and those using double extension on the internal faults is small for this time interval (Fig. 4.12). There is another small reduction in area between the restorations to 112 Ma and those to 150 Ma (cyan line), indicating a small quantity of extension during rift phase II (Fig. 4.13). Again the difference between the original maps and those using double extension on the internal faults is small for this time interval (Fig. 4.14). The largest reduction in area is seen between the restoration of the Top Basement Unconformity time structure map to 150 Ma and to 228 Ma (Fig. 4.15), indicating that there was the greatest amount of extension during rift phase I. There was a significantly larger reduction in area between the restoration of the Top Basement Unconformity time structure map to 228 Ma using the double extension values (Fig. 4.16). The total reduction in area of the Top Basement Unconformity time structure map between the present day and 228 Ma using the double extension values is 46% compared to a 22% reduction using the original extension values.

Chapter 5

Comparison of the restored time structure maps with the regional North Atlantic deformable plate reconstruction

Chapter 4 illustrated the time structure maps restored to before each rift phase using beta grids derived from fault heave measurements as input into GeoArctic Ltd.'s software (GeoArctic Ltd. website [13]). GeoArctic Ltd. and its subcontractors for the Petroleum Infrastructure Programme Rockall Studies Group (PIPCO RSG Ltd.) led a team of scientists, as part of the North Atlantic Petroleum Systems Assessment (NAPSA), to develop a new deformable/plate kinematic reconstruction of the North Atlantic between Ireland and Canada (GeoArctic Ltd. website, [13]). The GeoArctic Plate Model is derived from work funded jointly by the the Irish Shelf Petroleum Studies Group (ISPSG) of PIP and Nalcor Energy. This chapter integrates GeoArctic's regional North Atlantic reconstructions with the restorations from Chapter 4. Fault heave measurements from the 2D data underestimate extension by approximately 50% when compared with measurements from the 3D data (Section 2.2.5), hence the restorations using double extension estimates were deemed more accurate and used for the comparisons.

A plate kinematic model describes rigid plate motions on the Earth's surface using Euler poles of rotation and the angular velocity about the pole. Euler poles are calculated by matching magnetic anomalies, from transform faults and from Earthquake slip azimuths. However, continental crust is extended prior to breakup leading to plate overlap in reconstructions using a rigid model. A deformable plate margin model is integrated with a plate kinematic model to account for extension, transtension and compression prior to breakup. Srivastava and Verhoef, 1992 [47] produced plate reconstructions of the North Atlantic using a plate kinematic solution. They measured the plate overlap to account for the gross extension during rifting and used this to restore the plate margins and the basins on the margins to their pre-rift positions. GeoArctic's regional North Atlantic deformable plate reconstruction attempts to go a step further and account for the lateral, depth-dependent and time dependent variation in the amount and direction of extension. The plate overlap at any time is derived from a plate kinematic model in order to determine how much the plate has stretched. By measuring the overlap and removing it through time from grids of total crustal stretching (beta), the plates can be restored to their pre-extensional state. Regional 3D gravity inversion was used to determine crustal thinning and to produce total beta grids. Independent gravity inversion studies and subsidence analysis verified that the regional 3D gravity inversion provided reasonable values for total beta. Seventeen regional seismic lines were used to help establish the timing and amount of extension.

Figures 5.1 to 5.3 illustrate the present day unconformity time structure maps overlain on GeoArctic's regional tectonic elements map. Figures 5.4 and 5.5 compare the restorations using the deformable model from this study with the restorations using the regional North Atlantic deformable plate model. For rift phase III the extension direction is in agreement for both models, but the amount of extension is greater using the deformable model from this study than the regional model and there is a discrepancy between the timing (Fig. 5.4). It is proposed that the detailed fault mapping from this study provides insight into the quantity and timing of extension within the basin that is not possible to obtain from the regional picture. This information can be used to refine the regional North Atlantic deformable plate model. Rift phase II is omitted because the timing of the most significant extension is different between the two models, although the total extension shows an excellent correlation (Fig. 5.5).

The restorations of the Top Basement Unconformity time structure map to before rift phase I from the two models agree closely in the southern part of the Jeanne d'Arc Basin (Fig. 5.5). In the north of the basin the regional model has rotated the structure map during rift phase II, whereas the model from this study shows no rotation (Figs. 5.5 and 5.6). The regional North Atlantic deformable plate model proposes a rotation of the Flemish Cap between 136 and 140 Ma due to the differential extension between hyperextension in the East and West Orphan Basins to the north and normal extension in the surrounding basins to the south and west (Fig. 5.6). During rift phase II the Flemish Cap rotated 43 degrees relative to Galicia Bank and Iberia and moved 200-300 km southeast with respect to North America (Sibuet et al., 2007 [40]). However, there is no evidence, from the mapping in the north of the Jeanne d'Arc Basin, that this rotation affected the basin.

There is close agreement between the total amount of extension from this study and

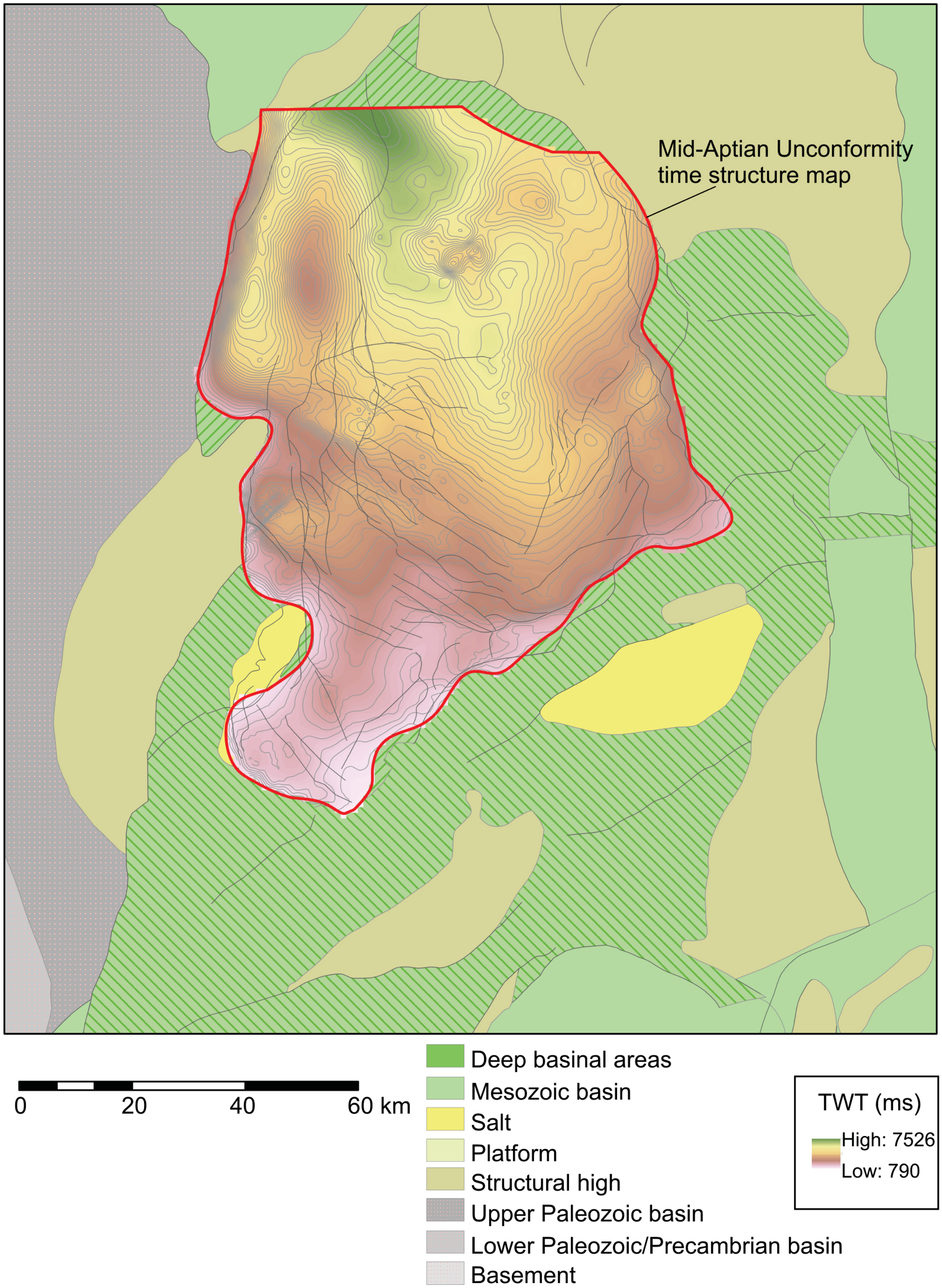

Figure 5.1: Present day Mid-Aptian Unconformity time structure map overlain on GeoArctic's regional tectonic elements map. GeoArctic data is derived from a project funded jointly by the ISPSG of the PIP and Nalcor Energy.

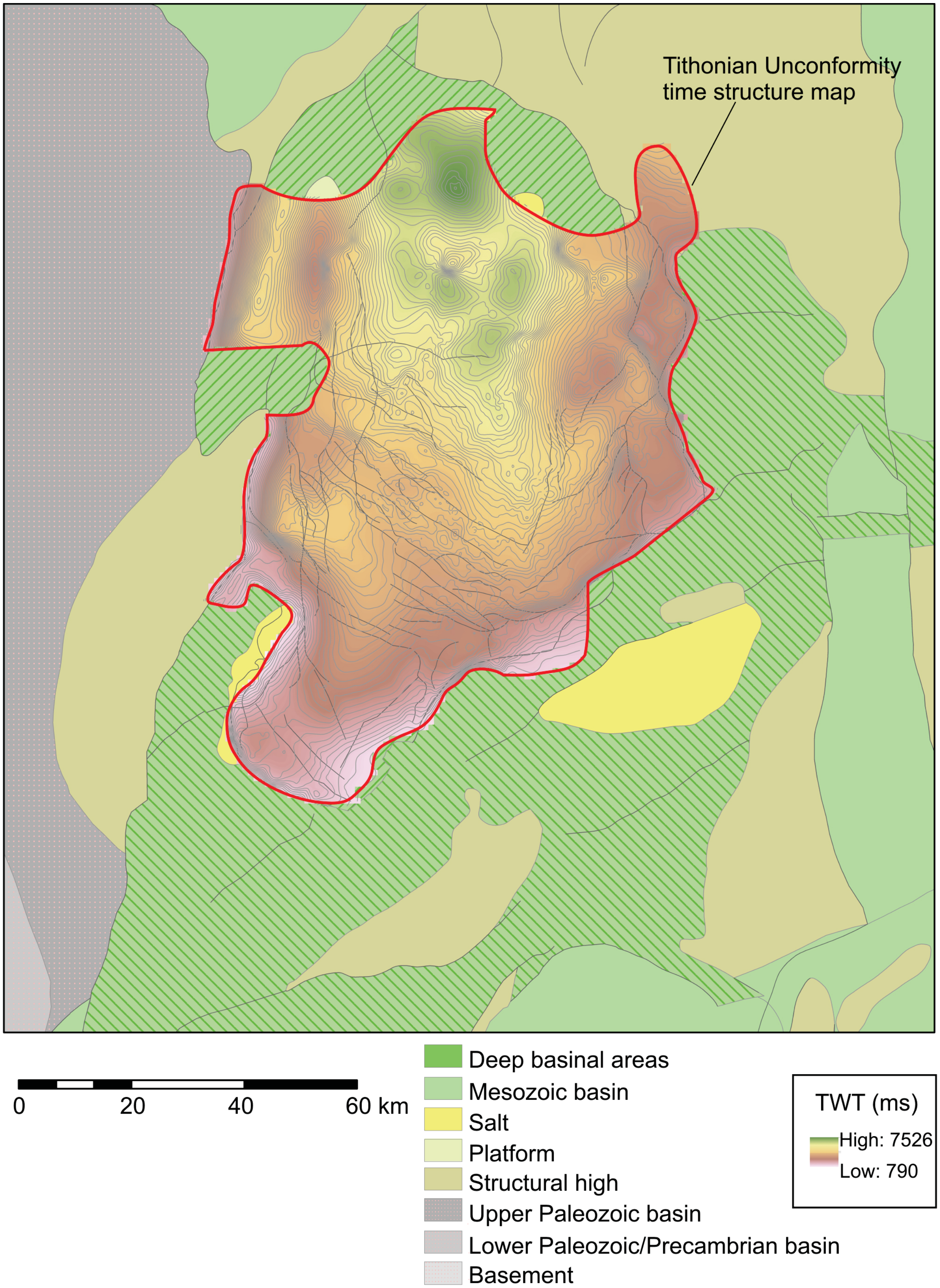

Figure 5.2: Present day Tithonian Unconformity time structure map overlain on GeoArctic's regional tectonic elements map. GeoArctic data is derived from a project funded jointly by the ISPSG of the PIP and Nalcor Energy.

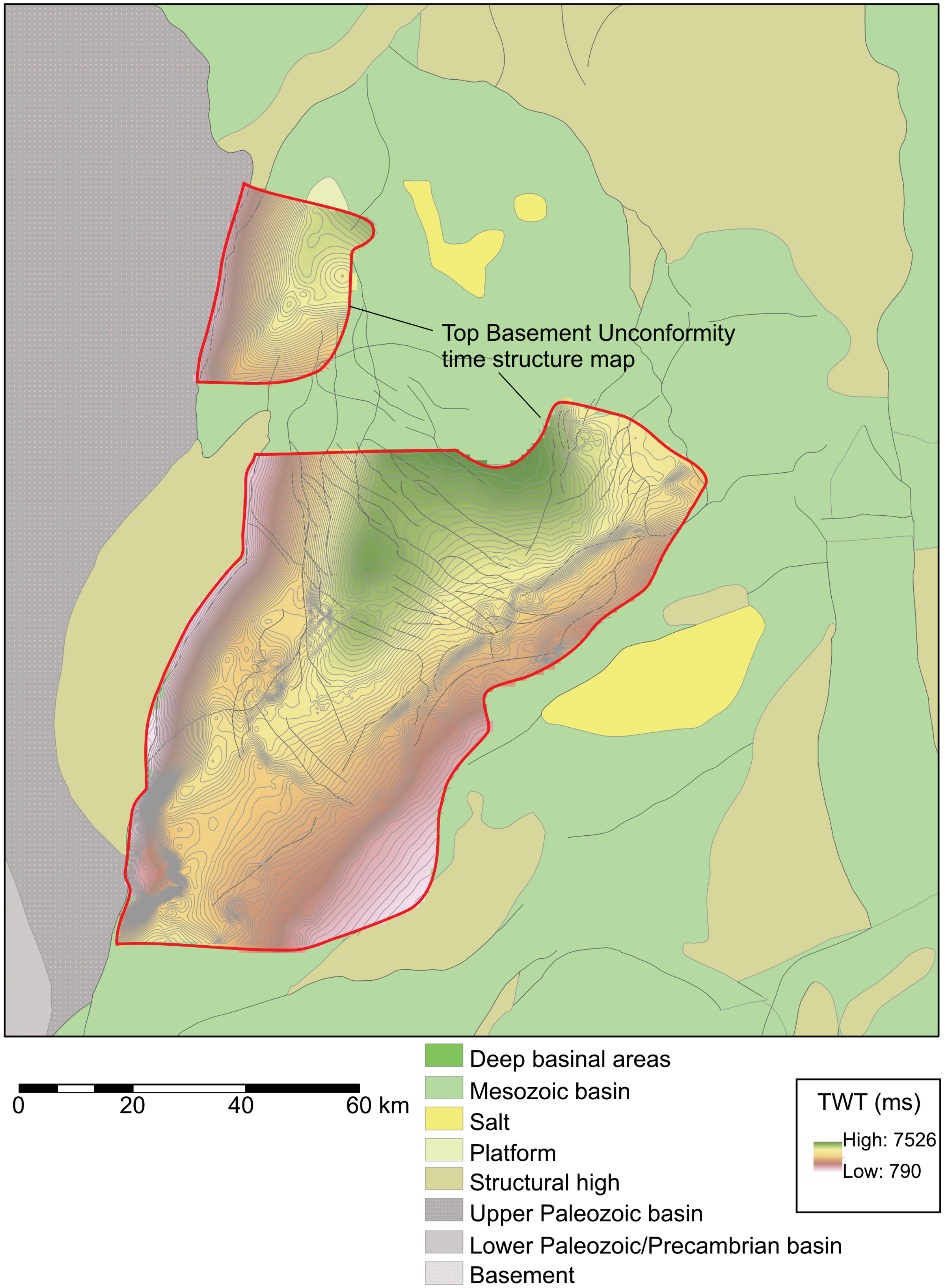

Figure 5.3: Present day Top Basement Unconformity time structure map overlain on GeoArctic's regional tectonic elements map. GeoArctic data is derived from a project funded jointly by the ISPSG of the PIP and Nalcor Energy.

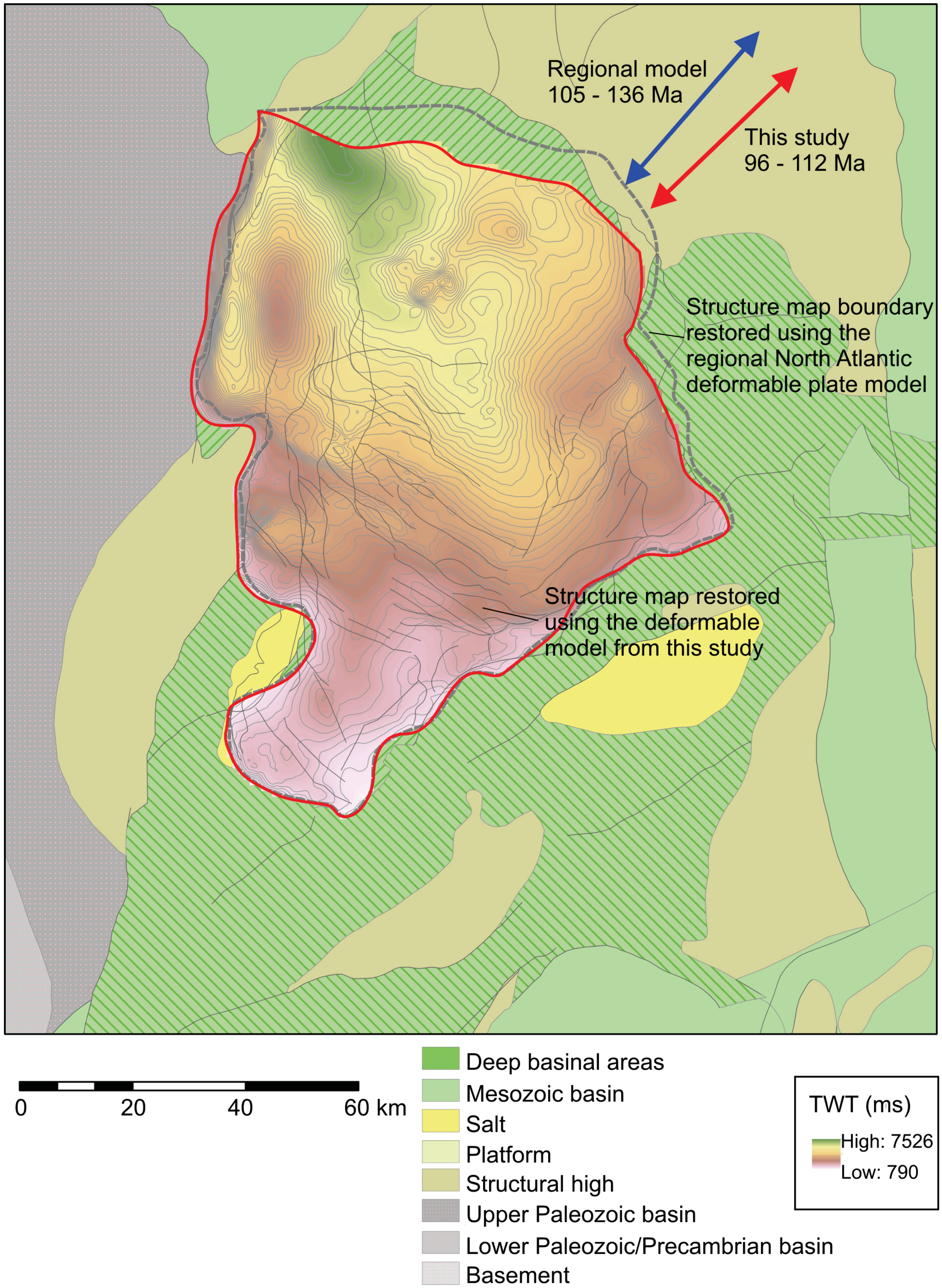

Figure 5.4: Mid-Aptian Unconformity time structure map restored to before rift phase III using the double extension values from this study, overlain on GeoArctic's regional tectonic elements map restored to before rift phase III using the regional North Atlantic deformable plate model. GeoArctic data and models are derived from a project funded jointly by the ISPSG of the PIP and Nalcor Energy.

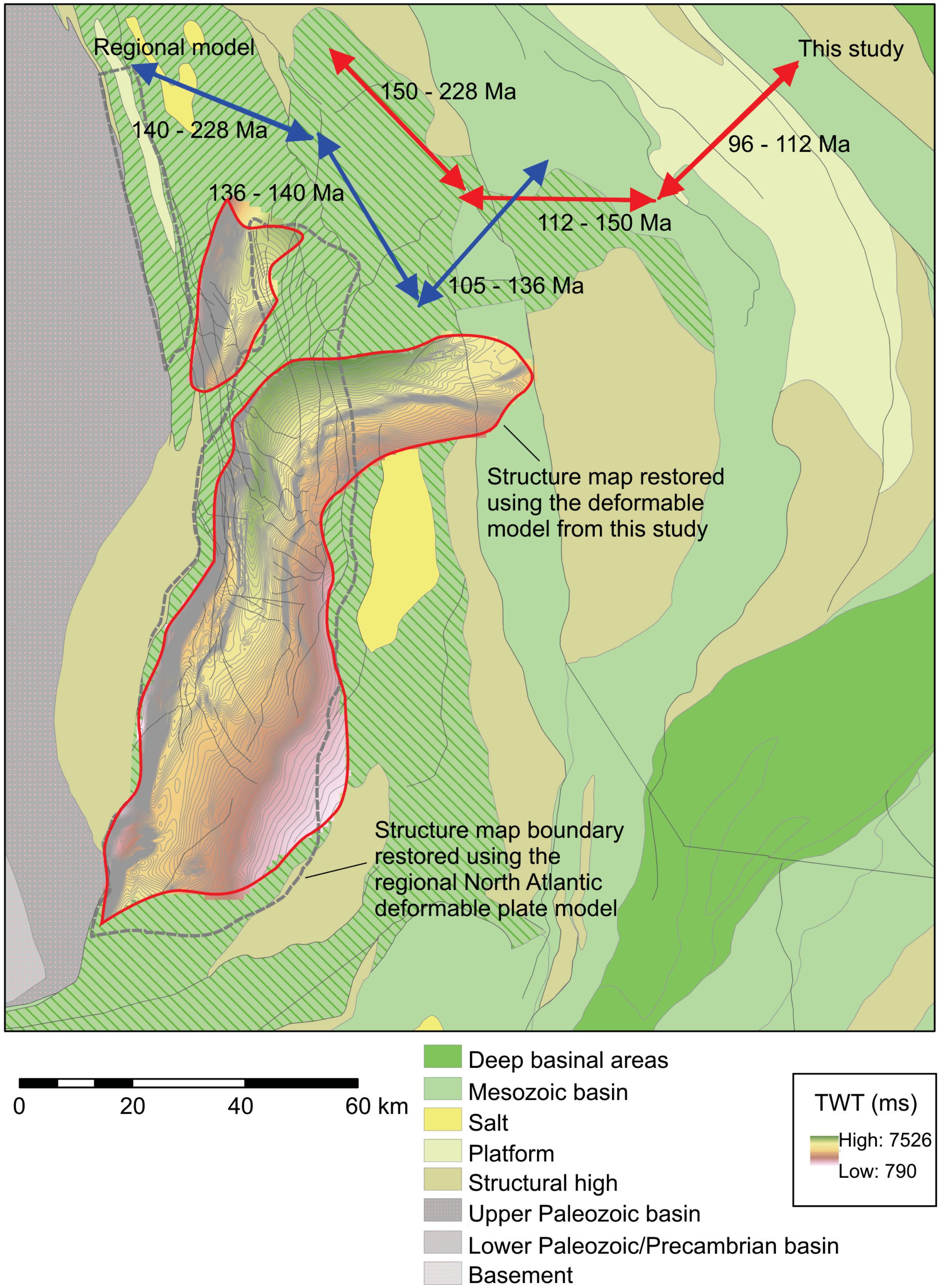

Figure 5.5: Top Basement Unconformity time structure map restored to before rift phase I using the double extension values from this study, overlain on GeoArctic's regional tectonic elements map restored to before rift phase I using the North Atlantic deformable plate model. GeoArctic data and models are derived from a project funded jointly by the ISPSG of the PIP and Nalcor Energy.

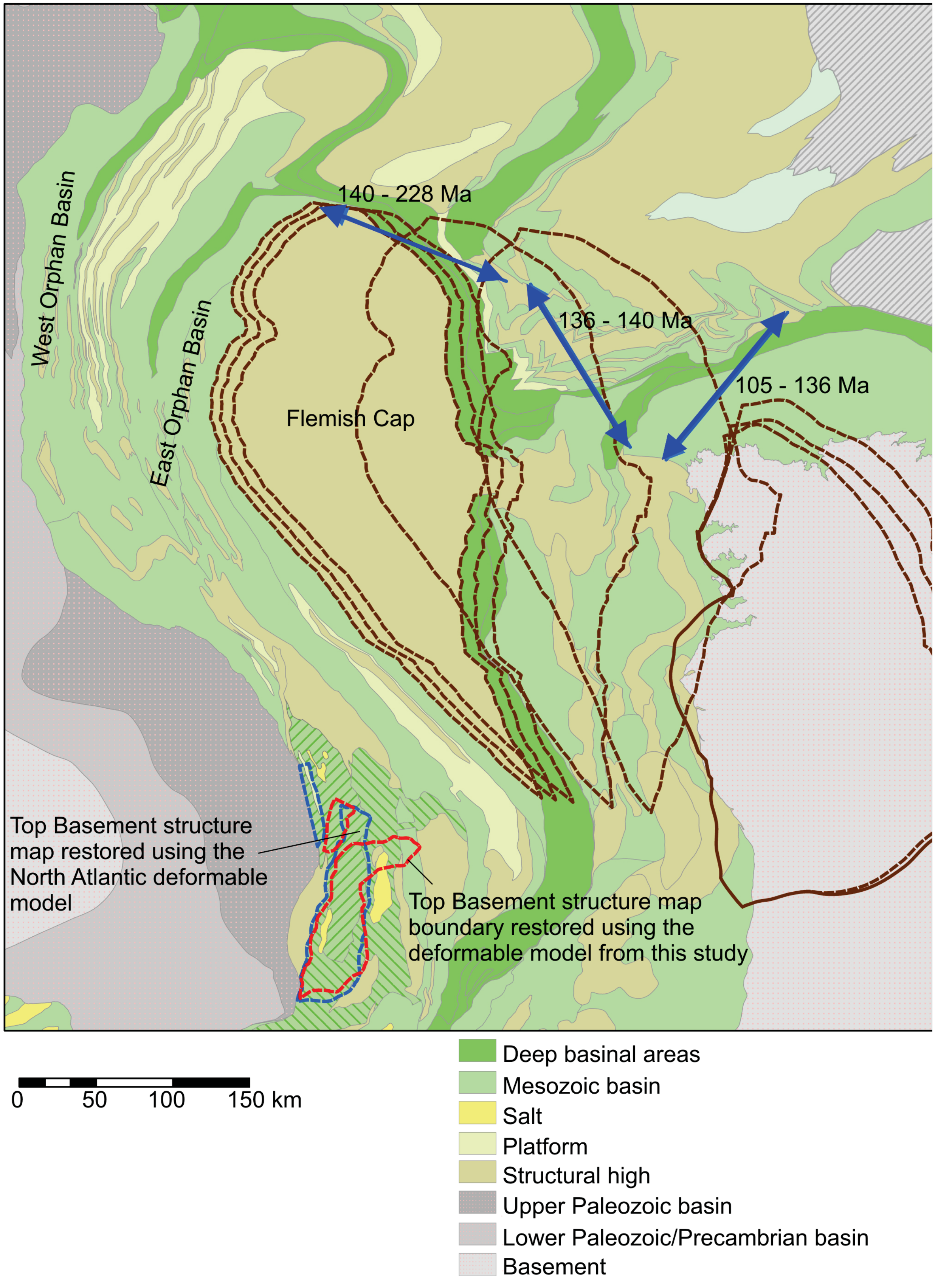

Figure 5.6: Deformable plate reconstruction from GeoArctic's regional model showing the rotation of the Flemish Cap. GeoArctic data and models are derived from a project funded jointly by the ISPSG of the PIP and Nalcor Energy.

from the regional study (Figs. 5.5). The restoration of the Top Basement Unconformity time structure map from the present day back to 228 Ma displays a 46% reduction in area using the deformable model from this study, compared with a 40% reduction using the regional model. In the non-hyperextended Jeanne d'Arc Basin, change in crustal thickness was considered an acceptable proxy for extension in the regional model. The close correlation between the results for the total extension using change in crustal thickness and fault heave measurements indicates that depth dependent stretching is not present in this area.

Chapter 6

A broader regional view of syn-rift and post-rift sedimentary thicknesses

6.1 Spatial discrepancy between syn-rift and post-rift

Figure 6.1 shows isochron maps illustrating the syn- and post-rift thickness across the Jeanne d'Arc Basin and into the southern Orphan Basin (see Fig. 1.4 for location). The syn-rift stratigraphy thickens towards the centre of the Jeanne d'Arc Basin from almost zero on the basin margins to a maximum thickness of 5600 ms two way time down the centre of the basin. It becomes predominantly 2000 ms two way time or less north of the Dominion O-23 well, with an area of 2500-3000 ms two way time thickness in a west-southwest-east-northeast zone just south of the Cumberland B-55

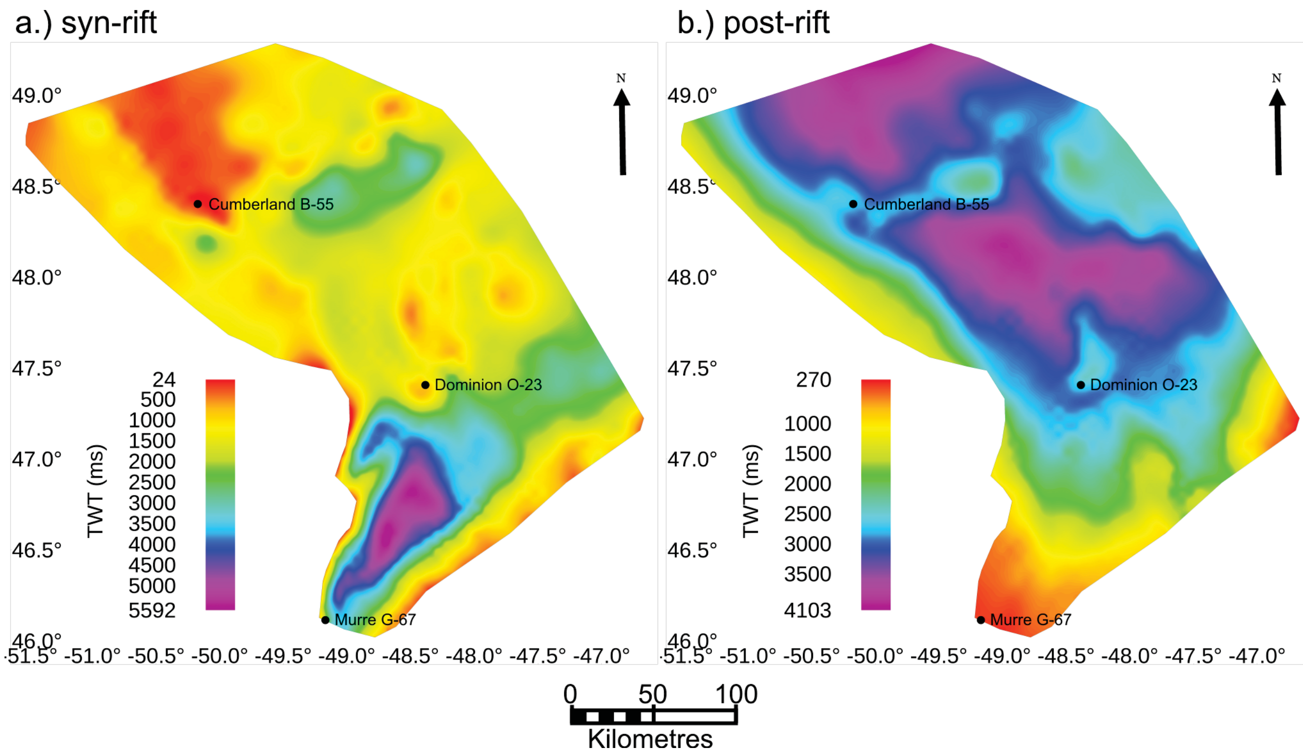

Figure 6.1: Isochron maps between a.) the Top Basement Unconformity and the Base Tertiary Unconformity, illustrating the approximate thickness of the syn-rift stratigraphy and b.) the Base Tertiary Unconformity and the waterbottom, illustrating the approximate thickness of the post-rift stratigraphy.

well. The post-rift stratigraphy thickens northwards from approximately 270 ms two way time near the Murre well to 3000 ms two way time just south of the Dominion O-23 well. North of the Dominion O-23 well the post-rift is predominantly 3500-4100 ms two way time except for a thinner area of around 2500 ms two way time at and just north of the Dominion O-23 well, and a thinner band of approximately 2000-2500 ms two way time running east-west from the Cumberland B-55 well.

A simple extensional model can be considered in which instantaneous and uniform extension of the crust and lithosphere is assumed (McKenzie, 1978 [30]). This is a pure shear model in which stretching is symmetrical with no solid body rotation. In order to maintain isostatic equilibrium following crustal extension there is passive upwelling of hot asthenosphere. Subsidence occurs because the crust is replaced by denser material. This creates accommodation space which can be filled by syn-rift sediments which in turn produces more subsidence due to loading. Following extension the isotherms in the lithosphere are closer together leading to high heat flow. As thermal equilibrium is slowly restored the rock contracts and gets denser. The isostatic response is subsidence. Sedimentation during this thermal subsidence phase is termed post-rift sedimentation. Assuming this simple model, subsidence can be measured as a function of the stretch factor (McKenzie, 1978 [30]; Fig. 6.2). This model predicts that thicker syn-rift should be overlain by thicker post-rift. The broad pattern of syn-rift thickness and post-rift thickness across the Jeanne d'Arc Basin and into the

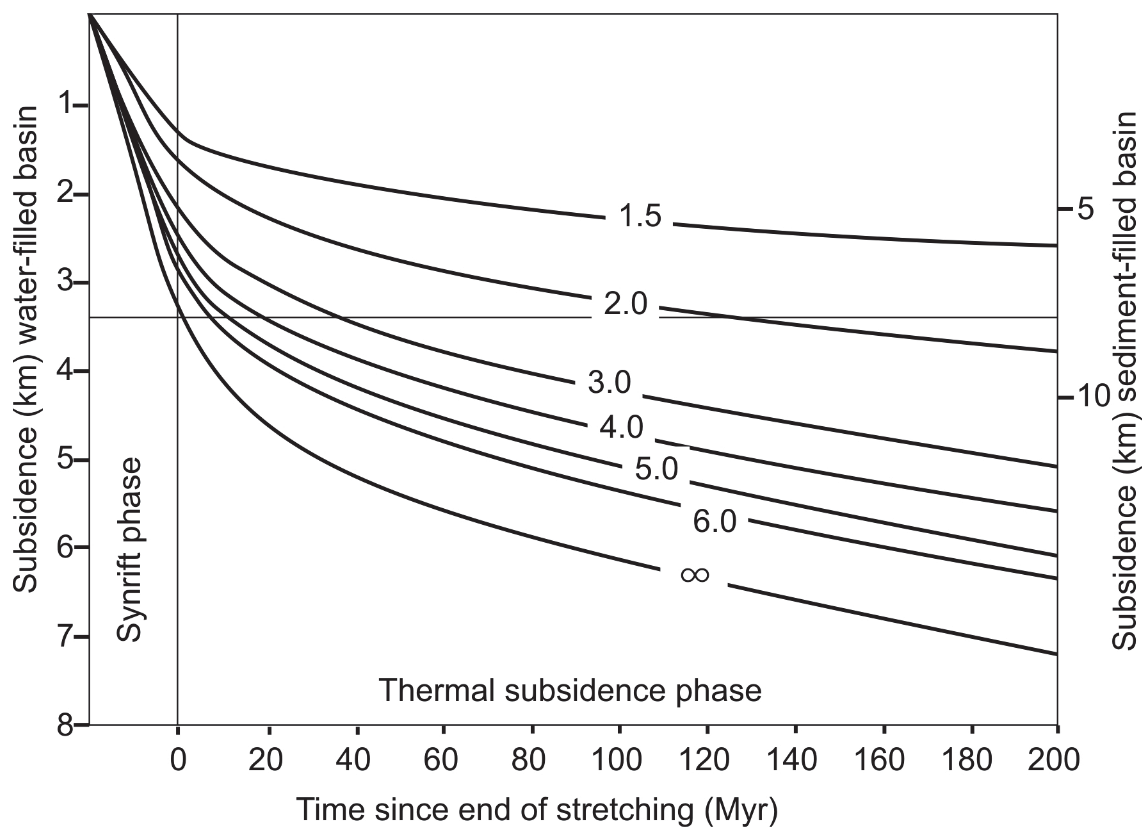

Figure 6.2: Subsidence as a function of the stretch factor using the uniform stretching model, showing the negative exponential post-rift thermal subsidence using the uniform stretching model (after Allen and Allen, 1990 [1]).

southern Orphan Basin is incompatible with this model. It is immediately apparent from Figure 6.1 that the thickness pattern of the post-rift does not follow the pattern of the syn-rift. The syn-rift in the main part of the basin thickens towards the centre in an east-west direction whereas the post-rift thickens northwards. The post-rift is thickest north of the Dominion well where the syn-rift is thin. North of the Cumberland well there is an area of very thin syn-rift (less than 500 ms two way time) overlain by very thick post-rift (around 4000 ms two way time).

A lateral offset between the syn- and post-rift stratigraphy could be explained by simple-shear dominated rifting . A simple shear model infers lithosphere extension by displacement on a large scale gently dipping shear zone that traverses the entire lithosphere (Wernicke, 1985 [59]). This is an asymmetric model where ductile sub-crustal stretching is laterally displaced from the zone of brittle crustal stretching, producing lateral displacement of thermal post-rift subsidence from brittle fault controlled subsidence. The Wernicke simple shear extension model predicts that the upper plate margin will be characterized by little faulting and abrupt crustal thinning and the lower plate margin has large scale faulting and gradual crustal thinning. This should lead to a discrepancy between the amount of extension measured by brittle faulting and that measured using crustal thinning for the upper plate margin. However there is found to be an extension discrepancy for both sides of the Newfoundland and Iberia conjugate pair (Pérez-Gussinyé, 2013 [32]).

Beaumont and Ings, 2012 [3] produced a depth dependent extension model which predicts symmetric margins as observed on the Newfoundland and Iberia margins. In their model, thick depleted continental mantle lithosphere flows laterally towards the rift axis under gravity to produce a wide zone of exhumed mantle (Beaumont and Ings, 2012 [3]). It is suggested that a thick, depleted lower lithosphere would be needed for lateral gravity flow of sub-continental lithosphere to be more efficient than upwelling asthenosphere and to suppress local decompression melting. Ductile flow of the continental mantle lithosphere leads to thinning of the lithosphere without brittle extension of the crust. Thus an anomalously thick post-rift sequence can be produced, as observed in the northern Jeanne d'Arc and into the Orphan Basin (Fig. 6.1). However, the total amount of extension in the Jeanne d'Arc Basin measured using fault heaves in this study corresponds closely with the total amount of extension measured using change in crustal thickness in the regional North Atlantic deformable plate model (Fig. 5.5), indicating that stretching is uniform with depth in this area. Uniform extension in the Jeanne d'Arc Basin can be reconciled with a depth dependent model in the northern Jeanne d'Arc and into the Orphan Basin by considering an evolution during passive margin formation from distributed extension, in this case the formation of multiple rift basins on the Grand Banks, to localized extension at the rift axis (Beaumont and Ings, 2012 [3]; Péron Pinvidic and Manatschal, 2010 [31]).

6.2 Polyphase rifting evolution

Drawing together information on the timing, direction and quantity of extension for the rift phases within the basin, along with a broader regional view of syn-rift and post-rift sedimentary thicknesses, a rifting evolution is proposed.

Initially extension was distributed over a broad region. Sites of rifting were dependent on zones of pre-existing weakness, therefore rifting was offset from the main axis. In the Jeanne d'Arc Basin old thrust faults were reactivated as normal faults. During the distributed extension phase, stretching can be approximated to a pure shear model thus producing the observed close correlation between extension due to brittle faulting and extension measured by change in crustal thickness in the Jeanne d'Arc Basin. However, an instantaneous model can not be assumed. Rifting of the Jeanne d'Arc Basin occurred over a total time span of approximately 132 Ma, hence some of the heat would have diffused away before stretching was complete, effectively transferring a portion of the thermal subsidence from the post-rift to the syn-rift phase. The most significant rifting in the Jeanne d'Arc Basin was during rift phase I (Fig. 4.16). This rift phase lasted until approximately 186 Ma, hence by the end of rift phase III (96 Ma) there had been 90 Myr for heat to diffuse after rift phase I. The majority of the thermal subsidence had occurred by 90 Ma (Fig. 6.2).

During rift phase II there was some ongoing east-west oriented extension in the Jeanne d'Arc Basin (Fig. 4.14), but extension became localized at the rift axis leading to intense crustal thinning. Uniform extension predicts that the crust and mantle rupture simultaneously and seafloor spreading commences. In the case of the Iberia-Newfoundland margin, the crust ruptured first and vast tracts of mantle lithosphere were exhumed (Huismans and Beaumont, 2011 [18]; Sibuet and Tucholke, 2012 [41]; Pérez-Gussinyé, 2013 [32]; Beaumont and Ings, 2012 [3]; Péron Pinvidic and Manatschal, 2010 [31]). The first mantle was exhumed in the Valanginian, approximately 137 Ma (Péron Pinvidic and Manatschal, 2010 [31]). It is proposed that in the northern Jeanne d'Arc and the southern Orphan Basin ductile flow of continental mantle lithosphere towards the rift axis led to depth dependent extension (Beaumont and Ings, 2012 [3]). The final rupture of exhumed mantle and onset of seafloor spreading was established in the late Aptian, 112 Ma (Péron Pinvidic and Manatschal, 2010 [31]).

Rift phase III in the Jeanne d'Arc Basin occurred after the onset of seafloor spreading between Newfoundland and Iberia. This rift phase produced a small amount of extension in the basin when compared with the extension from rift phase I, however it had a marked impact on the structuring of the basin due to the 90° rotation of extensional stress. This led to oblique slip reactivation of earlier faults, transpressional structures and a new set of faults orthogonal to previous faults.

It is proposed that the lithosphere had been thinned in the northern Jeanne d'Arc and southern Orphan Basin by the ductile flow of continental mantle lithosphere towards the rift axis between 137 Ma and 112 Ma. Thermal subsidence from this depth dependent extension produced a huge quantity (up to 4100 ms two way time) of post-rift stratigraphy during the Late Cretaceous and Cenozoic.

Chapter 7

Conclusions

7.1 Conclusions

- There were three rift phases that affected the Jeanne d'Arc Basin.
- Rift phase I was active during the Late Triassic to Early Jurassic (228 Ma - 150 Ma). It is estimated that there was up to 35 km of extension in a northwest-southeast direction. This was followed by a tectonically quiescent phase during the Early to Late Jurassic (186 Ma - 150 Ma).
- Rift phase II was active in the Late Jurassic to Early Cretaceous (150 Ma - 112 Ma). It is estimated that there was up to 12 km of extension in an east-west direction.
- Rift phase III was active during the Aptian to Albian (112 Ma - 96 Ma). It is estimated that there was up to 11 km of extension in a northeast-southwest direction. This resulted in oblique slip reactivation of earlier northeast-southwest and north-south striking faults.

- The most significant brittle extension in the Jeanne d'Arc Basin was during rift phase I.
- Fault interactions between faults from rift phase II and rift phase III are complex, hence fault interpretation and mapping is difficult even using the 3D data.
- Fault heave measurements from the 2D data underestimate extension by approximately 50% when compared with measurements from the 3D data.
- The total amount of extension measured using fault heaves in this study corresponds closely with the total amount of extension measured using change in crustal thickness in the regional North Atlantic deformable plate model. This would indicate that stretching is uniform with depth in this area.
- Detailed fault mapping provides valuable information on the orientation and timing of rift events within the Jeanne d'Arc Basin that can be used as input into a refined regional North Atlantic deformable plate model.
- In the northern Jeanne d'Arc and into the southern Orphan Basin there is a huge thickness of post-rift strata underlain by thin syn-rift strata. During rift phase II ductile flow of continental mantle lithosphere towards the rift axis led to depth dependent extension in this area.

7.2 Future Work

- Use the results from this study to feed back into the regional model to refine the regional North Atlantic deformable plate model.
- Fault mapping and extension estimates from a grid of high quality regional 2D seismic lines extending across the shelf edge and across the area between the

Jeanne d'Arc Basin and the Orphan Basin, to obtain a detailed regional picture. This information can be used to further refine the regional North Atlantic deformable plate model.

- Deeper high quality seismic, both 2D and 3D, to clearly image down to the Top Basement Unconformity across the full extent of the basin.
- 3D seismic mapping of the offset between the Murre fault and the Mercury fault. The geometry of this complex area requires the continuity of 3D data to be better understood.
- Geodynamic modelling of the Jeanne d' Arc Basin in order to better understand the processes controlling the evolution of the basin.
- Measure the total amount of extension using fault heaves in the northern Jeanne d'Arc and into the southern Orphan Basin and compare with the total amount of extension measured using change in crustal thickness in the regional North Atlantic deformable plate model to confirm that there was depth dependent stetching in this area.

Bibliography

[1] P. A. Allen and J. R. Allen. *Basin Analysis: Principles and Applications*. Wiley, 1990.

[2] BASIN. *Natural Resources Canada*, (accessed March 13, 2014). `http://basin.gdr.nrcan.gc.ca/wells/index_e.php`.

[3] C. Beaumont and S. J. Ings. Effect of depleted continental lithosphere counterflow and inherited crustal weakness on rifting of the continental lithosphere: General results. *Journal of Geophysical Research: Solid Earth*, 117(B8):B08407, 2012.

[4] CNLOPB. *Basins of Eastern Grand Banks Map*, 2003.

[5] S. Deemer, J. Hall, K. Solvason, K. W. H. Lau, K. Louden, S. Srivastava, and J.-C. Sibuet. Structure and development of the southeast Newfoundland continental passive margin: derived from SCREECH Transect 3. *Geophysical Journal International*, 178(2):1004–1020, 2009.

[6] M. C. Dentith and J. Hall. Application of section-balancing techniques to deep seismic reflection data from offshore eastern Canada: preliminary observations. *Canadian Journal of Earth Sciences*, 27(4):494–500, 1990.

[7] M. E. Deptuck, R. A. MacRae, J. W. Shimeld, G. L. Williams, and R. A. Fensome. Revised Upper Cretaceous and Lower Paleogene lithostratigraphy and

depositional history of the Jeanne d'Arc Basin, offshore Newfoundland, Canada. *AAPG Bulletin*, 87(9):1459–1483, 2003.

[8] K. Dickie, C. E. Keen, G. L. Williams, and S. A. Dehler. Tectonostratigraphic evolution of the Labrador margin, Atlantic Canada. *Marine and Petroleum Geology*, 28(9):1663–1675, 2011.

[9] N. W. Driscoll, J. R. Hogg, N. Christie-Blick, and G. D. Karner. Extensional tectonics in the Jeanne d'Arc Basin, offshore Newfoundland: implications for the timing of break-up between Grand Banks and Iberia. *Geological Society, London, Special Publications*, 90(1):1–28, 1995.

[10] W. F. Dula. Geometric models of listric normal faults and rollover folds. *AAPG Bulletin*, 75(10):1609–1625, 1991.

[11] M. E. Enachescu. Tectonic and structural framework of the northeast newfoundland continental margin. *Canadian Society of Petroleum Geologists*, Memoir 12:117–146, 1987.

[12] D. A. Ferrill, A. P. Morris, and R. N. McGinnis. Crossing conjugate normal faults in field exposures and seismic data. *AAPG Bulletin*, 93(11):1471–1488, 2009.

[13] GeoArctic. *Deformable plate reconstructions*, 2013 (accessed March 12, 2014). `http://www.geoarctic.com/home.html`.

[14] A. D. Gibbs. Balanced cross-section construction from seismic sections in areas of extensional tectonics. *Journal of Structural Geology*, 5(2):153–160, 1983.

[15] W. T. Holser, G. P. Clement, L. F. Jansa, and J. A. Wade. Evaporite deposits of the North Atlantic rift. In *Triassic–Jurassic Rifting and Opening of the Atlantic: Continental Breakup and the Origin of the Atlantic Passive Margin, Part A.*, pages 525–557. Elsevier, 1988.

[16] J. R. Hopper, T. Funck, and B. E. Tucholke. Structure of the Flemish Cap margin, Newfoundland: insights into mantle and crustal processes during continental breakup. *Geological Society, London, Special Publications*, 282(1):47–61, 2007.

[17] M. R. Hudec and M. P. A. Jackson. Terra infirma: Understanding salt tectonics. *Earth-Science Reviews*, 82(1–2):1–28, 2007.

[18] R. Huismans and C. Beaumont. Depth-dependent extension, two-stage breakup and cratonic underplating at rifted margins. *Nature*, 473(7345):74–78, 2011.

[19] M. P. A. Jackson and B. C. Vendeville. Regional extension as a geologic trigger for diapirism. *Geological Society of America Bulletin*, 106(1):57–73, 1994.

[20] C. E. Keen, R. Boutilier, B. De Voogd, B. Mudford, and M. E. Enachescu. Crustal geometry and extensional models for the grand banks, eastern canada: Constraints from deep seismic reflection data. *Canadian Society of Petroleum Geologists Memoir*, 12:101–115, 1987.

[21] N. J. Kusznir and G. D. Karner. Continental lithospheric thinning and breakup in response to upwelling divergent mantle flow: application to the Woodlark, Newfoundland and Iberia margins. *Geological Society, London, Special Publications*, 282(1):389–419, 2007.

[22] P.-H. Larsen. Relay structures in a Lower Permian basement-involved extension system, East Greenland. *Journal of Structural Geology*, 10(1):3–8, 1988.

[23] K. W. H. Lau, K. E. Louden, T. Funck, B. E. Tucholke, W. S. Holbrook, J. R. Hopper, and H. Christian Larsen. Crustal structure across the Grand Banks–Newfoundland Basin continental margin – I. results from a seismic refraction profile. *Geophysical Journal International*, 167(1):127–156, 2006.

[24] G. D. Lethbridge. *A geological model of the Hibernia Formation in the vicinity of the Terra Nova and Hebron/Ben Nevis oil fields, Jeanne d'Arc Basin, offshore Newfoundland*. M.Sc., Memorial University of Newfoundland, Canada, 2012.

[25] A. MacRae. *Tif2segy*, 2001 (accessed March 13, 2014). `http://seismic.ocean.dal.ca/~seismic/pwp_wiki/static/Tif2segy.html`.

[26] R. Marrett and R. W. Allmendinger. Estimates of strain due to brittle faulting: sampling of fault populations. *Journal of Structural Geology*, 13(6):735–738, 1991.

[27] R. Marrett and R. W. Allmendinger. Amount of extension on "small" faults: An example from the Viking graben. *Geology*, 20(1):47–50, 1992.

[28] K. D. McAlpine. Mesozoic stratigraphy, sedimentary evolution, and petroleum potential of the Jeanne d'Arc Basin, Grand Banks of Newfoundland. Technical Report 89-17, 1990.

[29] K. R. McClay. Physical models of structural styles during extension. *AAPG Memoir*, 46:95–110, 1989.

[30] D. McKenzie. Some remarks on the development of sedimentary basins. *Earth and Planetary Science Letters*, 40(1):25 – 32, 1978.

[31] G. Péron-Pinvidic and G. Manatschal. From microcontinents to extensional allochthons: witnesses of how continents rift and break apart? *Petroleum Geoscience*, 16(3):189–197, 2010.

[32] M. Pérez-Gussinyé. A tectonic model for hyperextension at magma-poor rifted margins: an example from the west Iberia–Newfoundland conjugate margins. *Geological Society, London, Special Publications*, 369(1):403–427, 2013.

[33] G. Péron-Pinvidic and G. Manatschal. The final rifting evolution at deep magma-poor passive margins from Iberia-Newfoundland: a new point of view. *International Journal of Earth Sciences*, 98(7):1581–1597, 2009.

[34] C. R. Ranero and M. Pérez-Gussinyé. Sequential faulting explains the asymmetry and extension discrepancy of conjugate margins. *Nature*, 468(7321):294–299, 2010.

[35] T. J. Reston. Polyphase faulting during the development of the west Galicia rifted margin. *Earth and Planetary Science Letters*, 237(3–4):561–576, 2005.

[36] T. J. Reston. The extension discrepancy and syn-rift subsidence deficit at rifted margins. *Petroleum Geoscience*, 15(3):217–237, 2009.

[37] T. J. Reston and J. P. Morgan. Continental geotherm and the evolution of rifted margins. *Geology*, 32(2):133–136, 2004.

[38] J. G. Sclater and B. Célérier. Errors in extension measurements from planar faults observed on seismic reflection lines. *Basin Research*, 1(4):217–221, 1989.

[39] J.-C. Sibuet, S. Srivastava, and G. Manatschal. Exhumed mantle-forming transitional crust in the Newfoundland-Iberia rift and associated magnetic anomalies. *Journal of Geophysical Research: Solid Earth*, 112(B6):B06105, 2007.

[40] J.-C. Sibuet, S. P. Srivastava, M. Enachescu, and G. D. Karner. Early Cretaceous motion of Flemish Cap with respect to North America: implications on the formation of Orphan Basin and SE Flemish Cap–Galicia Bank conjugate margins. *Geological Society, London, Special Publications*, 282(1):63–76, 2007.

[41] J.-C. Sibuet and B. E. Tucholke. The geodynamic province of transitional lithosphere adjacent to magma-poor continental margins. *Geological Society, London, Special Publications*, 369:429–452, 2012.

[42] I. K. Sinclair. Tectonism: the dominant factor in mid-Cretaceous deposition in the Jeanne d'Arc Basin, Grand Banks. *Marine and Petroleum Geology*, 10(6):530–549, 1993.

[43] I. K. Sinclair. Transpressional inversion due to episodic rotation of extensional stresses in Jeanne d'Arc Basin, offshore Newfoundland. *Geological Society, London, Special Publications*, 88(1):249–271, 1995.

[44] I. K. Sinclair, J. E. Evans, E. A. Albrechtsons, and L. J. Sydora. The Hibernia Oilfield – effects of episodic tectonism on structural character and reservoir compartmentalization. *Geological Society, London, Petroleum Geology Conference series*, 5:517–528, 1999.

[45] I. K. Sinclair and M. O. Withjack. Mid to Late Cretaceous structural and sedimentary architecture at the Terra Nova oilfield, offshore Newfoundland–implications for tectonic history of the North Atlantic. *Central Atlantic Conjugate Margins Conference, Halifax. Extended Abstracts volume*, pages 125–141, 2008.

[46] S. P. Srivastava and C. R. Tapscott. Plate kinematics of the North Atlantic: The geology of north america. In *The Western North Atlantic Region*, pages 379–404. The Geological Society of America, 1986.

[47] S. P. Srivastava and J. Verhoef. Evolution of Mesozoic sedimentary basins around the North Central Atlantic: a preliminary plate kinematic solution. *Geological Society, London, Special Publications*, 62(1):397–420, 1992.

[48] S. P. Srivastava, J. Verhoef, and R. Macnab. Results from a detailed aeromagnetic survey across the northeast Newfoundland margin, part II: early opening

of the North Atlantic between the British Isles and Newfoundland. *Marine and Petroleum Geology*, 5(4):324–337, 1988.

[49] A. J. Tankard and H. J. Welsink. Extensional tectonics and stratigraphy of Hibernia Oil Field, Grand Banks, Newfoundland. *AAPG Bulletin*, 71:10:1210–1232, 1987.

[50] A. J. Tankard, H. J. Welsink, and W. A. M. Jenkins. Structural styles and stratigraphy of the Jeanne d'Arc Basin, Grand Banks of Newfoundland. *AAPG Memoir*, 46:265–282, 1989.

[51] B. E. Tucholke, D. S. Sawyer, and J.-C. Sibuet. Breakup of the Newfoundland–Iberia rift. *Geological Society, London, Special Publications*, 282(1):9–46, 2007.

[52] B. E. Tucholke and J.-C. Sibuet. Leg 210 synthesis: Tectonic, magmatic, and sedimentary evolution of the Newfoundland-Iberia rift. In *Proceedings of the Ocean Drilling Program, scientific results*, volume 210, pages 1–56, 2007.

[53] B. E. Tucholke and R. B. Whitmarsh. The Newfoundland-Iberia conjugate rifted margins. In *Regional Geology and Tectonics: Phanerozoic Passive Margins, Cratonic Basins and Global Tectonic Maps*, pages 326–341. Elsevier, 2012.

[54] B. C. Vendeville, H. Ge, and M. P. A. Jackson. Scale models of salt tectonics during basement-involved extension. *Petroleum Geoscience*, 1(2):179–183, 1995.

[55] B. C. Vendeville and M. P. A. Jackson. The rise of diapirs during thin-skinned extension. *Marine and Petroleum Geology*, 9(4):331–354, 1992.

[56] J. D. Walker, J. W. Geissman, S. A. Bowring, and L. E. Babcock. The Geological Society of America Geologic Time Scale. *Geological Society of America Bulletin*, 125(3-4):259–272, 2013.

[57] J. Walsh, J. Watterson, and G. Yielding. The importance of small-scale faulting in regional extension. *Nature*, 351(6325):391–393, 1991.

[58] J. K. Welford, J. Hall, J. C. Sibuet, and S. P. Srivastava. Structure across the northeastern margin of Flemish Cap, offshore Newfoundland from Erable multichannel seismic reflection profiles: evidence for a transtensional rifting environment. *Geophysical Journal International*, 183(2):572–586, 2010.

[59] B. Wernicke. Uniform-sense normal simple shear of the continental lithosphere. *Canadian Journal of Earth Sciences*, 22(1):108–125, 1985.

[60] N. J. White, J. A. Jackson, and D. P. McKenzie. The relationship between the geometry of normal faults and that of the sedimentary layers in their hanging walls. *Journal of Structural Geology*, 8(8):897–909, 1986.

[61] M. O. Withjack and S. Callaway. Active normal faulting beneath a salt layer: An experimental study of deformation patterns in the cover sequence. *AAPG Bulletin*, 84(5):627–651, 2000.

[62] M. O. Withjack, Q. T. Islam, and P. R. La Pointe. Normal faults and their hanging-wall deformation: An experimental study. *AAPG Bulletin*, 79(1):1–17, 1995.

[63] M. O. Withjack and R. W. Schlische. A review of tectonic events on the passive margin of eastern North America. In *Petroleum Systems of Divergent Continental Margin Basins: 25th Bob S. Perkins Research Conference, Gulf Coast Section of SEPM*, pages 203–235. SEPM, 2005.

[64] H. Xiao and J. Suppe. Origin of rollover. *AAPG Bulletin*, 76(4):509–529, 1992.

[65] P. A. Ziegler. Evolution of the North Atlantic-an overview. *AAPG Memoir*, 46:111–129, 1989.

[66] P. A. Ziegler and S. Cloetingh. Dynamic processes controlling evolution of rifted basins. *Earth-Science Reviews*, 64(1–2):1–50, 2004.